(4)

GL-TR-89-0061

SIO Ref. 89-7
MPL-U-26/89

AUTOMATED VISIBILITY & CLOUD COVER MEASUREMENTS WITH A SOLID-STATE IMAGING SYSTEM

R. W. Johnson
W. S. Hering
J. E. Shields

March 1989
Final Report
26 Sept 84 - 25 Sept 88

UNIVERSITY OF CALIFORNIA SAN DIEGO

SCRIPPS INSTITUTION OF OCEANOGRAPHY

MARINE PHYSICAL LAB San Diego, CA 92152-6400

Prepared for
Geophysics Laboratory, Air Force Systems Command
United States Air Force, Hanscom AFB, Massachusetts 01731-5000

THE SELECTION AND USE OF THE COMPONENTS DISCUSSED HEREIN DOES NOT IMPLY ENDORESEMENT OR RECOMMENDATION OF THE TESTED PRODUCTS BY THE MARINE PHYSICAL LABORATORY OR ITS SPONSORS TO THE EXCLUSION OF OTHER PRODUCTS WHICH MAY BE SUITABLE.

"This technical report has been reviewed and is approved for publication"

Henry A. Brown

HENRY A. BROWN
Contract Manager

Bruce Kunkel

BRUCE KUNKEL
Acting Branch Chief

FOR THE COMMANDER

Robert A. McClatchey

ROBERT A. McCLATCHEY
Division Director

This report has been reviewed by the ESD Public Affairs Office (PA) and is releasable to the National Technical Information Service (NTIS).

Qualified requestors may obtain additional copies from the Defense Technical Information Center. All others should apply to the National Technical Information Service.

If your address has changed, or if you wish to be removed from the mailing list, or if the addressee is no longer employed by your organization, please notify AFGL/DAA, Hanscom AFB, MA 01731. This will assist us in maintaining a current mailing list.

Do not return copies of this report unless contractual obligations or notices on a specific document requires that it be returned.

UNCLASSIFIED

SECURITY CLASSIFICATION OF THIS PAGE

REPORT DOCUMENTATION PAGE

Form Approved OMB No. 0704-0188

1a. REPORT SECURITY CLASSIFICATION: Unclassified	1b. RESTRICTIVE MARKINGS
2a. SECURITY CLASSIFICATION AUTHORITY	3. DISTRIBUTION / AVAILABILITY OF REPORT: Approved for public release; distribution unlimited.
2b. DECLASSIFICATION / DOWNGRADING SCHEDULE	
4. PERFORMING ORGANIZATION REPORT NUMBER(S): SIO Ref. 89-7 MPL-U-26/89	5. MONITORING ORGANIZATION REPORT NUMBER(S): GL-TR-89-0061
6a. NAME OF PERFORMING ORGANIZATION: University of California, San Diego / 8b. OFFICE SYMBOL (If applicable): MPL	7a. NAME OF MONITORING ORGANIZATION: Geophysics Laboratory
6c. ADDRESS (City, State, and Zip Code): San Diego, CA 92093	7b. ADDRESS (City, State, and Zip Code): Hanscom AFB, MA 01731-5000
8a. NAME OF FUNDING / SPONSORING ORGANIZATION / 8b. OFFICE SYMBOL (If applicable)	9. PROCUREMENT INSTRUMENT IDENTIFICATION NUMBER: F19628-84-K-0047
8c. ADDRESS (City, State, and Zip Code)	10. SOURCE OF FUNDING NUMBERS

PROGRAM ELEMENT NO.	PROJECT NO.	TASK NO.	WORK UNIT ACCESSION NO.
63707F	317J	1C	AA

11. TITLE (include Security Classification)

Automated Visibility & Cloud Measurements With A Solid State Imaging System

12. PERSONAL AUTHOR(S)

Richard W. Johnson, Wayne S. Hering, Janet E. Shields

13a. TYPE OF REPORT	13b. TIME COVERED	14. DATE OF REPORT (Year, Month, Day)	15. PAGE COUNT
Final	FROM 26/9/84 TO 25/9/88	March 1989	128

16. SUPPLEMENTARY NOTATION

17. COSATI CODES			18. SUBJECT TERMS (Continue on reverse if necessary and identify by block number)
FIELD	GROUP	SUB-GROUP	Automation, Observations, Weather, Visibility, Cloud Cover, Weather Sensors, Sector Visibility, Aviation Weather Observations, Cloud Detection, Cloud-Free Arc Determination

19. ABSTRACT (Continue on reverse if necessary and identify by block number)

This Final Report, under Contract No. F19628-84-K-0047, summarizes the development status of two computer-controlled, video-based imaging systems, their initial deployment and the preliminary application of their output data for the objective determination of cloud free paths of sight, total cloud cover, and sector visibilities.

The research supporting these tasks has been a multi-year activity conducted at the Scripps Institution of Oceanography under the sponsorship of the Air Force Geophysics Laboratory. The effort has been directed toward the development of two related systems, one for the automatic assessment of total cloud cover and its related distributional statistics, and the other for the automatic determination of local sector visibilities. Both systems involve the use of similar hardware for image acquisition and manipulation, but quite different analytics and control algorithms, thus they are discussed separately in this Final Report.

The development status at the conclusion of this contract interval is such that two prototype systems, the Whole Sky Imager which is used for cloud cover assessments and the Automatic Horizon Scanner which is used for visibility determinations, are built, operational in several locations, and are producing image oriented data bases appropriate for computer analysis. Preliminary analytic algorithms for the use of these data in automated processes have been developed and are undergoing refinement.

20. DISTRIBUTION / AVAILABILITY OF ABSTRACT	21. ABSTRACT SECURITY CLASSIFICATION	
☐ UNCLASSIFIED / UNLIMITED ☐ SAME AS RPT. ☐ DTIC USERS	Unclassified	
22a. NAME OF RESPONSIBLE INDIVIDUAL: H. Albert Brown	22b. TELEPHONE (Include Area Code)	22c. OFFICE SYMBOL: GL/LYA

DD FORM 1473, JUN 86 *Previous editions are obsolete.*

SECURITY CLASSIFICATION OF THIS PAGE

UNCLASSIFIED

SUMMARY

This Final Report, under Contract No. F19628-84-K-0047, summarizes the development status of two computer-controlled, video-based imaging systems, their initial deployment and the preliminary application of their output data for the objective determination of cloud free paths of sight, total cloud cover, and sector visibilities.

The research supporting these tasks has been a multi-year activity conducted at the Scripps Institution of Oceanography under the sponsorship of the Air Force Geophysics Laboratory. The effort has been directed toward the development of two related systems, one for the automatic assessment of total cloud cover and its related distributional statistics, and the other for the automatic determination of local sector visibilities. Both systems involve the use of similar hardware for image acquisition and manipulation, but quite different analytics and control algorithms, thus they are discussed separately in this Final Report.

The development status at the conclusion of this contract interval is such that two prototype systems, the Whole Sky Imager which is used for cloud cover assessments and the Automatic Horizon Scanner which is used for visibility determinations, are built, operational in several locations, and are producing image oriented data bases appropriate for computer analysis. Preliminary analytic algorithms for the use of these data in automated processes have been developed and are undergoing refinement.

TABLE OF CONTENTS

Table of Contents con't.

LIST OF ILLUSTRATIONS

LIST OF TABLES

1.0 INTRODUCTION

It is clear that, in spite of substantial and well- documented study of the earth's atmosphere by a myriad of able and willing investigators, our ability to portray concisely the optical state of the local atmosphere in a manner suitable for many specific and immediate needs is severely limited. It is equally clear that a major and pervasive contaminant, from the point of view of image transmission scenarios, is the ubiquitous and ever changing cloud cover in any one of its infinite variations. Thus in an effort to provide an experimental approach that would enable automatic assessment of local cloud cover and sector visibility variabilities and statistics, two computer controlled video radiometer systems with appropriate control and analysis algorithms have been built and exercised by the Marine Physical Laboratory.

In its most basic form, each of these new and experimentally powerful devices consists of a computer- controlled solid-state video system that provides calibrated multi-spectral imagery suitable for the automatic extraction of local image transmission and cloud cover information. Imbedded within the control computer are prototype and proprietary extraction algorithms necessary to provide these numerical products. In addition to radiometrically calibrated imagery, advanced algorithm development is currently underway to provide near real-time products of the data acquisition, processing, and display system in the form of continuously updated digital presentations of selected operational quantities. The quantities most desired for describing the optical state-of-the-atmosphere in which these sensor systems operate are, of course, task dependent, but current algorithm development is slanted toward cloud detection, cloud-free arc determinations, sector visibilities and total cloud cover. The multi-spectral imagery is also applicable in more generalized search, detect and identify scenarios.

2.0 THE WHOLE SKY IMAGER

Responding to a well recognized need by many in both the modeling and operational communities for an improved capability in the collection and assessment of whole sky cloud characteristics, a new generation of whole sky, video based imaging systems has been developed and fielded by the Marine Physical Laboratory of Scripps Institution of Oceanography. These systems have been designed to acquire visible spectrum, whole sky images, *i.e.* Fields of View of approximately 175°, in pre-selected wavelength bands that can be recorded in a digital format suitable for subsequent automated cloud analysis. An additional goal of this developmental task was the creation of the algorithms necessary to exploit this class of data for the specification of cloud-free interval statistics and their related probabilities.

As can be expected in the development of most new hardware/software systems, several successive versions of the basic concept have been built and exercised. One of the earliest examples in this developmental sequence was fielded in September 1984 during a site characterization exercise at White Sands Missile Range (WSMR), New Mexico.

2.1 Preliminary System Configurations

The deployment of two prototype electro-optical (EO) camera systems, their general description, and an initial evaluation of their archived imagery were discussed in a limited edition, Technical Note No. 200, which was issued in May 1986. This note has been reproduced herein as Appendix A, with several summarizing comments abstracted for review in the following few paragraphs.

2.1.1 Electro-optic Camera Systems

Both EO camera systems consisted primarily of a GE solid state camera, with Visibility Laboratory optical and filter assemblies attached. In each case, the camera contained a CID (charge injection device) sensor. The external optics were designed to allow the use of a fisheye lens, for nearly full hemisphere coverage, as well as smaller field of view lenses. The filter assembly, which physically contained part of the optics mentioned above, allowed the spectral filtering of the light, as well as the control of light levels through use of neutral density filters. Finally, each system included control electronics as well as data archival electronics and systems.

There were several important design considerations affecting the development of these instruments. Some of these are given below.

a) In the analysis of the images, it may be necessary to know the absolute radiance of each point in the image, in order to compare this radiance with a model or standard value. Even if knowledge of absolute radiance is not required, many of the potential techniques for cloud identification require knowledge of relative radiance within the image. In either case, this implies the use of a fixed gain system, *i.e.*, one which does not change the electronic amplification as a function of the image itself. This was a major reason for choosing a CID imager with fixed gain.

b) It is convenient to obtain data for the whole sky in one image. In this particular application, it was deemed adequate to obtain all but near-horizon look angles.

Consequently an upward looking fish eye lens was used. A related consideration, however, is that optical resolution must be adequate to image sufficiently small clouds. Whereas the backup system, EO Camera I, had a 128 x 128 picture element (pixel) array, with a resulting resolution of approximately 1.5° (zenith angle) per pixel, the prototype system, EO Camera II, had approximately 256 x 256 pixels, with a resolution of approximately 0.7° per pixel.

c) To obtain maximum radiometric resolution between clouds and sky, a filter changer was used to allow data to be collected through a red filter. In this wavelength regime, the sky is relatively dark in comparison with the clouds. In addition, as backup, it was desirable to obtain data through a blue filter, so that clouds might be potentially identified through analysis of the measured spectral radiance ratios. For this deployment, the backup EO Camera I was fitted with a blue filter in addition to the red, whereas the prototype EO Camera II had only a red filter.

d) Since the range of the CID cameras was rather limited in comparison with observed sky and cloud radiances (just over 1 log of radiometric sensitivity), a number of neutral density filters were included in the filter changer in order to allow the input flux level to be changed in a controlled way. The use of the f-stops on the fisheye lens offered additional ranging capability.

Figure 2-1(a) illustrates the optical layout of the EO Camera I. EO Camera I could be run with either the 425nm filter or the 605 nm filter, either with or without a .3 log neutral density filter. Additional control of flux level was obtained through the use of the various f-stops on the fisheye lens. Also, a 555nm filter was included in this system for acquiring pseudo-photopic test data.

The system block diagram for EO Camera I is illustrated in Fig. 2-2(a). The camera was a GE solid state CID camera, Model 2200. Camera control and data logging were accomplished through an HP mini-computer in conjunction with a Chieftan frame grabber. The data were recorded digitally on magnetic tape, and viewed simultaneously on a monitor. Digital tapes were returned to the laboratory for analysis. In this system, the iris assembly was manually controlled, as was the occultor assembly. The occultor assembly consisted of a shading device placed external to the fisheye lens to shade it from sunlight, thus reducing stray light within the system.

The optical layout for EO Camera II is illustrated in Fig. 2-1(b). This system is similar to EO Camera I, with a somewhat more compact optical assembly and a higher resolution sensor array. The sensor was a GE Model 2505 CID Camera. Data could be obtained either with a 650nm filter or spectrally unfiltered, and with any of four neutral density filters (or none) superimposed in the path.

Figure 2-2(b) illustrates the system block diagram for EO Camera II. Figure 2-2(c), showing the "Proposed" system, illustrates the Zenith-driven system which was originally intended for this deployment, but not utilized. Third party delivery delays resulted in the deployment of the "As-built" system in Fig. 2-2(b). In this system, the video signal was routed through a time/date generator to a video recorder and a monitor. The primary disadvantage of the prototype system was the variable gain inherent in the VCR. The video tapes of data from this system were transported to the laboratory where they could be digitized and read into the mainframe computer for analysis. With this system, the iris assembly and occultor assembly were controlled remotely.

For a more detailed description of these early hardware systems, their operation, data collection and subsequent data analysis, the reader is referred to Appendix A.

After the successful proof of concept operations at WSMR, an intensive period of system upgrade and sophistication was launched to exploit more fully the most attractive aspects of this video based radiometric system.

The proliferation of advanced military electro-optical (EO) systems designed for visible spectrum operations in the troposphere has greatly increased the need for a compact automatic system to assess and predict the optical and meteorological properties of this operational medium.

Under the sponsorship of the Air Force Geophysics Laboratory, the Visibility Laboratory, which has subsequently been re-organized as part of the Marine Physical Laboratory, began developing a family of small, solid-state imaging systems to address this need. Several existing and developing versions of these devices and their proposed uses are described briefly in the following paragraphs and illustrations which have been abstracted from Technical Note No. 201. (See Appendix B for more detail discussion)

2.1.2 First Generation Instrumentation, E/O Camera III

The system block diagram shown in Fig. 2-2(c) illustrates configurational relationships common to all sys-

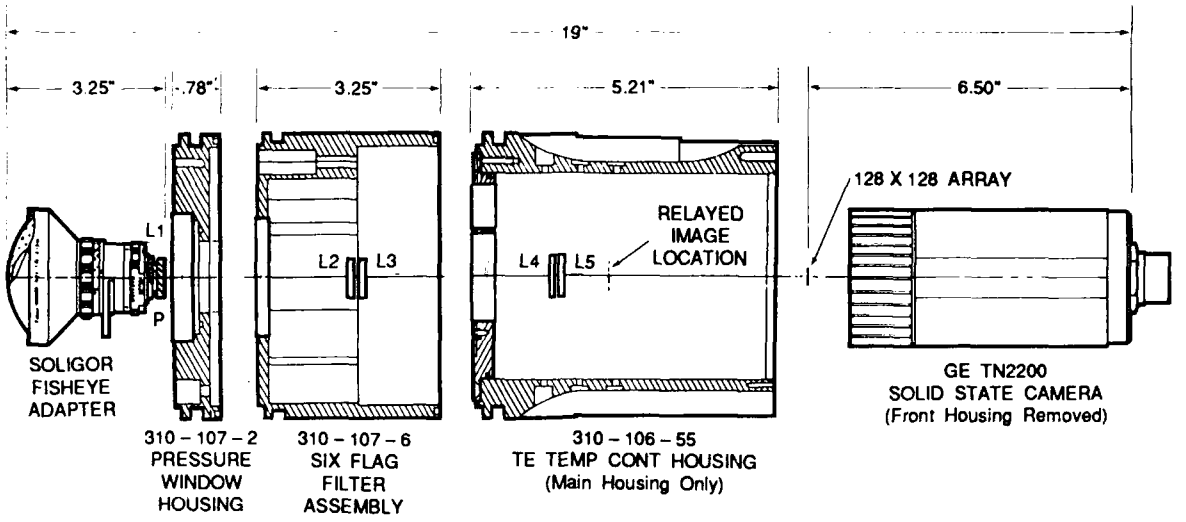

(a) Multi-spectral imaging fisheye scanner (EO Camera I)

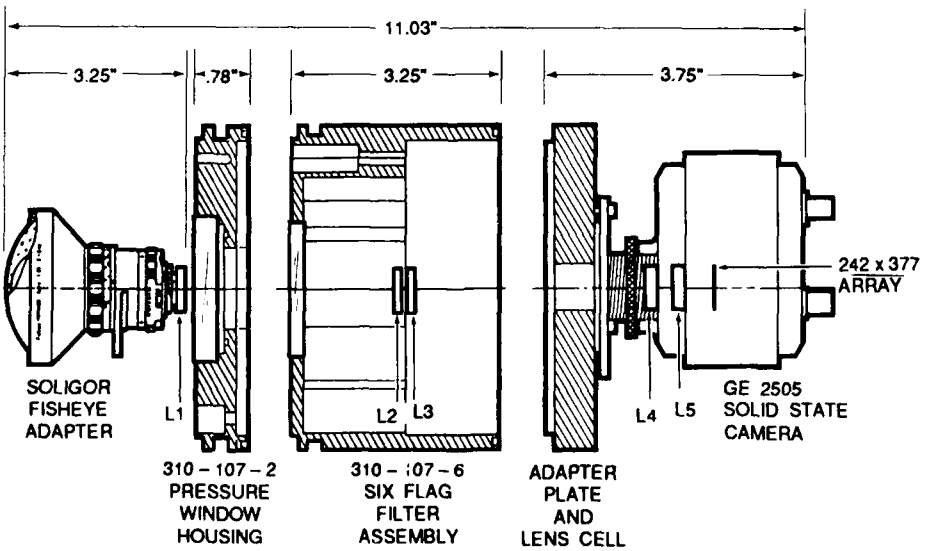

(b) Multi-spectral whole sky imager (EO Camera II)

Fig. 2-1. EO Camera optical layout.

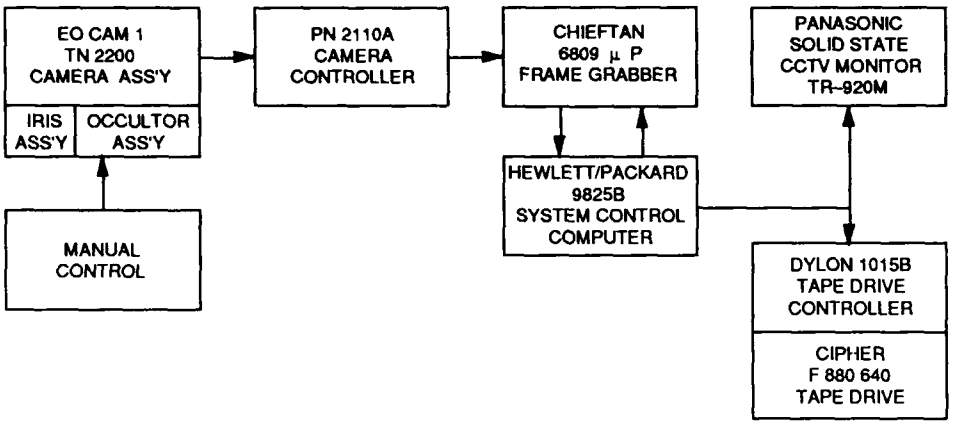

(a) Back-up system as-built for AUG '84 deployment. (EO Camera I)

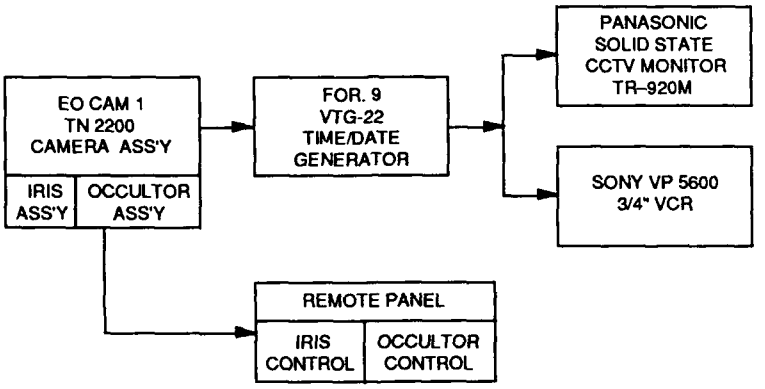

(b) Prototype system as-built for AUG '84 deployment. (EO Camera II)

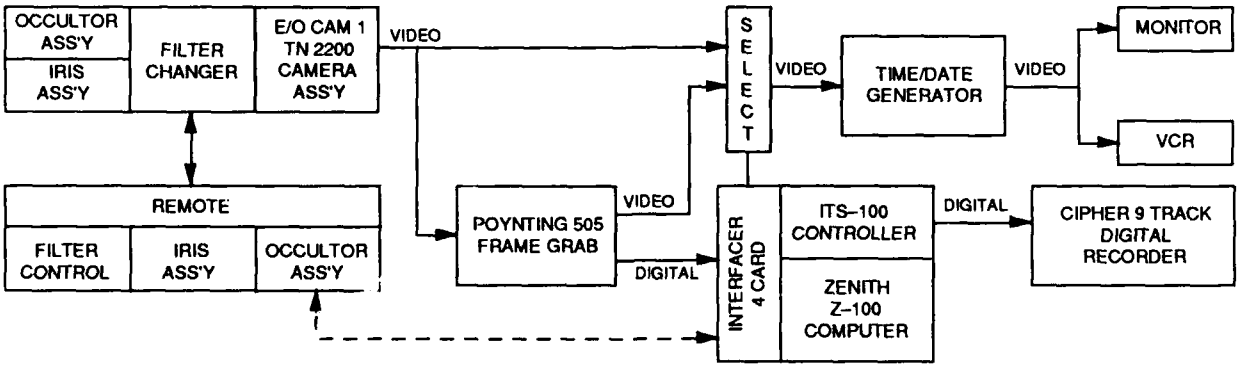

(c) Composite system proposed for CFLOS Algorithm development.

Fig. 2-2. Equipment organization schematic.

tems described herein, and is not necessarily an as-built drawing. For example, the "select" function linking the Z-100 computer and the Time/Date Generator is conceptual only. Both the video and digital data are routed through the system simultaneously and independently. The parallelism is an operator convenience, not a necessity. Most of the operational characteristics illustrated in Fig. 2-2(c) are included in each of the currently evolving hardware configurations.

A typical version of the basic computer controlled systems designed for the semi-automatic acquisition and archival of calibrated imagery is illustrated in Fig. 2-3. Typical component sub-assemblies are listed in Table 2.1.

The schematic drawing of the multi-spectral imager shown in Fig. 2-4 illustrates the Filter Changer Assembly, an important feature of the camera system that contributes greatly to its general utility. The Filter Changer Assembly contains two independently controlled filter locations on the optical axis. This assembly contains two filter wheels, each holding four separate filters in addition to the five lens optical relay. Each wheel can position any one of its four filters into the optical path under either manual or computer control. In its present configuration, the forward wheel contains four glass absorption neutral density filters, while the rear wheel contains four spectrally different interference filters. Thus, both spectral band and flux level can be controlled either manually or by predetermined computer program.

The multi-lens Turret Assembly (shown pictorially, not as built), provides an efficient method of modifying the overall optical path to meet task specific requirements. In the prototype systems currently in use, the two lens assemblies require manual substitution into a fixed adapter. The remotely controlled turret assembly is no longer under development.

The composite, as-built system shown in Fig. 2-3 is the original operating Z-100 system. Both the video and digital options previously illustrated are contained in the two instrument racks. The camera, filter changer, and fisheye lens assembly are supported on the temporary camera pedestal. This successfully deployed operational system is designed primarily for image acquisition and archival only. The computer does not contain the programmed algorithms necessary for sophisticated image manipulation and analysis, although relatively simple data extractions and numerical computations are readily available. The system can reliably acquire an image every two seconds and store it on the internal hard disk. Identifying time/date and filter information is imbedded within each image data array for subsequent processing and analysis control. In this design, 360 images are stored on disc prior to their batch mode downloading to magnetic tape.

The fundamental shortcoming of this computer system is its limitation to eight bit I/O, and lack of image-oriented, third party software/firmware support. The first generation system shown in Fig. 2-3 uses the GE2505A2 solid-state CID video camera as the primary detector. This camera outputs a standard RS170 composite video signal which is grabbed and digitized by the Poynting 505 frame grabber. The resultant 8-bit 256x256 data array is subsequently operated upon to yield an image that is radiometrically calibrated in absolute radiance units traceable to the National Bureau of Standards. Geometric calibrations are performed on the array such that with the 174(degree) Fisheye adapter lens in place the system yields an angular resolution of approximately 0.7 deg/pixel, and with the 30(degree) small FOV lens in place yields approximately 0.1 deg/pixel resolution.

2.1.3 Second Generation Instrumentation, E/O Camera IV

Having satisfactorily demonstrated the ability to rapidly and reliably acquire and archive calibrated whole sky imagery with the Z-100 based systems described above, there was an immediate recognition that an even more powerful tool was clearly within our grasp. By increasing the image manipulation capabilities within the host computer, and by further customizing the optical collection optics, it seemed possible to create an acquisition and computational environment suitable for more advanced, automatic determinations of the optical state of the atmosphere. The following paragraphs describe the cogent electro-optical and computational characteristics of this emerging system.

The evolution of the second generation system is defined by two basic changes. First to an enhanced host computer, and second to a more exotic optical "turret". Other than that the system concept remains the same, calibrated imagery is manipulated to mimic the observational skills of a human observer.

With regard to the first change, it was felt that a true 16-bit machine was necessary to handle the data flows and computational techniques anticipated. Since the early Z-100 systems had performed well, it was decided to stay within the Zenith environment but to upgrade to their IBM clone, the Z-200 series, in order to avail ourselves of the rapidly expanding IBM support within the third party vendor market. Following this plan, the second generation system outlined in Table 2.1 has been par-

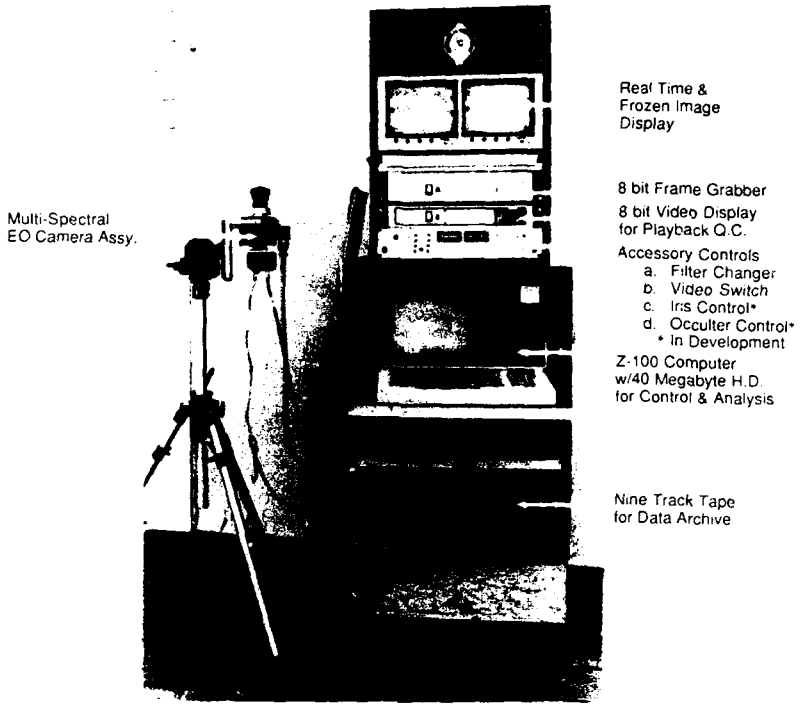

Fig. 2-3. Z-100 system for whole sky image archival.

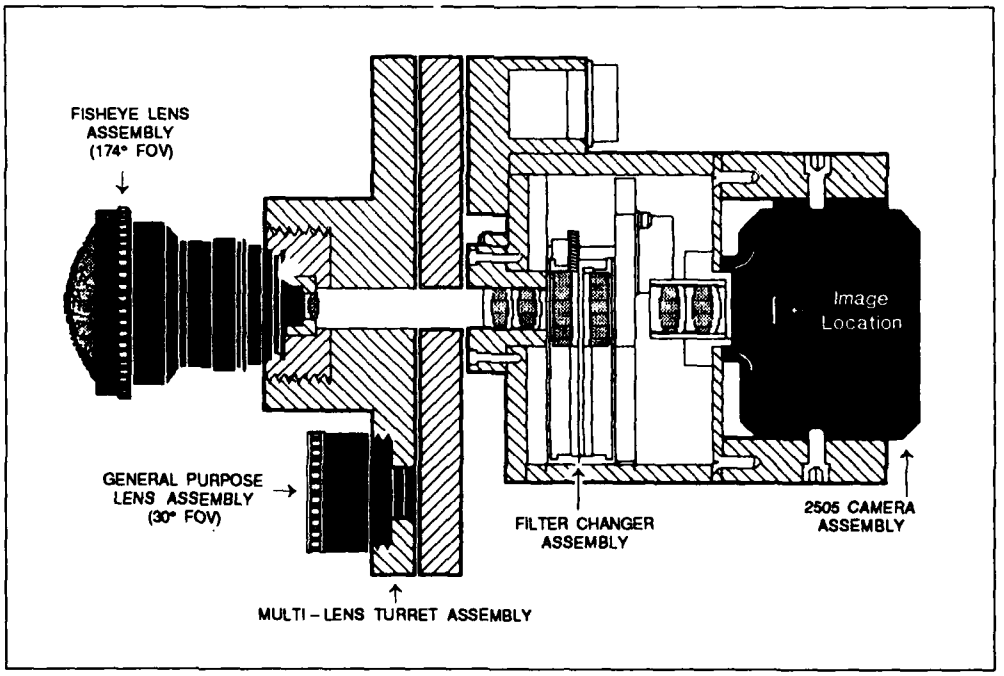

Fig. 2-4. Multi-spectral EO Camera III Assembly.

Table 2.1 Hierarchy of Prototype Imaging Systems
(Not Including Optical Accessories & Housings)

First Generation, Z-100 Based System

Item No.	Item Description
1	ZENITH Z-100 COMPUTER, 8088/8085 μP, enhancements, 40 MB hard disk
2	Poynting 505, Video Frame Grabber
3	Poynting 208, Digital Video Memory
4	Cipher F880640, Microstreamer Tape Drive
5	RCA TC1910 CCTV Monitors
6	GE2505A2 CID Video Camera
7	VisLab Dual Wheel Optical Filter Changer
8	VisLab Accessory Control Panel
	Archival Only, No Image Processing (*i.e.* I.P.) Software

Second Generation, Z-200 Based System

Item No.	Item Description
1	Zenith Z-200 Computer, 80286 μP, enhancements, 40 MB hard disk
2	ITI, PFG-8-1-U-XT Video Frame Grabber (Internal Board)
3	Zenith ZVM-135 Hi Resolution Monitor
4	Cipher 540 Streaming Cartridge Tape Drive (Proposed)
5	Sony PVM 1271(Q) Hi. Res. Video Monitor (Proposed)
6	GE2505A2 CID Video Camera
7	VisLab Dual Wheel Optical Filter Changer
8	VisLab Accessory Control Panel
9	Okidata m83A MicroLine Printer
	Designed to run LOTUS 1-2-3 and PC Vision/Image Lab I.P. Software

Third Generation, Z-241 Based System

Item No.	Item Description
1	Zenith, Z-241 Computer, 80286 μP, enhancements, 40 MB hard disk
2	Imaging Technology FG-100 AT Frame Grabber
3	Zenith ZVM-133 RGB Video Display
4	Cipher 540 Streaming Cartridge Tape Drive
5	Sony PVM 1271(Q) Hi. Res. Video Monitor
6	GE2710 CID Video Camera
7	VisLab Dual Wheel Optical Filter Changer
8	VisLab Accessory Control Panel
9	Epson FX85 Printer
	Designed to run LOTUS 1-2-3 and PC Vision/Image Lab I.P. Software

tially acquired and exercised. Most of the algorithm development and preliminary computations discussed later in this note have been performed in the Z-200 environment. Other than some minor inconveniences in fully exploiting the computer's enhanced RAM (1.2 MB) via the LOTUS 1-2-3 code, the computer system has performed well. It is anticipated that both the second and third generation systems may continue to use the Z-200 class computer. Only the tenant IP (Image Processing) systems will change, in association with future task specific I/O and display requirements.

The entire electro-optical assembly is contained within an insulated weatherproof housing. The remaining design problems are associated with maintaining optically clean windows through which the lenses must collect their imagery. While the solution of these problems will involve some severe aggravation, the fundamental concept of the device should remain uncompromised.

The third generation system summarized in Table 2.1 represents two refinements to the basic Z-200 system. The first is a change to the more powerful Image Technology FG-100 Frame Grabber which provides a 1024x1024 pixel image memory, and the second is a change to the 2710 camera which provides improved 512x512 pixel resolutions. Both changes are directed toward improving the precision and accuracy of the radiometric calibrations and do not imply a change in the basic philosophy underlying the systems performance.

2.2 Current Generation Instrumentation, EO Camera V

Building on the experience gained through the development and operation of the computer controlled video radiometers reviewed in the preceding paragraphs, the Optical Systems Group at the Marine Physical Laboratory has produced a compact and reliable system for the automatic acquisition and archival of whole sky imagery specifically tailored to the assessment of daytime cloud distributions and subsequently their spatial and temporal variations.

Dedicated video based systems of the sort described herein offer the combined capabilities of solid-state imaging technology and fast, efficient micro-computer processing.

The as-built configuration for the systems currently (Sept 88) being fielded in a seven station network covering large portions of the continental U. S. is illustrated in Figs. 2-5, 2-6, and 2-7. A brief discussion of the most significant features of this EO Camera V system is contained in the following paragraphs. More specific details are contained in Appendix C.

The exterior sensor assembly, shown schematically in Fig. 2-5 and photographically in Fig. 2-6, is a relatively

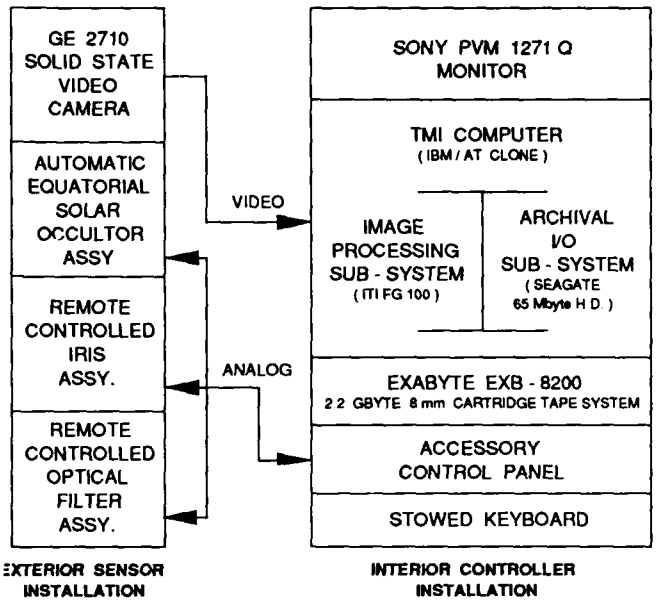

Fig. 2-5. Image Acquisition & analysis system, hardware block diagram, EO Camera V.

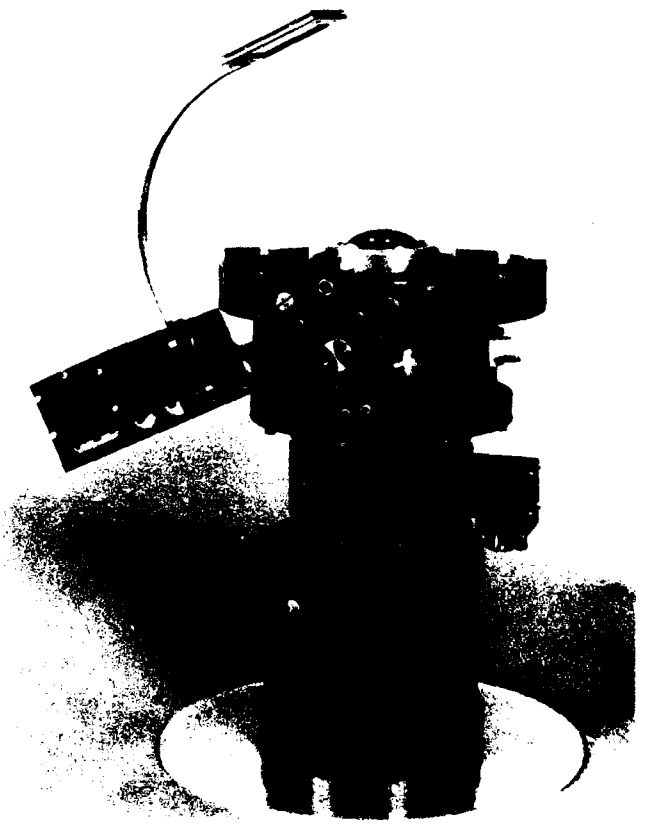

Fig. 2-6. As-built exterior sensor.

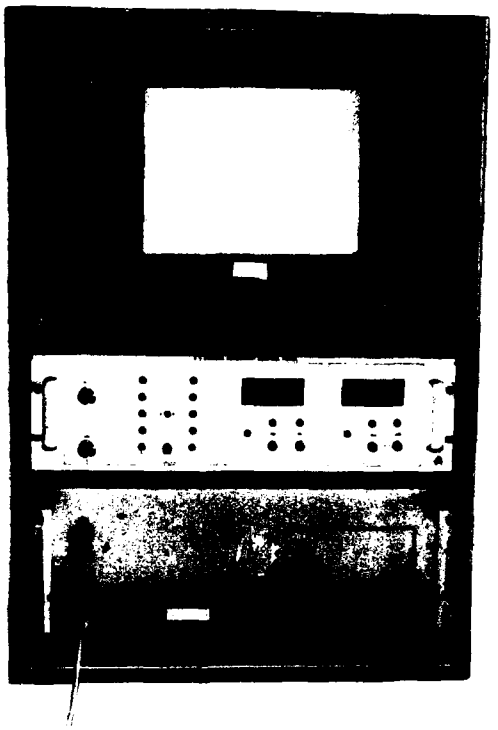

Fig. 2-7. As-built interior controller

compact, weatherproof housing which contains four independent but inter-related sub-systems. The detector component is the CIDTEC (formerly General Electric) model 2710 solid state video camera. This small, solid-state monochrome camera is well suited to this whole-sky imaging application. The CID sensor has a 512Vx776H pixel array yielding excellent angular resolutions even with the super wide-angle (174°) fisheye optical system. The charge injection device has inherently low blooming characteristics resulting in no smear and no lag highlight handling. Background fixed pattern rejection circuitry contributes to excellent low illumination image quality, and the camera's RS-170 compatible video output makes interfacing with peripheral display and processing devices straightforward.

The three associated sub-assemblies, the solar occultor, the remote controlled iris and the remote controlled optical filter assembly have been fabricated at the Marine Physical Laboratory. These peripheral components provide stray light and flux control to ensure optimum image quality over a broad range of illumination levels, and also to provide for the selection of the task specific spectral filters. The optical filter assembly contains two independently controlled four position filter wheels, one contains four neutral density filters for flux level control, and the other contains four spectral filters for spectral pass band selection. All three sub-assemblies are controllable through the accessory control panel, located within the interior controller installation. Each sub-assembly can be operated under either manual or computer control.

The interior controller installation is also shown schematically in Fig. 2-5, and photographically in its as-built configuration in Fig. 2-7. The majority of the systems primary control and archival processes are enclosed within the AT class microcomputer. They include the video frame grabber which accommodates a 1024x1024 image memory, the 80286 based CPU card, and the 8mm cartridge tape system whose 2.2 Gigabyte storage capacity makes possible the seven day duty cycle of the overall camera system.

As illustrated in Appendix C, the components selected for use within the EO Camera V System were selected from a broad variety of commercial vendors. These selections were made on the basis of suitability for minimal interface problems, competitive unit costs, and good delivery schedules at the time the design configuration was frozen.

2.3 E/O Camera V, Operational Characteristics

The use of the dedicated video systems described herein offers the combined capabilities of solid-state imaging technology and fast, efficient micro-computer processing. Measurement accuracy is achieved through excellent control over both spatial resolution and relative brightness accuracy. The solid-state sensor array has exact pixel element placement. Thus, any individual element imperfections can be recognized and specific corrections applied. The sensor responses tend to be highly linear and discrete pixel corrections once applied tend to be valid for extended time periods.

2.3.1 In House Calibration

Whereas many useful algorithms for the determination of atmospheric properties can be devised to require only the input of the relative values of radiant flux fields, it is generally true that far more redundant and reliable methodologies are available when absolute values of radiance are available. Thus, to enable an optimum selection of techniques for analytic applications, the camera systems described in this note are all calibrated against standards of radiant intensity traceable to N.B.S. using standard radiometric procedures in association with optical calibration facilities established at the Marine Physical Laboratory. In practice, each measurement system is subjected to a systematic series of calibration procedures consisting of the operational steps outlined in Fig. 2-8. It should be recognized that although the exact data flow through the computerized processing schedule

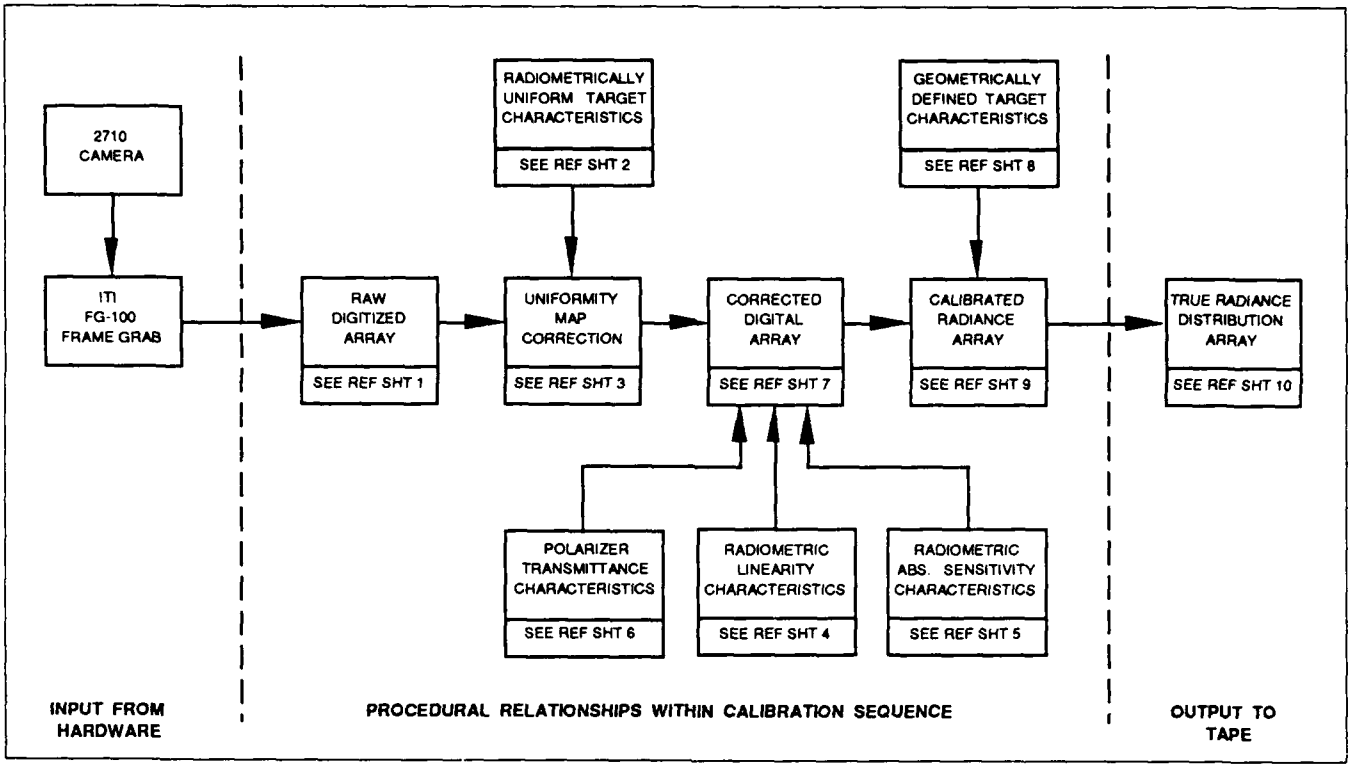

Fig. 2-8. EO Camera V, system calibration procedures.

may not be as illustrated in Fig. 2-8, each item illustrated is in fact addressed for each individual camera. Several specialized facilities and fixtures are of course necessary to implement the calibrations specified for these camera systems, one of which is illustrated in Fig. 2-9. The three meter optical bench in conjunction with a selection of standard lamps and calibration targets can create the various radiance fields necessary to characterize the camera's performance in each of the following regions of interest.

a) Radiometric linearity - radiative flux vs byte value output.

b) Absolute radiative response - absolute spectral flux input vs byte value output.

c) Relative radiance shifts - systematic changes in flux/byte relationships as a function of f-stop and neutral density changes.

d) Geometric mapping - pixel element vs object space geometry as diagnosed with Hemispheric Dome Attachment.

Calibrations of the sort outlined above are conducted in each of the spectral response bands illustrated in Fig. 2-10.

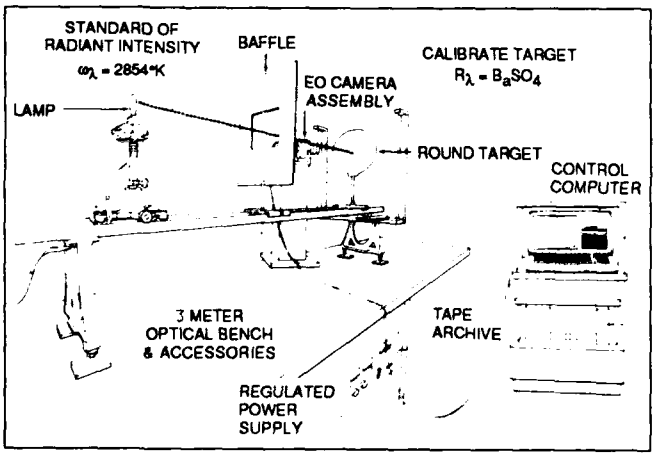

Fig. 2-9. Radiometric calibration facility layout.

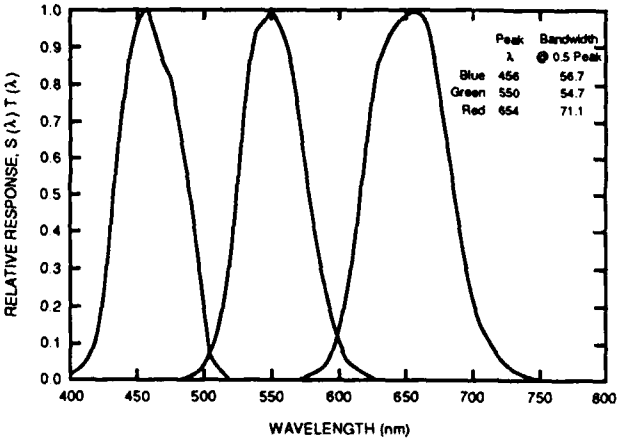

Fig. 2-10. Relative spectral responses.

2.3.2 Field Data Acquisition

The as-built configuration of EO Camera V, discussed in Section 2.2, has been commonly referred to as the Whole Sky Imager (WSI) as a conversational simplification. Several WSI systems have been built, calibrated and deployed to several test sites as illustrated in Fig. 2-11. The geographical distribution is currently (Sep '88) biased toward the southwestern deserts areas, however additional sites in Missouri and Florida, when operational, will provide a better balance between geographical and meteorological regimes.

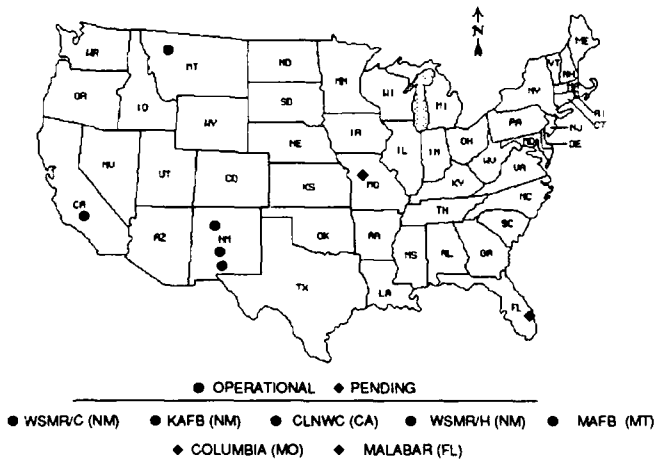

Fig. 2-11. Whole Sky Imager data sites.

As will be discussed further in the following Section 3 of this report, each WSI system has been designed to acquire automatically, whole sky imagery in two spectral bands, i.e. Blue @ ~ 450nm and Red @ ~ 650nm, at a rate of one set per minute for twelve hours a day over a period of two years. The basic data acquisition and archival schedule is illustrated in Fig. 2-12. In accordance with this general time line, a basic set of four images is captured during the first eight seconds of each minute. These four images, two red and two blue, are digitized by an 8 bit A/D converter and subsequently stored at either 512X512 pixel resolution or in a lower resolution sub-set of 33 rows and 33 columns.

An example of the digitized resolutions appearing in the raw imagery is shown in Fig. 2-13. This monochromatic image displays both the full 512x512 resolution initially captured minute by minute in each of the four images per set, and as an overlay, the 33 rows and columns that comprise the archived one minute sub-sets. As noted in the archival schedule of Fig. 2-12, full resolution 512x512 imagery is archived every ten minutes, and low resolution 33 row x 33 column sub-set of each full image is archived every minute throughout each twelve hour day, *i.e.* Local Apparent Noon (LAN) ± 6 hours.

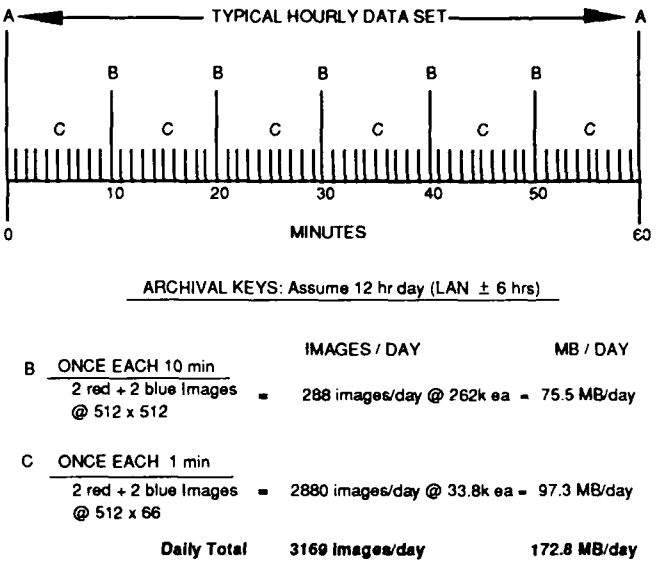

Fig. 2-12. WSI data acquisition and archival schedule.

Scene identification information is automatically imbedded into each image at the time of acquisition which specifies site, location, time, date, and accessory control settings. These data are decoded by the systems post-archival quality control programs and superimposed on all displayed imagery as seen in the upper left corner of Fig. 2-13. The black square area near the center of the image in Fig. 2-13 is an equatorially-driven solar occultor to shadow the fisheye lens, thus preventing undesired stray light from entering the optical path.

Each WSI field is designed to run automatically and without operator intervention for seven days, at which time the system shuts down, ejects its 8mm data cassette, and asks the field operator to insert a new tape into the recorder, which automatically restarts the system on a new seven day cycle. Data cassettes containing approximately 1.5 to 1.7 Gigabytes of digitized imagery are mailed to the Marine Physical Laboratory for post-archival quality control checks and analysis. Host facility support which is requested from each test site custodian is illustrated in Table 2.2 which has been abstracted from the WSI Preliminary Operations Manual. This instructional document is attached to this report as Appendix D. A typical field installation, in this case a site near the Atmospheric Sciences Laboratory on the White Sands Missile Range in New Mexico, is illustrated in Fig. 2-14.

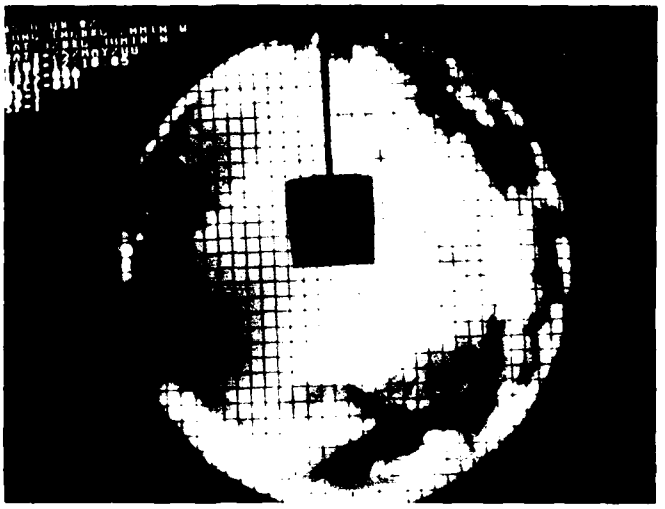

Fig. 2-13. WSI imagery, 512 x 512 with 33 x 33 overlay.

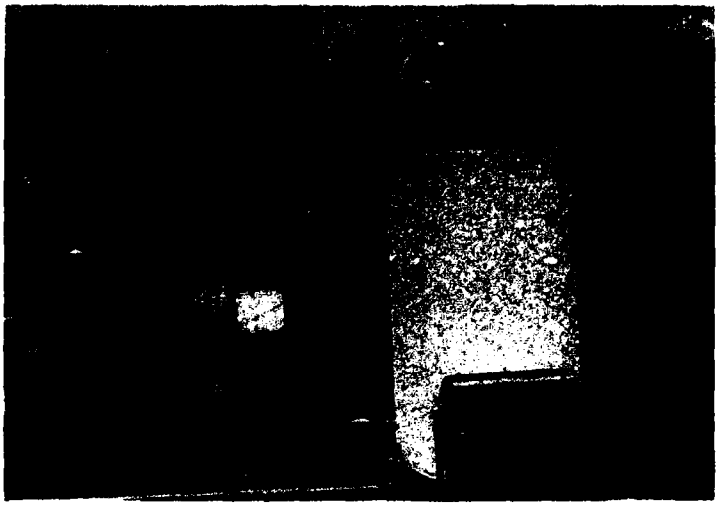

Fig. 2-14. WSI data site, WSMR.

Table 2.2

WSI Data Site:
Host Support Notes During Data Collection Interval
(Estimated 2 Yrs.)

1. Provide daily visual inspection of camera assembly. Wipe or brush optical dome lightly if required to remove snow, heavy dew, thick dust, etc.

2. Provide daily visual inspection of console assembly. Observe video monitor to determine normal image quality and solar attenuator position.

3. Provide weekly unloading and replacement of data cassette with subsequent mailing to UCSD/MPL. (Cassettes provided by UCSD/MPL as well as procedural training).

4. Provide periodic substitution of solar attenuator arms to compensate for seasonal declination changes. (Change schedule and appropriate arms provided by UCSD/MPL. Normal change cycle is at two week intervals, extending to twelve weeks twice a year).

5. Provide telephone contact with UCSD/MPL in the event of system malfunction, and assist in preliminary fault assessment.

6. Permit intermittent access to site by UCSD/MPL personnel to effect system repair/replacement as required.

NOTE: UCSD/MPL will provide written instruction manuals as required to assist host personnel in accomplishing items listed above.

3.0 CLOUD DISCRIMINATIONS FROM WHOLE SKY IMAGERY

A variety of techniques for objective cloud/clear-sky discrimination with the solid-state imagery system are being investigated. Single image (monochromatic) analysis with simple brightness contrast and/or edge depiction techniques often provides excellent results. The cloud radiances are in general larger than the background clear-sky radiances, especially in the red portion of the visible spectrum. Although the qualitative brightness contrast is readily apparent in most images, obvious difficulties are involved in the development of objective depiction criteria using single wavelength image analysis. As summarized in the list of caveats in Fig. 3-1, the cloud and clear-sky radiances vary over broad limits, requiring complex analytic adjustments to the appropriate cloud/clear-sky threshold radiance values. Furthermore, dense and/or shadowed cloud radiances are comparable to and sometimes become less than, the corresponding background sky radiances.

1. **Radiance Threshold Techniques**
   a. Sky & Cloud Radiances Vary Over Large Excursions
   b. Threshold Radiances Require Continual Analytic Updates
   c. Dark or Shadowed Clouds Mimic Background Sky Radiances
2. **Edge Gradient Techniques**
   a. Cloud Imabedded in Cloud Background Yields Redundant Boundaries
   b. Fails as Scene Approaches Uniform Overcast

Fig. 3-1. Single wavelength discriminators: Caveats.

On the other hand, experimental results clearly demonstrate the effectiveness of color contrast, as derived from multi-spectral imagery, for objective sky-cover analysis. Dedicated systems with the dual filter wheel option can easily be configured to acquire sequentially narrow-passband blue and red imagery with variable neutral density control. Objective cloud depiction algorithms based on the ratio of the all-sky blue and red radiance fields provide good specification accuracy over a broad range of sky and visibility conditions. The blue/red spectral radiance ratios are characteristically near 1

for the white or grey cloud elements in contrast with significantly larger values for the background clear sky.

3.1 Current Cloud Discrimination Procedures

Numerical examples demonstrating the efficacy of using blue-red radiance ratios for cloud discrimination can be readily generated using standard radiative transfer models with assumed levels of atmospheric aerosol loading.

Calculations made with the Hering atmospheric radiance model FASCAT (AFGL-TR-84-0168), indicate the blue/red radiance ratio for cloud-free sky to be substantially elevated above the same ratio for those sky regions containing clouds. Sample calculations illustrating this characteristic are shown graphically in Figs. 3-2 and 3-3. In these figures, the blue/red sky radiance ratio has been plotted versus zenith angle along an east-west horizon to horizon sky arc for each of several surface visibilities. Equivalent blue/red ratios for clouds fall near the 1.0 line. Current data base searches are directed toward defining the real world variance of the cloud ratio from its characteristic value near unity. The eastern sky

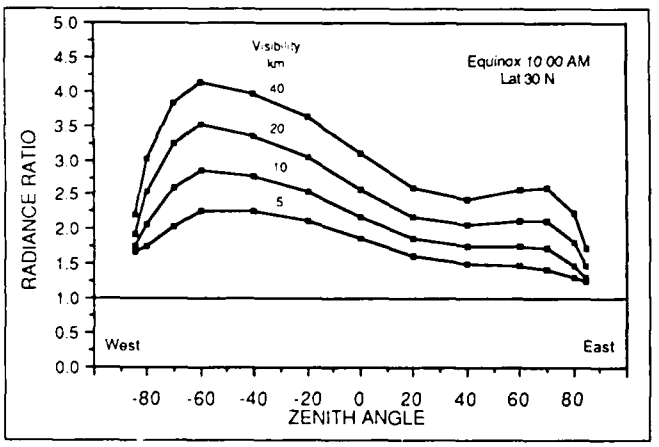

Fig. 3-2. Blue-Red sky radiance ratios, 10 A.M.

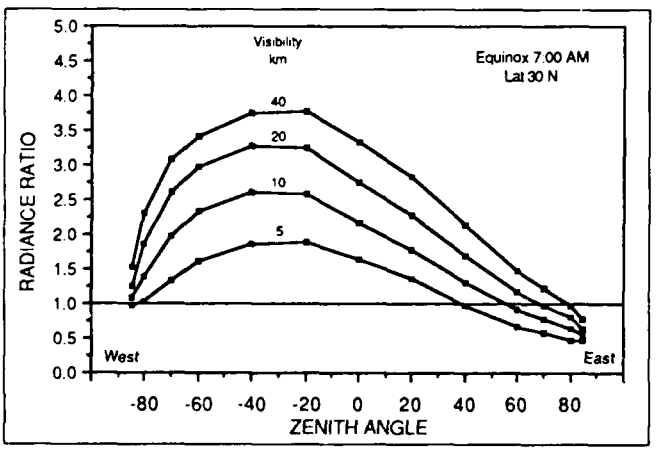

Fig. 3-3. Blue-Red sky radiance ratios, 7 A.M.

near sunrise, Fig. 3-3, continues, for example, to be a difficult region; however, the blue/red radiance ratio will surely continue as the basis for a reliable, consistent cloud detection methodology. These early morning eastern skies with their anticipated, yet procedurally aggravating ratio cross-overs must have their discriminations resolved through the application of supplementary decision algorithms.

Related problem areas associated with the independent use of the blue-red ratio algorithm for cloud discrimination center primarily on paths of sight near the horizon, especially the upsun direction near sunrise and sunset, where the blue-red spectral ratio of the background clear-sky typically becomes less than one in hazy atmospheres. The problem also extends to the solar aureole region at higher solar elevation angles in dense haze conditions where little color contrast exists between the white aureole region and the existing clouds. The information content of the multi-spectral image patterns is being investigated in an effort to develop helpful supplementary techniques to extend the limits of cloud detection in these areas.

Post archival data processing is an inherent characteristic of the WSI operating concept. The various field units are designed to automatically provide optimized imagery for on-site archival only. There is no attempt to make real-time, on-site cloud/no cloud decisions within the current operating system. The post archival data processing follows the general procedures illustrated in Fig. 3-4. The intent of this methodology is to impose strict quality and calibration controls on the raw data, while simultaneously reducing the number of images required for insertion into the optimized cloud/no cloud decision processes. As implied in the processing flow chart, it is inevitable that there will be a variety of specialized decision algorithms which must be applied to provide accurate cloud discriminations under the myriad of real world meteorological circumstances. Determining these specialized techniques is the meat of the research effort required to exploit the capabilities of this system.

Preliminary results indicate that the cloud analysis based upon the radiance ratio imagery might be extended effectively beyond a simple yes-no representation. For example, studies are underway to explore the correspondence between the measured radiance ratios and the opacity of thin, semi-transparent cloud elements.

An example of the semi-automatic process is illustrated in Figs. 3-5 and 3-6. Figure 3-5 is one of the "basic imagery" images acquired and archived every ten min-

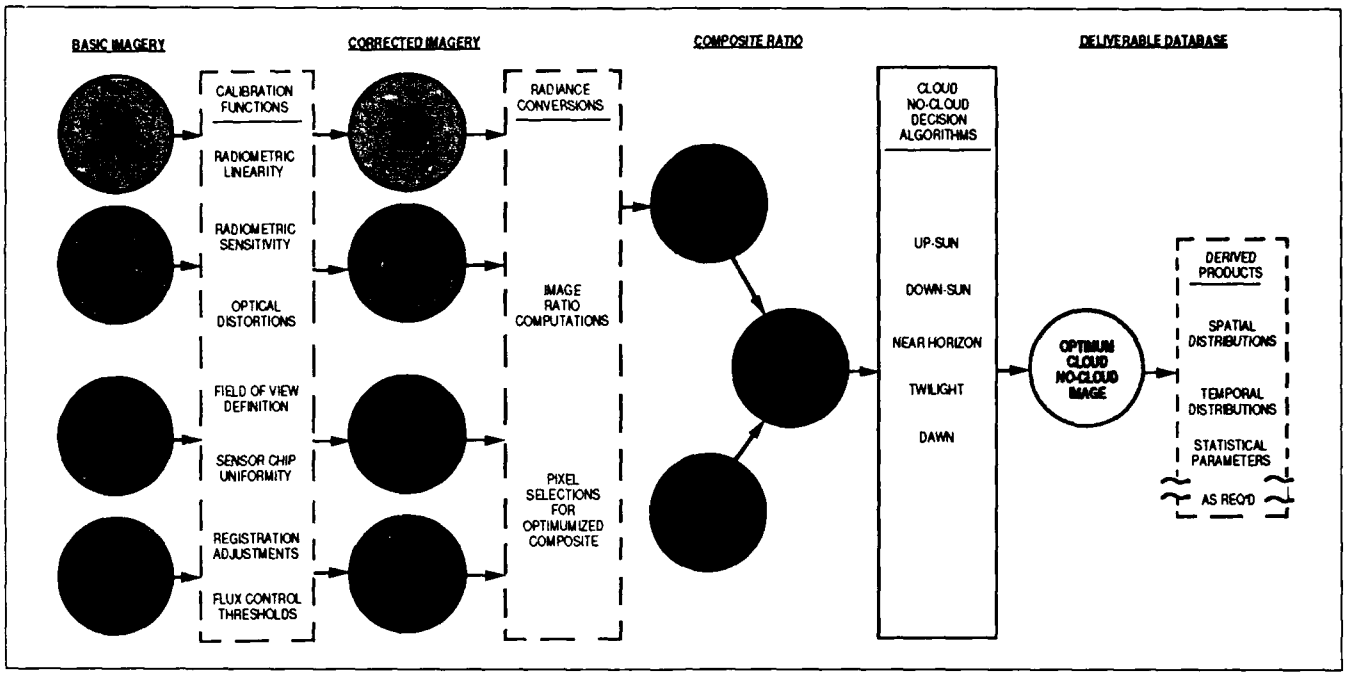

Fig. 3-4. WSI basic image processing flow chart.

utes by the WSI system at WSMR. This high contrast whole sky image, in addition to being a basic data input to the processing cycle, also can be usefully employed as the bogey "sky truth" image against which the automatic determination of cloud/no cloud can be judged. The false colored image shown in Fig. 3-6 represents the results of a computerized pixel by pixel discrimination of whole sky cloudiness. It was derived by exercising the processing sequences illustrated in Fig. 3-4.

4.0 DATA BASE MANAGEMENT & ANALYSIS

The data base to be generated with the whole sky multi-spectral image system will provide cloud discrimination with significantly greater spatial and temporal resolution than has been possible in the past. Program objectives require that vast amounts of data be gathered and analyzed. In terms of individual visible images, existing requirements call for over 1 million whole-sky images to be acquired per year per station. Thus, it is important to plan the data management program with care and understanding at the outset, since subsequent procedural changes may be very costly, simply because of the large additional amount of data manipulation that may be involved.

Multi-spectral visible imagery data is being acquired and stored at frequent intervals during the daylight hours

Fig. 3-5. WSI basic imagery, 650 nm.

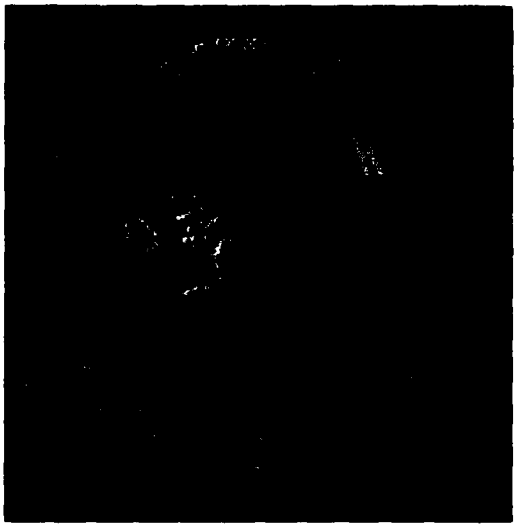

Fig. 3-6. WSI derived CLD/NO CLD image.

at each site. It is important to note that the basic data archive will consist of the pixel by pixel image brightness data and the relevant calibration information. Thus the fundamental radiance values are stored for each of two narrow wavelength intervals centered near 450 nm (blue) and 650 nm (red). Conversion to binary cloud/no cloud imagery data will occur as a separate second stage in the data processing program. Cloud discrimination algorithms may be changed as desired depending upon individual cloud analysis requirements.

As noted in Section 2.3.2, the input format to the basic radiance archive is different depending upon the interval of observation. At ten-minute intervals, 4 images (512 X 480) will be acquired and stored in rapid fire sequence (8 sec grab, 20 sec download for 4 images). A pair of images, one with a blue and one with a red passband filter will be acquired in full, followed by a second pair of red-blue images buffered by offset neutral density filters to help insure that the full range of sky/cloud brightness in the scene is accommodated. The complete imagery for each of the 4 scenes will be stored in radiance format (about 1 megabyte for the 4 images).

Some compromises must be made to handle the vast increase in data volume associated with the measurements at 1-minute intervals. Complete imagery for a set of 4 images will be acquired as for the 10-min data, but the pixel by pixel data for a prescribed screen as illustrated in Fig. 2-13 will be extracted from each image and stored each minute. Complete radiance data along each of 33 preselected rows and 33 columns is archived as opposed to simply retaining pixel data at the grid intersections. Transformation of the 1-min brightness data to binary cloud/no cloud data occurs later. The basic 1-min brightness data extracted from the red and blue imagery is placed in the radiance archive prior to the application of conversion algorithms.

As a supplement to the basic WSI data archive, concurrent conventional weather observations from the nearest local weather station will be stored in a separate data file in a form suitable for quick and easy data retrieval. All cloud data on Federal Meteorological Form MF 1-10 will be retained.

4.1 Cloud/No Cloud Data Archive

As discussed in Section 3, cloud discrimination is achieved through analysis of spectral ratio imagery. Threshold cutoff values of blue-red ratio are determined as dictated by the cloud properties to determine the corresponding discrete cloud/no cloud binary images. Since operational systems such as ground-based lasers may show a range of line-of-sight sensitivity, depending upon system characteristics as well as the optical properties of the cloud elements, two distinct cloud/no-cloud classifications will be analyzed. One will identify only the opaque clouds in the scene including thick cirrus clouds, and a second will identify both the opaque and the thin, semi-transparent clouds. The second determination which includes the semi-transparent clouds will be set-up as far as practicable to discriminate all clouds normally identified and reported by the experienced weather observer including those he labels with a "thin" designation. Thus, the "optimized cloud/no cloud image" illustrated as the deliverable data base in Fig. 3-4, will contain four discrete data values representing opaque cloud, thin cloud, clear and no data.

The image based format for the separate cloud/no-cloud archives (one for opaque clouds only and one for all clouds) is the same as the format used for the basic radiance archive (which is left intact), except that the pixel by pixel data now have been converted to discrete, four level cloud/no-cloud representations.

4.2 Applications To Cloud Model Evaluation

The solid-state, Whole Sky Imagery systems have been installed in the network configuration shown in Fig. 2-12. The WSI field program will provide continual concurrent measurements of sky cover and cloud free line of sight from the network sites with one-minute resolution. A central goal is to acquire the data base required to evaluate and extend cloud models. The stochastic models are to be used to estimate the impact of clouds on ground-based systems that depend upon unobscured paths of sight to satellites in space.

A comprehensive statistical model has been developed by Boehm, et al, (1986) that specifically provides estimates of the duration of cloud free lines of sight from multiple ground sites to orbiting and geostationary satellites. The innovative method establishes the climatic probabilities through repetitive simulations of sky cover distributions with the multidimensional Boehm Sawtooth Wave Model. The simulation model and its many component approximations are the prime candidates for test and evaluation with the new WSI data base.

An alternate and purely analytic approach is under development by the Marine Physical Laboratory. The modeling procedure is based on the Ornstein-Uhlenbeck (0-U) class of the simple Markov process (Gringorten, 1982). This approach has been applied successfully both in analytical form and by Monte Carlo simulation of probability distributions to estimate the joint occurrence and duration of a variety of weather events (Gringorten

1966, 1968, 1972). This study is directed toward extension of the analytical form of the 0-U Markov model to yield estimates of the joint occurrence and persistence probability of cloud free lines of sight in time and space.

4.3 Sub-Element Test and Evaluation

Both the simulation and analytic cloud model systems are complex and involve a variety of simplifying assumptions and procedures. Careful model evaluation should involve a wide variety of comparisons between model components, assumptions and output with the actual cloud structure and behavior as defined by the WSI data base.

Some key elements in the evaluation process are summarized in the following paragraphs.

4.3.1 Sky Cover Comparisons

A principal input variable to the stochastic cloud models is the climatic frequency of sky cover as derived from conventional weather records, based on human observer estimates of sky/cloud conditions. For model evaluation purposes, the cloud discrimination algorithms in the WSI system are set up initially to achieve as close a correspondence as possible with the estimates of sky cover reported by an experienced weather observer. As part of the model evaluation program it is important to establish the degree of correspondence between the WSI measurements and weather observer estimates of sky cover. Emphasis should be placed also on analysis of azimuthal differences in measured sky cover due to both the natural systematic variations caused by local influences and by systematic variations in apparent sky cover as perceived by an observer due to directional scattering properties of cloud particles. The following specific sky cover data/model comparisons should be included in the evaluation program:

a) Compare WSI sky cover with corresponding human observations for both "opaque" and "all cloud" classifications.
b) Determine and compare by quadrant the cumulative frequency of WSI sky cover as a function of time of day, season, and location.
c) Compare sky cover as determined from 10-min WSI data with sky cover as determined from the subset of screen data (32 rows x 32 columns) that is archived at 1-min. intervals.

4.3.2 Cloud-Free-Line-Of-Sight (CFLOS) As A Function of Sky Cover and Zenith Look Angle

Variations in the angle of view through the atmosphere coupled with the 3-dimensional structure of cloud forms result in a systematic decrease in the average relative frequency of CFLOS with an increase in the zenith angle of the ground-based observer's path of sight. The probability of CFLOS as a function of sky cover, cloud type and zenith viewing angle was determined empirically by Lund and Shanklin (1973). Three years of hourly summer data were used to establish the model estimates. The smoothed and adjusted probabilities were derived from whole-sky photographs using infrared film and companion observations of cloud amount by National Weather Service observers at Columbia, Missouri. The relative frequencies of CFLOS have been summarized for individual cloud types as well as a composite of all cloud types by Lund and Shanklin (1973). The model estimates have been refined and upgraded by Allen and Malick (1983), removing apparent observer bias through geometric modeling procedures. The revised model presented in analytical form yields the distribution of relative frequency of CFLOS as a function of sky cover.

For the objective at hand, this class of model approximation is a necessary first step, serving to convert climatic probabilities of ground to space CFLOS for designated viewing angles. The accuracy and general applicability of the CFLOS models can be subjected to close analysis with the greatly enhanced data base produced by the WSI network program.

4.3.3 Correlation of Sky Cover and CFLOS In Time and Space

The other primary input variable to the cloud models is a functional representation of the temporal and spatial correlation of sky cover and CFLOS. In the case of the Boehm simulation model, a two-part scale distance approximation is used involving the specification of a small-scale or short relaxation time and a broad-scale or long relaxation time. Both short and long temporal changes are approximated to conform with the 0-U Markov process. In the case of the purely analytical model development noted above, both the temporal and spatial variations of sky cover and CFLOS are modeled with the 0-U Markov process.

The WSI data base can be processed into a form convenient to explore in detail the behavior of these correlation parameters as a function of geographical location, day of the year, and time of day.

4.3.4 Overall Tests of Model Performance

An ultimate objective of the modeling process is to determine the joint climatological probability of the duration of cloud free lines of sight to a point in space from one or more preselected ground sites given the climatic summaries of sky cover at each site. Straight-

forward tests of overall model performance can be achieved through direct comparisons of observed down time duration with model estimates for prescribed operational scenarios. Both model and real data summaries are to be generated consisting of chronological listings of binary down/up conditions at successive one-minute intervals at each network ground site. A "down" condition is defined as a cloud-obscured line of sight from a ground location to a prescribed satellite position in space. In turn, the chronological tables for individual sites may be combined to determine the estimated and the WSI observed "downtime" duration statistics for selected combinations of sites and prescribed configurations of geosychronous and orbiting satellites.

5.0 THE HORIZON SCANNING IMAGER

Although the use of television systems for the determination of local visibilities has been considered by many early investigators, at least as early as 1955 (Douglas, *et al*, 1977), the systems, in general, have provided less than adequate performance. For a variety of engineering reasons, the video picture on the user's monitor was quite difficult to assess from a radiometric point of view, and therefore was inappropriate for the extraction of contrast reduction due only to atmospheric influences. In many situations the operation of the camera's automatic gain circuitry in conjunction with the monitor's contrast enhancement circuitry could completely mask the often subtle changes in target and background radiances that are at the heart of contrast transmittance determinations, and therefore the specification of local and sector visibilities.

More recently, the availability of solid-state video cameras and reliable high resolution video frame grabbers has reopened the door to the use of video-based radiometric systems in a variety of technical applications. In few areas of research has this resurgence been more welcome than in those related to the automatic measurement and specification of the optical state of the atmosphere. The application of these new instrument systems to the determination of surface visibility has been underway at the Marine Physical Laboratory for several years, and is at this point a relatively mature technology. This Chapter describes the basic concepts of the technique, the current status of the as-built instrumentation, and a selection of the systems performance characteristics.

5.1 Preliminary System Configurations, Horizon Scanning Imager

In overall chronology, the Horizon Scanning Imager (HSI) began its hardware development after the WSI system described in Sections 2.1 and 2.2 of this report, and in fact during the early stages of system development there was a strong symbiotic relationship between the two prototype packages.

The initial design concept for the automatic observing system reported herein was for a combined WSI & HSI instrument package which shared a single camera, but used two different customized optical paths for image definition. An artist's conception illustrating one of several early prototypes is shown in Fig. 5-1. For a variety of engineering and cost considerations, it was

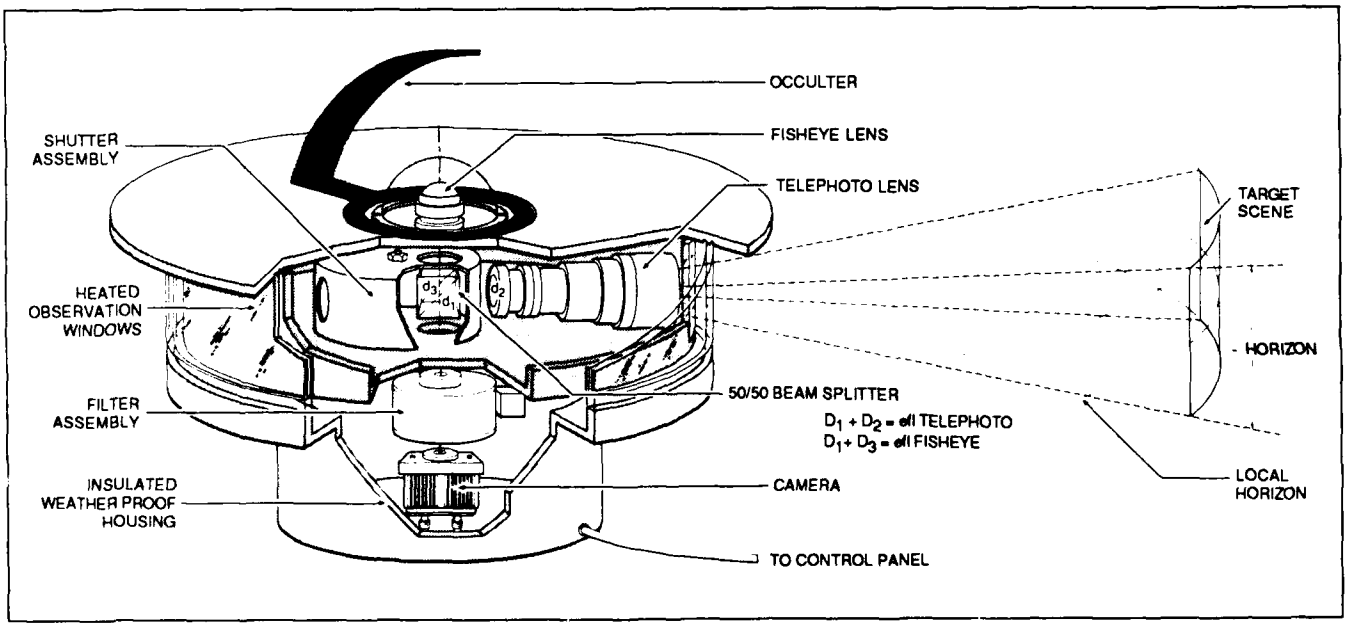

Fig. 5-1. Artists conception, automatic observing system.

decided relatively early in the program to abandon the composite system concept in favor of a parallel development for each individual function. Further work on the composite package has been deferred pending additional studies on the applicability of newer three chip color camera systems to the joint discernment task.

With the decision to develop a single function device whose only task was the automatic determination of local sector visibilities, several design simplifications became appropriate. Specifically, unlike the WSI package, the horizon scanner could operate in the photopic spectral region only, thus obviating the requirement for the relatively complex and expensive optical filter changer previously illustrated in Fig. 2-5. Also, since maximum angular resolutions were required in the near horizon regions, a small field of view lens assembly was preferred over the fisheye used by the WSI. And thirdly, rather than a fixed path of sight staring system, a revolving path of sight sweeping the local horizon was found to be a more practical design concept.

An additional procedural simplification evolved from the analytic form of the visibility expression discussed in detail in Section 6.0. Once it became apparent that the defining equations needed for the computational aspects of the HSI system could readily be expressed as a combination of discrete ratios, then the need for precise inter-frame flux control became severely relaxed. It was demonstrated in early mock-ups that the system concept retained its operational integrity even with the video camera running under full auto-iris control, rather than requiring fixed, discrete aperture setting. The suitability of running under auto-iris control further obviated the requirement for the discrete flux control increments provided by the original optical filter changer.

With the radiometric and field of view aspects of the HSI system concept thus modified, the assembly of the prototype hardware was straightforward. Figure 5-2 illustrates schematically the arrangement of the physical components, and Figs. 5-3 and 5-4 illustrate photographically the external transducer assembly in its weather proof enclosure, and the interior control console, both in prototype configuration.

5.1.1 External Sensor Assembly and Weatherproof Enclosure

In the initial configuration shown in Figs. 5-2 and 5-3, the external sensor assembly consisted of only four interrelated sub-systems, the solid state video camera, the auto-iris attachment, the precision rotary table, and the weatherproof enclosure.

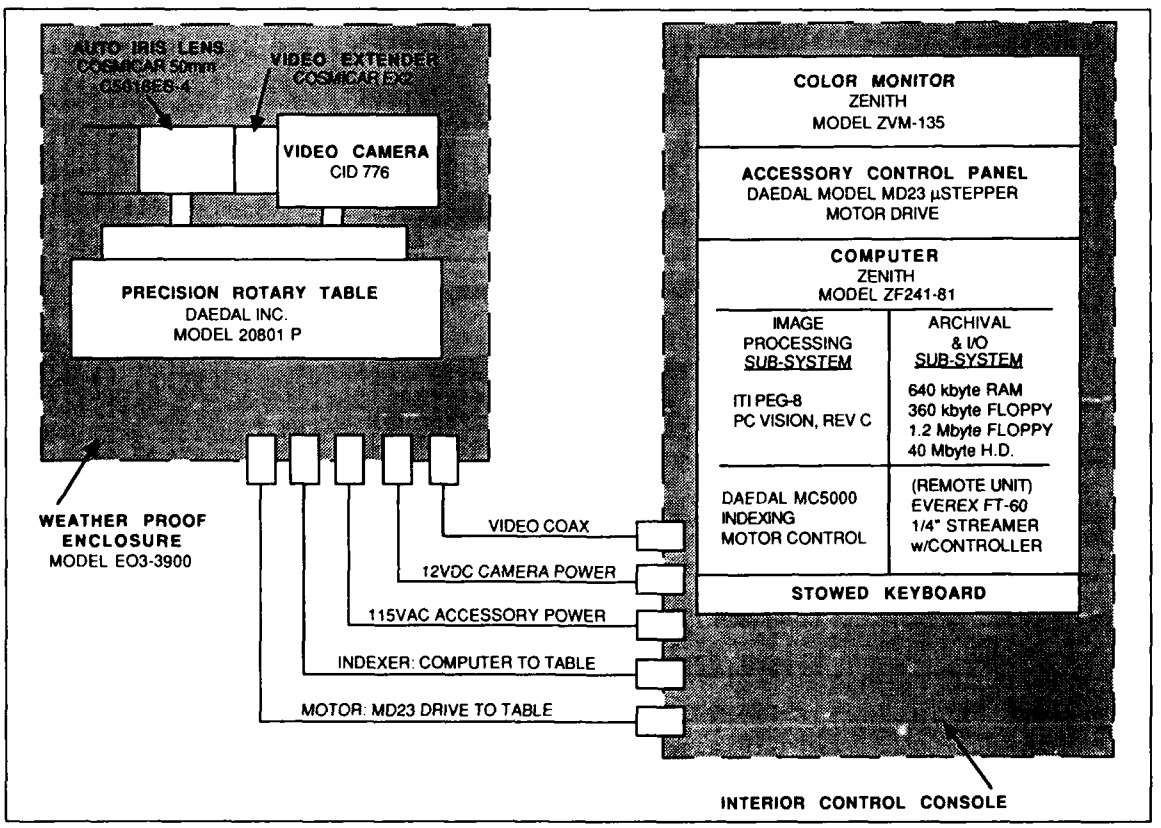

Fig. 5-2. Automatic visibility system, hardware layout.

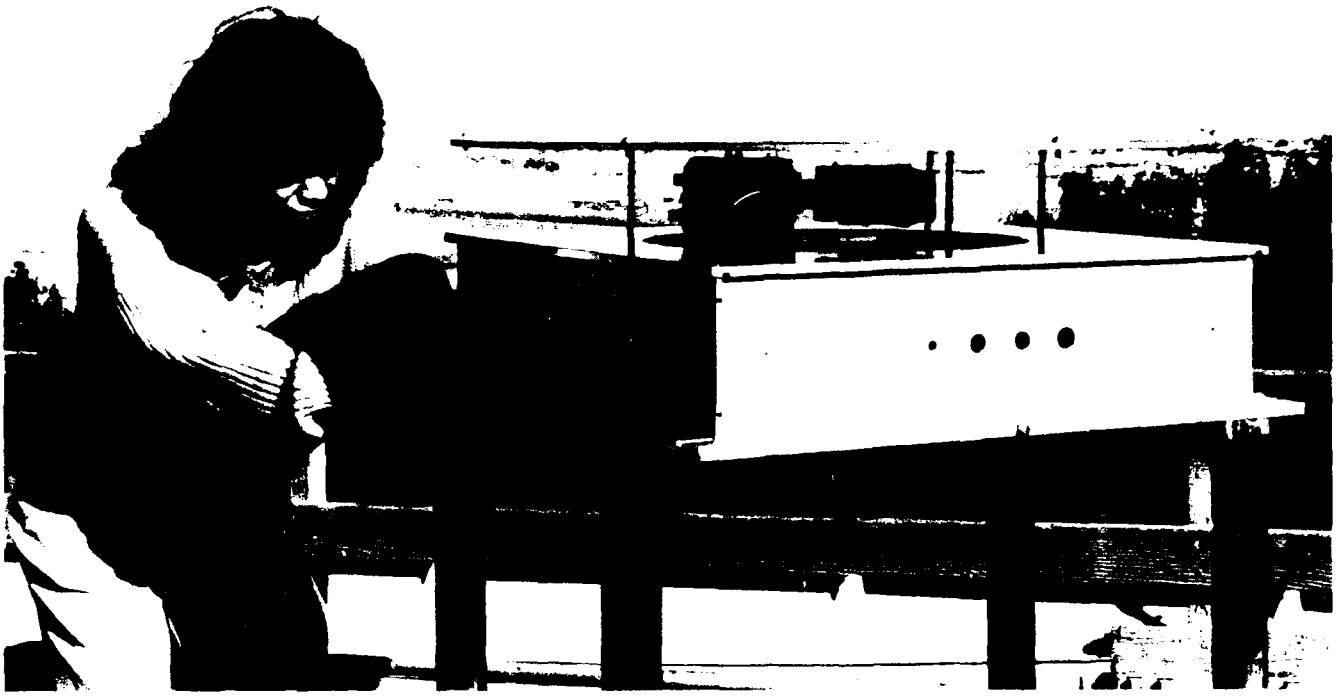

Fig. 5-3. Exterior sensor assembly, prototype.

As in the earlier development of the WSI system, the initial choice for the video camera was the GE Model 2505. This solid state Charge Injection Device (CID) camera was appropriate for use with the remotely located PC Vision frame grabber to yield 256x256 digital imagery. Used in conjunction with the Cosmicar 50mm Auto-Iris Lens with a X2 video extender, the sensor subassembly delivered good quality imagery to the controller for subsequent digitization.

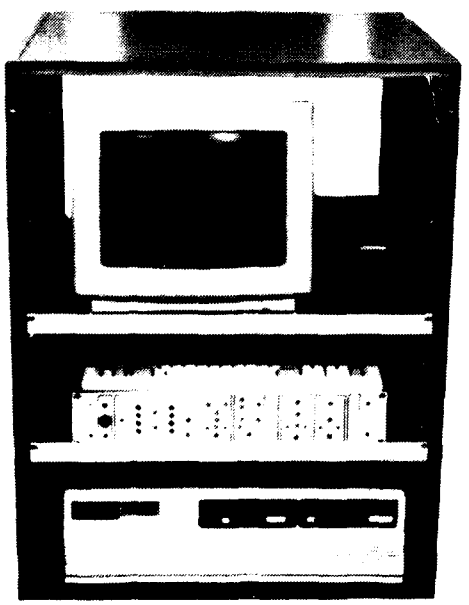

Fig. 5-4. Interior control console, prototype.

The analytic procedures to be discussed in Section 6.2 will address the need for precise relocation of the camera's field of view as it automatically searches the local horizon for suitable visibility targets. To assure the desired positional accuracies to within ±1 pixel element on the camera array, a precision mechanical stage is required on which to mount the camera. After several mock-up efforts and substantial testing using the desired optical magnifications, the Daedal Series 20000 Rotary Indexing Table was incorporated into the prototype design. (See Appendix C.) Since the Horizon Scanning Imager is conceived as a fully automatic system, the control of the rotary table must be via the computer associated with the interior control console. Thus, the Daedal Model MC5000 IBM Compatible Indexing Motor Control and Model MD23 Micro Stepper Motor Drive were also included in the prototype system.

The weatherproof enclosure for the exterior sensor assembly was fabricated by the Marine Physical Laboratory. Its design features are straightforward with only the observation window being a critical element. The photograph in Fig. 5-3 was taken before a satisfactory window was selected. Several attempts to acquire optically clear glass in a suitable shape, *i.e.* equivalent to an 18" diameter tube 4" long, were unsuccessful due to either quality or cost considerations. The prototype windows in the as-built configuration were made of 1/4" thick strips of clear LEXAN, cold bent into the required circular shape and mechanically bonded at the point of overlap. The result-

ing window was inexpensive, of good optical quality and durable during subsequent field operations.

5.1.2 Interior Control Console

The prototype interior console for the HSI system is illustrated in Figs. 5-2 and 5-4. It is similar to that used in early versions of the WSI, but with several significant differences, primarily in the configuration of the Accessory Control Panel.

A quick review of Table 2.1 with its hardware listing for the Second Generation Z-200 Based System, and of the schematic configuration in Fig. 5-2 illustrates the similarity in early computer hardware used in the two emerging automatic video radiometer systems. The major hardware difference is the inclusion of the appropriate Daedal Rotary Table control elements within the HSI accessory panel in lieu of the Iris, Occultor, and Filter control circuitry associated with the WSI cloud system.

The archival and I/O sub-systems contained within the prototype HSI were selected for ease and convenience of interactive system control and procedure development. These relatively low capacity components were not anticipated for use in an on-going collection and archival sequence.

After the fabrication, check-out and deployment of two Horizon Scanning Imager systems as illustrated in Figs. 5-2, 5-3 and 5-4, it was decided to upgrade several system components to improve interchangeability with the WSI cloud system.

This involved two refinements to the basic Z-200 system, and a repackaging of the Daedal control elements. Since prototype system number one was then running under Z-248 control at the Air Force Geophysics Laboratory, the upgrade retrofits were made only to prototype system number two which was still operational at the Marine Physical Laboratory.

5.2 Current Generation Instrumentation

Building on the experience gained through the development and operation of the computer controlled video radiometers reviewed in the preceding paragraphs, the Optical Systems Group at the Marine Physical Laboratory has produced a compact and reliable system for the automatic acquisition and archival of local horizon imagery specifically tailored to the determination and assessment of daytime sector visibilities, and subsequently their spatial and temporal variabilities.

The as-built configuration for the system currently in operation at the Marine Physical Laboratory in San Diego is illustrated schematically in Fig. 5-5 and photographically in Figs. 5-6 and 5-7. The hardware listing appropriate to the illustrated configuration is given in Table 5.1.

The exterior sensor assembly shown in Figs. 5-5 and 5-6 is a relatively compact, weatherproof housing which contains several inter related components and sub-systems. The detector component is the CIDTEC (formerly General Electric) model 2710 solid state video camera. This small, all solid state monochrome camera is well suited to this horizon scanning task. The CID sensor has a 512V x 776H pixel array yielding excellent angular resolutions particularly using the 100mm efl optical system which yields an approximate field of view of 5.4 degrees.

The associated sub-assemblies most important to the reproducibility of the systems suite of selected target scenes are the Precision Rotary Table itself and the Microstepper Motor Drive. These two components, now co-located in the external housing, were originally isolated with the μ stepper motor drive located within the accessory control panel (ACP). A variety of cabling and signal quality problems in the prototype configuration of Fig. 5-2 were resolved by this relocation and no further operational peculiarities have developed.

The interior control console illustrated in Figs. 5-5 and 5-7 contains a computer configuration identical in most respects with that in the WSI cloud system. In a like manner, most of the systems primary control and archival processes are enclosed within the AT class micro computer. They include the video frame grabber which accommodates a 1024x1024 image memory, the 80286 based CPU card, and the 8mm cartridge tape system whose 2.2 Gigabyte storage capacity enables an extended automatic duty cycle for the fully automatic system.

As illustrated in Table 5.1, as well as in Appendix C, the components in the Horizon Scanning Imager system were selected from a broad variety of commercial vendors. These selections were made on the basis of suitability for minimal interface problems, competitive unit costs, and good delivery schedules at the time the design configuration was frozen.

5.3 HSI, Operational Characteristics

The use of the dedicated video system described in Section 5.2 of this report for the automatic determination of local sector visibilities, as with the Whole Sky Imager described earlier, offers the combined capabilities of solid state imaging technology and fast, efficient micro-

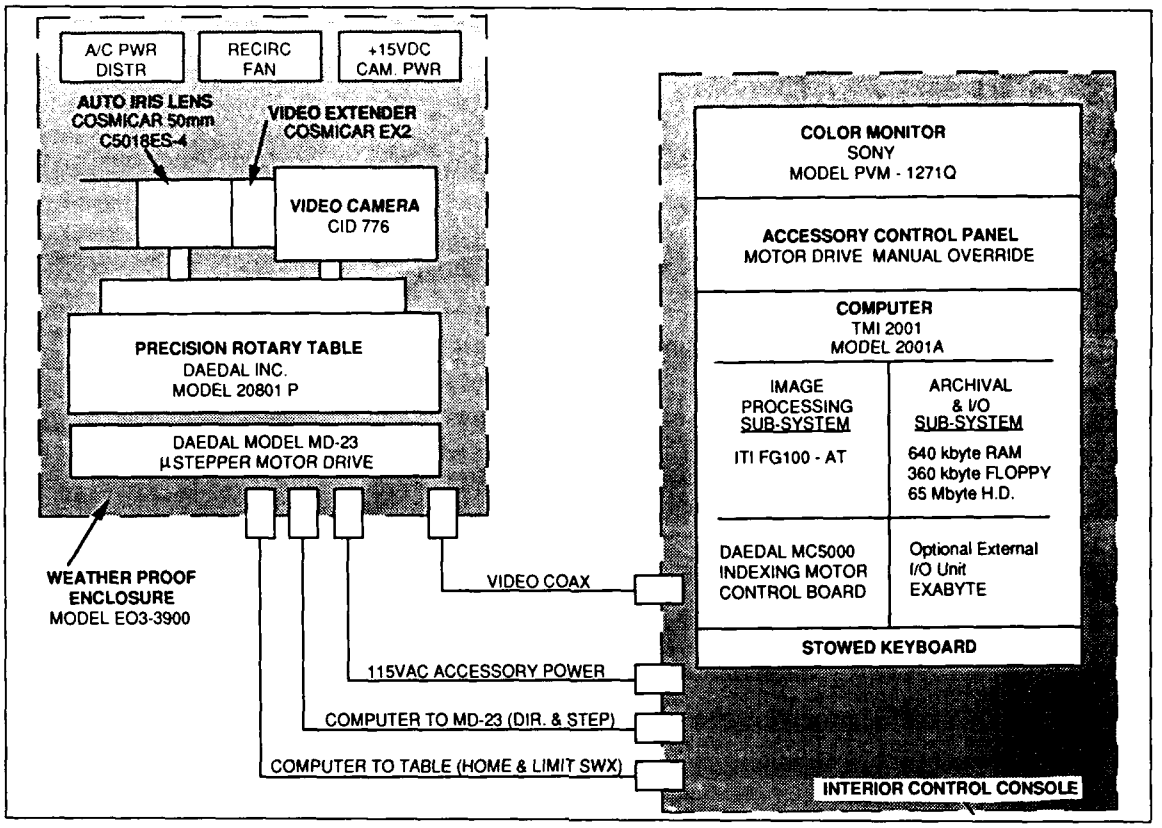

Fig. 5-5. Automatic visibility system, as-built.

Fig. 5-6. As-built exterior sensor configuration.

computer processing. In the ratio oriented techniques associated with frame by frame assessment of the video imagery, the geometric stability of the silicon array with its exactly reproducible pixel placement is an outstanding advantage in assuring precise target/background definitions. Similarly advantageous to frame-by-frame analysis is the auto-iris characteristic of maintaining a video lines average detected radiance at approximately mid-scale on the detectors radiant flux versus analog voltage output curve. Due to the imaging chips reliably linear output in this mid-range region, highly precise ratios of target to background pixel radiances are readily obtainable.

5.3.1 In-House Calibration

Whereas many useful algorithms for the determination of atmospheric properties can be devised to require only the input of the relative values of radiant flux fields, as with the HSI system, it is generally true that far more redundant and reliable methodologies are available when absolute values of radiance are available. The need for

Fig. 5-7. As-built interior control console.

Table 5.1. Auto-VIS Horizon Scanning Imager (HSI) As-Built September 1988

Exterior Sensor Assembly

1. WXP Housing, EO3-3900
2. CID TEC, 2710 Video Camera
3. Daedal, 20801P, Precision Rotary Table
4. Daedal, MD23, μStepper Motor Drive
5. Cosmicar, C5018ES-4 Auto-Iris Lens
6. Cosmicar, EX-2, Video Extender
7. Recirculation Fan
8. 15VDC Camera Power Supply

Interior Control Assembly

1. TMI, 2001A, AT Compatible Computer
   a. TMI, B286-IM-AT CPU Board
   b. TMI, 80287-8, Math Co-processer
   c. TMI, BVC-1, Color Video Card
   d. TMI, KB1AT, Keyboard
   e. Seagate, ST-277R, 65MB Hard Disc
   f. Western Digital, HCRA2, Disc Controller
   g. Exabyte, EX-8200, 2.2GB Tape Streamer
   h. Adv. Storage Concepts, ASC-88, SCSI Host
   i. ICS Computer Products, DIO-96, TTL/IO Ports
   j. ITI. FG-100-1024-U-AT-A, Video Frame Grabber
   k. Compumotor, MC5000 Controller with PC-21 Indexer
2. Sony, PVM 1271Q, Color Monitor
3. MPL, E03-3000, Accessory Control Panel

measuring absolute radiance levels is an optional procedure within the HSI concept, which at this point in the system's development is not normally selected.

The HSI camera system described in this note may readily be calibrated against standards of radiant intensity traceable to N.B.S. using standard radiometric procedures in association with optical calibration facilities established at the Marine Physical Laboratory. In practice, each measurement system is subjected to a systematic series of calibration procedures consisting of the operational steps outlined in Fig. 2-9. Although the exact data flow through the computerized processing schedule may not be as illustrated in Fig. 2-9, each item illustrated is in fact addressed for each individual camera. In the simplified case of the HSI system, the determination of radiometric absolute sensitivity, specified under procedure number 5 in Fig. 2-9, is only accomplished if specifically requested by the data analyst. Several specialized facilities and fixtures are necessary to implement the calibrations specified for these camera systems, one of which is illustrated in Fig. 2-10. The three meter optical bench in conjunction with a selection of standard lamps and calibration targets can create the various radiance fields necessary to characterize the camera's performance in each of the following regions of interest.

a) Radiometric linearity: radiative flux vs byte value output.

b) Absolute radiative response: absolute spectral flux input vs byte value output. (Not normally applicable to HSI systems)

c) Relative radiance shifts: systematic changes in flux/byte relationships as a function of f-stop and neutral density changes.

d) Geometric mapping: pixel element vs object space geometry as diagnosed with Precision Calibration Target.

Calibrations of the sort outlined above for the HSI system, are conducted in the green spectral response band illustrated in Fig. 2-11.

5.3.2 Field Data Acquisition

Two exterior sensor assemblies as shown in Fig. 5-6, and three interior control consoles similar to that shown in Fig. 5-7 were built during this contractual effort. By September 1988, two full systems were in operation, one at the Air Force Geophysics Laboratory (AFGL) near Boston, and the other at the Marine Physical Laboratory (MPL) in San Diego.

Both the AFGL unit and the MPL unit use the external sensor configuration illustrated in Fig. 5-6 and specified in Table 5.1. The interior control consoles associated with the two field units however, are not the same physically although functionally they are equivalent.

The AFGL control console is configured similar to that illustrated in Fig. 5-2. The basic difference being that it uses a Zenith Z-248 series computer rather than the earlier Z-241. Functionally both of these micro-computers are IBM/AT compatibles running under a version of Z-DOS which for the most part is compatible with MS-DOS.

The MPL control console has been revised from its original Z-241-based configuration to a TMI-2001-based system as illustrated in Fig. 5-5 and specified in Table 5.1. The TMI is another IBM/AT compatible which runs directly under MS-DOS, and is exactly the same machine used in the sister WSI clouds system discussed earlier. The conversion to the TMI configuration was driven by the desire to share peripheral sub-systems,

control codes and archival techniques with the more mature WSI instrumentation package. To a large degree, this commonality was particularly attractive with respect to the EXABYTE tape sub-system. The 2.2 Gigabyte capacity of the 8mm tape streamer made it practical to save digitized imagery representing the original data from which each visibility determination might be made. The ability to save automatically, all pertinent imagery is particularly useful during initial set-up and target selection sequences, as well as during unsupervised daily data collection sequences.

A composite system consisting of two external assemblies running under the control of a single computer is currently in development at the Marine Physical Laboratory. In this emerging package, an exterior sensor assembly from the WSI clouds system and an exterior sensor assembly from the HSI visibility system are being jointly controlled by a single TMI based interior control console. The continuing development of this joint visibility/cloud cover determination system was an additional element in the decision to convert from the Z-241 to the TMI 2001 micro-computer with its associated peripheral devices and operational software.

In its current field configuration, the Horizon Scanning Imager sweeps its field of view through the entire 360° local horizon in approximately one minute. The sweep is momentarily interrupted at up to 32 pre-selected azimuths for target assessment and line of sight visibility determinations. At each stop, up to six different targets of opportunity may be selected for use in ratioing against the local horizon radiance. The field of view of the camera system is approximately 5.4 degrees which produces an image at each azimuth stop similar to that shown in Fig. 5-8.

The typical data scene illustrated in Fig. 5-8 contains a variety of targets of opportunity, those outlined in red having been selected to determine the visibility for this specific scene. One should recall that daytime visibility determination, either instrumentally or by a human observer, ultimately involves the resolution of the distance from pre-selected targets that the apparent contrast, C_r, reduces to some minimum (threshold) value needed for detection. The threshold contrast depends on a number of factors including the visual acuity of the observer as well as the angular subtense of the target, its shape and its location with respect to background features. Human estimates of visibility result from adaptive integration by the eye in time and space of all scene features. The World Meteorological Organization (WMO) and the Federal Meteorological Handbook (FMH) recommend that daytime visibility targets be

Fig. 5-8. Typical HSI imagery.

black or very dark targets viewed against the background sky. However, in order to achieve adequate areal coverage, objects selected for visibility markers for routine meteorological observations often are less than ideal both in angular size and inherent optical properties.

If one assesses the scene captured in Fig. 5-8 it is clear that a solid state imaging system, in this case the HSI, can provide highly accurate and readily updateable measurements of the apparent contrast of all identifiable objects within its field of view.

Whenever practicable, as illustrated in Fig. 5-8, the selection of visibility targets should be adjusted for each scene in accordance with observed conditions. In the absence of ideal dark targets viewed against the background horizon sky, priority should be shifted as necessary to objects at distances close to the limit of detection, where the most consistent and representative calculations of visual range can be made.

The important consideration is that the objects in a selected-area ensemble be located at approximately the same azmuth angle and as close in range as practicable to the limit of visibility. A discussion of the detailed elements involved in the determination of atmospheric visibility is contained in Section 6 of this report.

As noted earlier, in its automatic data collection mode the HSI system acquires a set of images similar to that shown in Fig. 5-8 every minute. In each image a series of targets at known ranges have been pre-selected by the operator in an initial set-up sequence. Using these images the machine is programmed to simulate the human observer's assessment of the scene in a manner consistent with the appropriate definitions and methodologies discussed in Section 6.

The goal is to develop a completely automated system to provide objective quantitative estimates that are consistent regardless of time and location. The degree of visual modeling required to provide, for example, the visual range along specific pre-selected horizontal or slant paths depends upon the accuracy needed to satisfy the individual user requirements. In the HSI, we limit attention to the more general problem of determining prevailing visibility, which is defined by Douglas and Booker (1977) as the greatest visibility equal or excluded through at least half of the horizon circle which need not be continuous, *i.e.* the median visibility around the horizon circle. The E/O camera system provides a continuously updated representation of the detailed radiance scene for the discrimination of prevailing visibility and its sector variations. The objective is to exploit the measured apparent radiance contrast for all suitable objects in the scene, adjusting the resultant visibility estimates as necessary to compensate for the non-standard nature of individual targets.

Several computer displays of the measured and derived data used by the machine in its computations have been devised to assist the operator during initial set-up sequences, and later for either archival or quality control procedures. Two examples of these displays are illustrated in Figs. 5-9 and 5-10.

Figure 5-9 is a representation of an early display typifying a situation where an interactive operator has selected six different visibility targets, *i.e.* A through F, in a specific scene such as in Fig. 5-8, and asked the machine to estimate the sector visibility for diagnostic assessment. In this diagnostic procedure, the operator is free to select the computational parameters, r, and ε as noted along the top of the tabulation, and for each set of selections the computer will calculate the apparent contrast C_r, and thus the visibility based on each individual targets set of parameters, for eleven different inherent contrast values, C_o. A more complete discussion of these essential relationships is provided in Section 6.0, and the analytic expression being exercised is specified in Eq. 6-19.

A more recently developed display is presented in Fig. 5-10. This display is the output from a fully automatic sequence, in which the operator's set-up parameters have been pre-selected and frozen into the computational algorithm. At this point, the camera system goes through its automatic horizon sweep routine, stopping at pre-designated azimuths and calculating the visibility for each scene. Each designated target within the scene is used to make an independent estimate of visibility, and the result displayed as illustrated. Computed values of

Diagnostic Display for Automatic Visibility Assessments

	Target A	Target B	Target C	Target D	Target E	Target F
AP CR = C_r	.206	.186	.173	.235	.209	.269
RANGE = r	6.000	5.000	5.000	4.000	4.000	4.000
EPSON = ε	.030	.030	.030	.030	.030	.030
.50	19.03	14.24	13.24	14.94	12.93	18.21
.55	17.77	13.43	12.56	13.72	12.06	16.31
.60	16.81	12.80	12.03	12.81	11.39	14.97
.65	16.06	12.30	11.61	12.12	10.86	13.97
.70	15.45	11.89	11.26	11.56	10.44	13.20
C_o .75	14.94	11.55	10.96	11.11	10.09	12.58
.80	14.52	11.26	10.71	10.74	9.80	12.07
.85	14.15	11.01	10.50	10.42	9.55	11.64
.90	13.84	10.79	10.31	10.15	9.33	11.28
.95	13.56	10.60	10.14	9.91	9.14	10.97
1.00	13.32	10.43	9.99	9.70	8.97	10.70

DO YOU WANT A NEW TARGET SET AND NEW IMAGE?
YES=1, NO=0

Fig. 5-9. Typical diagnostic display (interactive).

STOP (2-106)	RANGE (MILES)	THRESHOLD CONTRAST	INHERENT CONTRAST	APPARENT CONTRAST	HORIZON BRIGHTNESS	VISIBILITY (MILES)
TARGET 1	25.00	.030	.800	< .030	161.	< 25.0
TARGET 2	15.00	.030	.800	< .030	161.	< 15.0
TARGET 3	6.00	.030	.800	.185	161.	13.5
TARGET 4	3.00	.030	.800	.349	161.	11.9

Fig. 5-10. Menu driven display (automatic).

visibility are tagged to indicate whether or not the target used is appropriate for optimum computational reliability. For targets with ranges too near, the computed visibility is tagged " > ", *i.e.* greater than, similarly for targets deemed too far, *i.e.* undetectable, the computed visibility is tagged " < ", *i.e.* less than.

6.0 THE DETERMINATION OF ATMOSPHERIC VISIBILITY FROM DIGITAL IMAGERY: CONCEPTS

6.1 Introduction

The potential for fully automated measurements of the visibility of distant objects has improved substantially with the recent advances in the development of digital, image-acquisition systems. Dedicated systems which combine solid-state image sensing capability with microcomputer control and processing functions can handle the imagery data transfer, processing and storage requirements for real time measurements. Thus, we are challenged to exploit this capability through the development of operationally efficient algorithms, which extract the useful information from the imagery and provide continuously-updated, numerical representations of the visibility. The purpose of this Section is to review

briefly the factors that are important for determining daytime visibility, both instrumentally and by the human observer, and to set forth techniques for objective measurements of prevailing visibility with the digital imagery system.

6.2 Basic Concepts; An Overview

The solid state video camera in combination with a digitizer-processor board (frame grabber) provides an output of relative pixel-to-pixel brightness to the microcomputer for further processing. Each picture element (pixel) in the resultant 2-dimensional array defines the relative brightness of the corresponding element of the actual image. With careful radiometric and geometric calibration of the system, each pixel in the fixed array may be transformed to the calibrated apparent radiance of the elemental fraction of the target or background area in the scene that corresponds to the pixel location at the instant of recording.

6.2.1 Expression for Contrast Transmittance

Let us review the procedures involved in determining visibility from the measured radiance distribution through reference to the basic expressions for contrast transmission in the atmosphere as given by Duntley, Boileau and Preisendorfer (1957). Reference to these basic concepts is of particular interest for understanding the effects of simplifying assumptions and for identifying the factors important for the selection of the best available visibility targets.

The expression for the (monochromatic) apparent spectral radiance ${}_tL_r$ of a target t at range r along the path of sight specified by zenith angle θ and azimuthal angle ϕ is

$$ {}_tL_r(\theta, \phi) = {}_tL_o(\theta, \phi)\, T_r(\theta) + {}_pL_r(\theta, \phi) \qquad (6.1) $$

where ${}_tL_o$ is the inherent target radiance and ${}_pL_r$ is the path radiance generated by the scattering of direct sunlight and diffuse light from the surrounding sky, clouds and terrain into the path of sight. The radiance transmittance of the path, $T_r(\theta)$ is given by

$$ T_r(\theta) = \exp - \overline{\alpha}\, r\,, \qquad (6.2) $$

where $\overline{\alpha}$ is the average attenuation coefficient.

Similarly, the expression for the apparent spectral radiance of the adjacent background ${}_bL_r$ is

$$ {}_bL_r(\theta, \phi) = {}_bL_o(\theta, \phi)\, T_r(\theta) + {}_pL_r(\theta, \phi) \qquad (6.3) $$

where ${}_tL_o$ is the inherent radiance of the background.

Thus the measured pixel radiance is the sum of the residual, image-forming light from the target (or background) and the path radiance due to aerosol and molecular scattering throughout the path. Strictly speaking, Eqs. (6.1) and (6.3) apply only to monochromatic radiance and ignore the effects of small scale turbulence on atmospheric transmission.

Subtracting Eq. (6.1) from Eq. (6.3) we have

$$ {}_tL_r(\theta, \phi) - {}_bL_r(\theta, \phi) = $$
$$ T_r(\theta)\,[{}_tL_o(\theta, \phi) - {}_bL_o(\theta, \phi)]. \qquad (6.4) $$

Note the radiance differences are transmitted along atmospheric paths with the same attenuation as the individual target and background radiances.

The apparent spectral contrast C_r of a target with respect to the background is defined by

$$ C_r = ({}_tL_r - {}_bL_r)/{}_bL_r \qquad (6.5) $$

For convenience the notation with respect to viewing angle has not been continued in this and following expressions. However, it is important to remember that the apparent and inherent contrast as well as the spectral radiance have strong directional dependence.

The corresponding definition of the inherent spectral contrast is given by

$$ C_o = ({}_tL_o - {}_bL_o)/{}_bL_o \qquad (6.6) $$

Finally, the expression for contrast transmittance in its most general form is obtained by combining Eqs. (6.4), (6.5) and (6.6) to yield

$$ C_r/C_o = T_r\, {}_bL_o/{}_bL_r\,. \qquad (6.7) $$

Duntley, *et al.*, (1957) state that the above equations *"apply rigorously to any path of sight regardless of the extent to which the scattering and absorbing properties of the atmosphere or the distributions of lighting exhibit non-uniformities from point to point", and the "equations can be used in treating all real atmospheres and all real lighting conditions."*

6.2.2 Visibility and Equilibrium Radiance

Under computer scan control, the digital image-acquisition system continuously maps the apparent radiance distribution and the relative apparent contrast of objects within the view of the observation point. The measurements are immediately applicable to the determination of the optical and meteorological properties of the ambient atmosphere. In the case of meteorological visibility, the objective is to extract numerical estimates commensurate with the human perception of visibility. In this regard, guidance given by the World Meteorological Organization (1971) to help ensure observation com-

patibility and representativeness prescribes: "Meteorological visibility by day is defined as the greatest distance at which a black object of suitable dimensions, situated near the ground, can be seen and recognized, when observed against a background of fog or sky."

For both practical and theoretical reasons, the technique for the instrumental determination of visibility should conform with all elements of the definition. As discussed in the following paragraphs, strict adherence to these criteria for target/background selection results in a simple direct relationship between the numerical representation of visibility, V , contrast transmittance, C_r/C_o, and radiance transmittance, T_r, greatly enhancing the interpretation of measurements made in different places at different times.

The basic relationships can be shown by substituting for the path radiance ${}_pL_r$ such that Eq. (6.3) may be written

$$ {}_bL_r = {}_bL_o\, T_r + L_q(1 - T_r). \qquad (6.8) $$

where L_q is defined as the equilibrium radiance (Duntley, *et al.*, 1957) and is the same as the incremental source function as given by Chandrasekhar (1960). As the radiance transmittance decreases with increasing range r between the target (and/or background) and observer the apparent radiance ${}_bL_r$ approaches the source function L_q.

6.2.3 Special Case: Objects Viewed Against Horizon Background

In the case of a cloudless sky background, the apparent horizon radiance tends to remain unchanged as the observer backs away from the target. Assuming horizontal uniformity, the apparent horizon radiance ${}_hL_r$ at that azimuth is equal to the equilibrium radiance (source function) for the path of sight as follows,

$$ {}_bL_r(90, \phi) = L_q(90, \phi) = $$
$$ {}_bL_r(90, \phi) = {}_bL_o(90, \phi). \qquad (6.9) $$

Under these special conditions, Eq. (6.7) for the contrast transmittance becomes

$$ C_r/C_o = T_r. \qquad (6.10) $$

Early on in the development of visual range concepts, Koschmieder (1924) determined through consideration of the process of light scattering in a uniform atmosphere that the apparent radiance of a black object at range r viewed against the horizon sky is given by

$$ {}_tL_r = {}_hL_r(1 - \exp - \sigma r). \qquad (6.11) $$

In addition, Koschmieder extended the development to the more general case where the inherent target radiance is not zero, deriving the expression

$$ {}_tL_r = {}_tL_o \exp - \sigma r + {}_hL_r(1 - \exp - \sigma r), \qquad (6.12) $$

where σ is the average scattering coefficient. With respect to objects viewed against a cloudless or overcast horizon sky, Eq. (6.12) as determined by Koschmieder is equivalent to Eq. (6.8) except that the attenuation due to atmospheric absorption is neglected. In most instances when reference is made to "Koschmieder's Law" the reference is to the special case of Eq. (6.10) for a black object, ($C_o = -1$), viewed against the horizon sky where

$$ C_v = \varepsilon = T_v = \exp - \sigma V \qquad (6.13) $$

and ε is the threshold of apparent contrast needed for the detection of the distant object, and V is the visual range.

6.2.4 General Expression for Visibility Determination

Finally in this brief review of the general principles for the determination of visibility, let us return to the complete expressions for contrast transmittance and visibility that apply to objects viewed against any background. Solving for the radiance transmittance in Eq. (6.7), the expression may be written

$$ T_r = \frac{C_r}{C_o} \frac{{}_bL_r}{{}_bL_o} \exp - \overline{\alpha}\, r\,. \qquad (6.14) $$

Consistent with the basic definition of visibility, as the distance to the target increases there is a distance V where the apparent contrast C_r becomes numerically equal to the prescribed threshold contrast ε. The corresponding equation for the radiance transmittance at this range is

$$ T_v = \frac{\varepsilon}{C_o} \frac{{}_bL_v}{{}_bL_o} \exp - \overline{\alpha}\, V, \qquad (6.15) $$

where ${}_bL_v$ is the apparent background radiance at distance V.

Dividing Eq. (6.15) by Eq. (6.14), we have the general expression for the determination of visibility from digitally acquired imagery,

$$ \frac{V}{r} = \frac{\ln \frac{\varepsilon}{C_o} + \ln \frac{{}_bL_v}{{}_bL_o}}{\ln \frac{C_r}{C_o} + \ln \frac{{}_bL_r}{{}_bL_o}}. \qquad (6.16) $$

Thus, the ratio of the apparent to the inherent background radiance is an important factor in the determination of

visibility from the apparent contrast of objects in the scene that are viewed against backgrounds other than the clear horizon sky. For further analysis of this aspect, let us consider yet another form of Eq. (6.7) obtained by substituting from Eq. (6.8) to obtain

$$\frac{C_r}{C_o} = \left[1 + \frac{L_q(1 - T_r)}{{}_bL_o\, T_r} \right]^{-1} \qquad (6.17)$$

Here we note that the contrast transmittance is related to the radiance transmittance by the ratio $L_q/{}_bL_o$ which is termed the "sky-ground ratio", S, by Duntley (1948), so that

$$S(\theta, \phi) = L_q(\theta, \phi)/{}_bL_o(\theta, \phi). \qquad (6.18)$$

Sky refers to the fact that the clear-sky horizon radiance for the horizon path having the same scattering angle with respect to the sun as the path to the target is to a good approximation equal to the equilibrium radiance or source function for that path of sight. *Ground* refers to the inherent radiance of the background adjacent to the target, and the term therefore is dependent upon the reflectance and orientation of the surface as well as the downwelling irradiance. The directional notation is retained for this expression to emphasize the importance of the directional dependence, particularly with respect to the variations with sun angle as a function of time of day.

Now substituting Eq. (6.18) in Eq. (6.16), we have

$$\frac{V}{r} = \frac{\ln\left\{ S\left(\frac{\varepsilon}{C_o}\right) \Big/ \left[1 - \frac{\varepsilon}{C_o}(1 - S) \right] \right\}}{\ln\left\{ S\left(\frac{C_r}{C_o}\right) \Big/ \left[1 - \frac{C_r}{C_o}(1 - S) \right] \right\}} \qquad (6.19)$$

which is the general equation expressed in terms of sky-ground ratio.

Figure 6-1 is a graphical representation of Eq. (6.19), and shows the dependence of the visibility/target-range ratio on the measured apparent contrast for the normal range of sky-ground ratio that is observed in clear-sky conditions. Low values of S near 0.25 are associated with a surface covered with freshly fallen snow, whereas values near 4.0 correspond, for example, with forest canopy backgrounds. Large fractional changes in the calculated visibility ratio result as the inherent terrestrial background radiance departs from the horizon radiance, particularly when the measured apparent contrast is rather high (*i.e.* nearby target in good visibility conditions). The disparity becomes significantly less when the apparent target contrast is near the limit of detectability. It is important to note that in overcast sky conditions, the

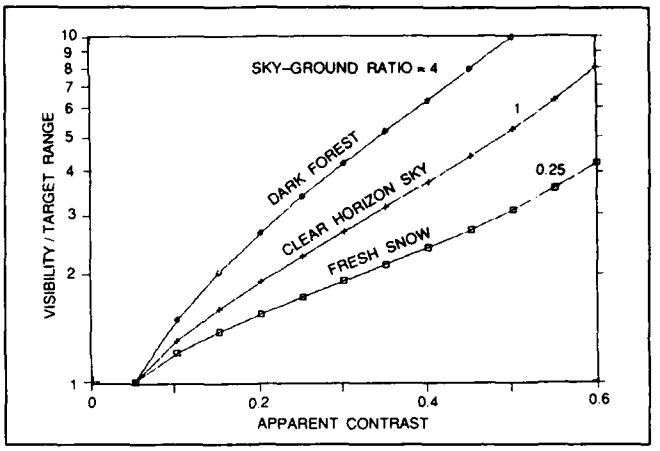

Fig. 6-1. Calculated values of the visibility/target range ratio as a function of the observed apparent contrast for the typical range of sky-ground ratio. For these calculations, the assumed values for the inherent contrast and the threshold contrast were 0.85 and 0.05, respectively.

range of values for the sky-ground ratio increases substantially to near 20 for forest cover backgrounds and about 1 for fresh snow surface backgrounds.

It is evident from Fig. 6-1 and Eq. (6.19) that one must be careful in the interpretation of visibility observations where the human observer finds it necessary to depart from the guidelines as given in Section 6.2.2, and selects non-standard targets with backgrounds other than the adjacent horizon. Although digital imagery offers added opportunity to extract information with respect to the optical properties of the ambient atmosphere, considerable sophistication must be built into algorithms that diagnose effectively the detection range of many non-standard targets against variable backgrounds. On the other hand, the wealth of information generated by repetitive horizon scans with a digital imagery system enables straightforward determinations of prevailing visibility and visual range from a hierarchy of targets. The resultant measurements can be designed to conform in accuracy and representativeness with the highest standards of current practice.

6.3 Determination of Prevaling Visibility

The preferred approach for instrumental determinations of visibility from radiometrically calibrated imagery follows directly from the discussion of the factors that govern image transmission in the atmosphere. First and foremost it is important, insofar as possible, to direct attention to the measured apparent contrast between the horizon sky and objects in the scene. It is desirable but not strictly necessary that the objects stand above the horizon as viewed from the ground observation point.

The major consideration is that the extinction and directional scattering properties along the paths of sight to the object and horizon correspond closely. As discussed in the previous section, with the horizon sky as the background, the sky ground ratio is 1 and Eq. (6.19) simplifies to

$$\frac{V}{r} = \ln\left(\frac{\varepsilon}{C_o}\right) / \ln\left(\frac{C_r}{C_o}\right). \qquad (6.20)$$

With careful selection of visibility targets on or near the horizon, Eq. (6.20) becomes the basic expression for the determination of visibility from the horizon scan imagery. Criteria for target selection and the specification of inherent contrast C_o and threshold contrast ε as input variables to Eq. (6.20) are reviewed in the following sections.

6.3.1 Target Selection

The prime requirement for reliable determination of prevailing visibility is an ample supply of suitable targets, well distributed in range and azimuth. On the one hand it is important to make use of all objects in the horizon scan imagery that may serve as visibility targets. On the other hand, because of their intrinsic properties, potential targets are not equal in a given situation as effective determinants of the prevailing visibility. The basic properties of individual targets must be predefined by the input variables to Eq. (6.20). In addition to the target distance from the observation point, the input variables are the inherent contrast of the target and the contrast threshold for detection. Stability in the input variables over the full range of atmospheric conditions is the major consideration in the selection of specific objects to be included in the accepted group of visibility targets.

6.3.2 Inherent Contrast

For visibility determination using Eq. (6.20), we must prescribe the relative contrast between the inherent radiance of the selected object and the adjacent horizon sky radiance. In the case of the ideal, non-reflecting, black target the relative contrast is always -1. (Note that the measured apparent contrast of a given target-background does not change sign with increasing path length so that the absolute value of contrast can be used for calculation purposes). However, the reflectivity of even natural dark targets is seldom zero so that careful attenuation must be given to the estimates of inherent contrast and the vulnerability of the target to fluctuations in C_o due to changes in the directional distribution of lighting reaching the target from the sun, sky and surrounding terrain.

The sensitivity of visibility determinations to the uncertainties in the estimates of the inherent contrast as an input variable is illustrated in Fig. 6-2. Trial calculations were made of the visual-range/target-range ratio as a function of measured apparent contrast for selected values of assumed inherent contrast. Shown here are the disparities in V/r associated with departures from an assumed inherent contrast of 0.8 for natural dark targets in the acquired imagery. The range of assumed values, -0.6 to -0.1, is representative of this class of targets. Note in particular that the visibility determinations are not sensitive to errors in the input values of C_o when the object is near the maximum distance at which it can be seen so that the apparent contrast is close to the threshold detection contrast. However, the error sensitivity increases substantially for nearby targets in good visibility conditions when the measured apparent contrast is relatively large. Thus, the relative accuracy of visibility as determined from a given non-standard target is in part a function of the visibility itself. Most weight in a given situation should be applied to the fraction of preselected targets where the measured contrast transmittance of the intervening path is relatively low.

6.3.3 Threshold Contrast

Experiments by Taylor (1964) have shown that the visual contrast threshold does not vary significantly with

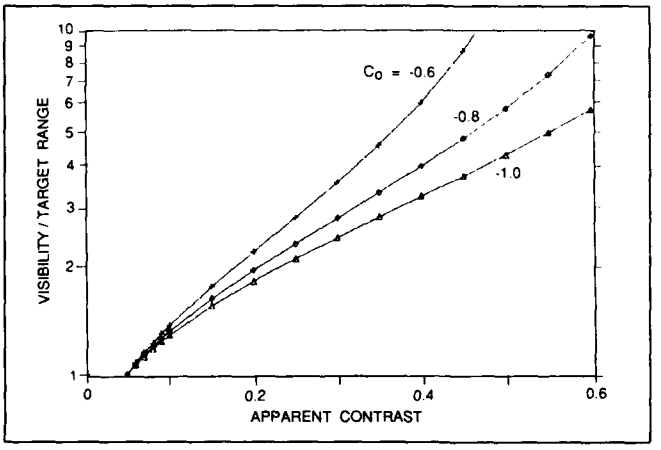

Fig. 6.2. Calculations of visibility/target range ratio using Eq. 20, illustrating the sensitivity of the resultant values to the assumed inherent contrast.

background luminance over the normal range of daylight conditions. However, the contrast threshold does vary markedly with the angular subtense of the target at the point of observation. With dwell times commensurate with normal visual search (1/3 sec), the minimum contrast for confident detection by the human eye is about .025 for objects with an angular size greater than 0.5 deg,

as determined from the laboratory experiments. Based upon general field experience, Douglas and Booker (1977) recommended "—a recognition contrast threshold value of about 0.05 when measurements of transmittance are used for determining the visual range equivalent to that reported by meteorologists and the use of a value of ε in the region of 0.035 to 0.04 for the detection contrast threshold under field conditions". The sensitivity of the visibility determinations to the assumed value of threshold contrast is illustrated in Fig. 6-3.

6.3.4 Overcast Sky Conditions

As in the case of a cloudless horizon sky, the apparent horizon radiance of an overcast sky tends to remain unchanged as the observer backs away from the target. Thus, Eq. (6.9) also holds for the overcast horizon case, and the resultant determinations of visibility using Eq.

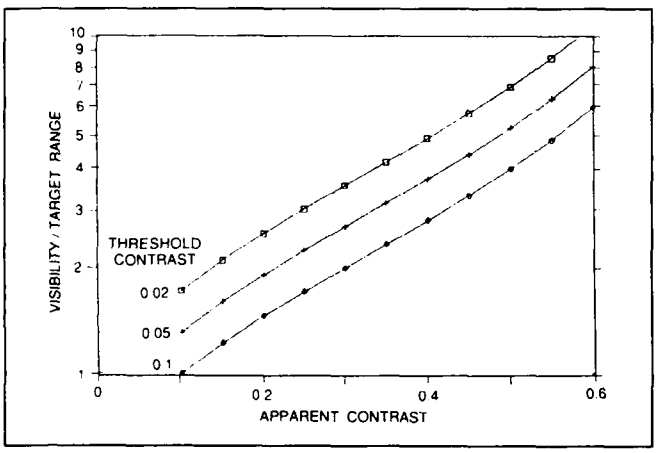

Fig. 6.3. Calculations of visibility/target range ratio using Eq. 20, illustrating the sensitivity of the resultant values to the assumed threshold contrast.

(6.20) are commensurate with the fundamental definition of meteorological visibility given in Section 6.2.2 above. However, the inherent contrast of dark objects with the overcast horizon is normally greater than the corresponding inherent contrast with the cloudless horizon, yielding an overestimate of the visibility to the extent indicated in Section 6.2.2, unless proper adjustment is made in the input values of inherent contrast.

6.3.5 Partly Cloudy Horizon Sky Conditions

Horizon sky backgrounds with variable cloud conditions introduce additional uncertainty into the visibility determinations. Shown in Figs. 6-4 and 6-5 are the results of trial calculations illustrating the errors in V associated with the presence of isolated clouds on the horizon when a cloudless horizon is assumed for the calculations. Key factors are the distance of the cloud background relative to the target and the brightness of the cloud relative to the corresponding clear sky horizon radiance. Again we see that the resultant disparities are small when the contrast transmittance of the path of sight is small, regardless of the cloud position or brightness. The errors increase substantially in the case of targets having a range much less than the existing visual range.

As shown in Fig. 6-4, without an appropriate change in C_o, the presence of a dark cloud results in progressively larger underestimates of visual range with increasing apparent contrast. The errors due to clouds much brighter than the corresponding clear sky horizon radiance are

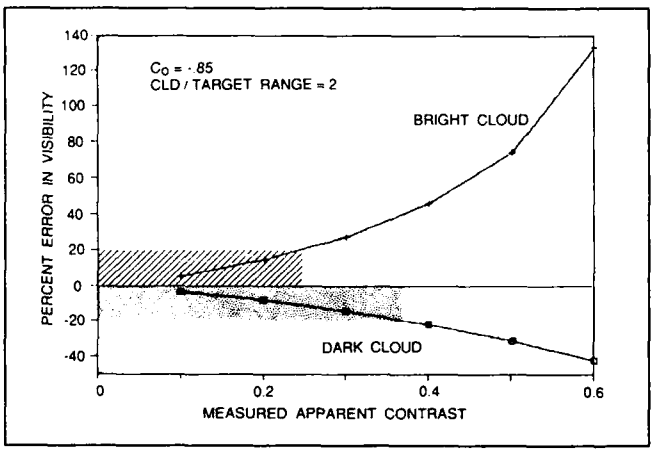

Fig. 6.4. Sample calculations illustrating the percent error in the determination of visibility due to isolated cloud of variable brightness obscuring the horizon sky.

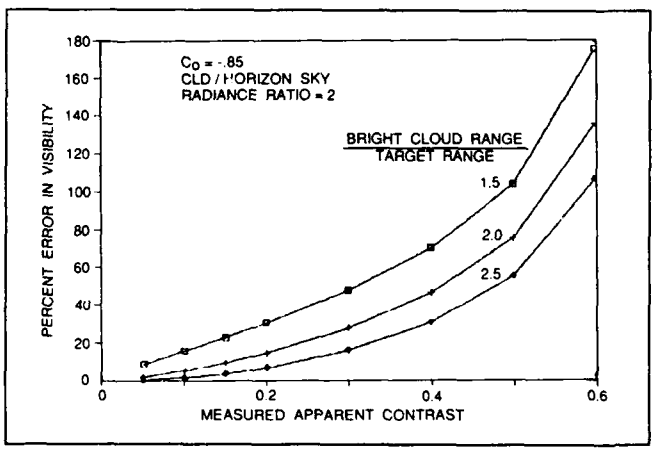

Fig. 6.5. Sample calculations illustrating the percent error in the determination of visibility due to isolated cloud at variable distance obscuring the horizon sky.

opposite in sign and more severe. The comparison in Fig. 6-4 gives results for horizon cloud radiances equal to twice and one-half the cloudless horizon radiance. The assumed inherent contrast with the clear-sky horizon is -.85 and the assumed cloud/target range ratio is 2.

The sensitivity with respect to relative cloud distance is shown in Fig. 6-5. A cloud/clear-sky brightness ratio of 2.0 and C_o equal to -0.85 was assumed. For this bright cloud example, the error increases well beyond 50% for a cloud positioned at a range less than 1.5 times the target range when the apparent contrast is greater than 0.3. The error diminishes significantly for cloud ranges more than twice the target range, and of course for cloud brightness closer to that of the clear sky horizon brightness.

7.0 RECOMMENDATIONS FOR FURTHER RESEARCH

The primary characteristics of several compact, solid-state imaging systems for the automatic measurement of atmosphere optical and meteorological properties have been presented and discussed. The modular design of the systems allows for both manual and/or computer control of both spectral band and flux level selections as required by the measurement task. In addition, absolute radiometric calibration of the sensor array enables a variety of reliable methodologies for the assessment of atmospheric properties to be employed with objective confidence.

Experimental results have clearly demonstrated the effectiveness of color contrast, as derived from multispectral imagery, for objective sky cover analysis over a broad range of sky and visibility conditions.

A solid-state imaging system provides highly accurate and continuously updated measurements of the apparent contrast of all identifiable objects within its field of view. Early experience indicates that consistent and reliable estimates of visual range can be obtained from these target-background ensembles as well as with isolated targets.

From our experience to date, it is clear that a small relatively automatic system for the assessment of these key atmospheric properties is now readily available to the experimental and modelling communities. This report has described the as-built status of an automatic system designed to accumulate the imagery required to address these and related optical phenomena. The application of these prototype systems to the task of multipurpose local area measurements should be the harbinger of a new standard of consistent and reliable weather related observations. Several comments appropriate to the extension of these research applications are summarized in the following paragraphs.

7.1 Daytime/Night-Time Considerations

The basic concepts underlying the operation and the interpretation of data from the prototype electro-optical visibility/cloud sensor outlined in this report were derived initially to support the systems daytime operation. A future goal is to extend the utility of the system into the night-time hours. There are several considerations one must address in this regard which are conveniently separated into either the visibility or the cloud detection schemes. However, the prototype visibility and cloud detection systems, while very similar in nature and using many common hardware sub-assemblies, are two separate hardware/software entities which have not been integrated into a single unit. Each stands alone and functions independently. This separation was intentional during the preceding stages of development such that each could be optimized in its task performance attributes without being compromised by conflicting packaging constraints. It is fortuitous that extending both subsystems into a night operation configuration might use yet again a common component.

The cloud discrimination task seems most straightforward from a basic concept of view, so it will be addressed first.

7.1.1 Night-Time Cloud Discrimination

The detection and measurement of cloud field characteristics with the whole sky imager depends primarily upon the radiometric sensitivity of the camera system, and the spectral relationship between the background clear sky and the cloud elements superimposed against it. It has been well demonstrated that during the daylight hours, the requirements for both of these parameters are quite satisfactory, *i.e.* the camera can readily acquire high resolution imagery, and the blue/red sky radiance ratio clearly discriminates between clear blue sky and the non-blue cloud elements. It is reasonable to assume that if these two conditions were to be extended into the night-time hours, then the cloud detection system would continue to function normally. It is our contention that for many circumstances, this extension is reasonably attained by the simple substitution of an image intensified camera. There are commercially available intensified cameras which should yield gains approaching 10^5 which is adequate to transfer the camera's operation from daytime levels of 10^3 lum/m^2 down to quarter moon levels of approximately 10^{-2} lum/m^2. Thus sensor sensitivity enhancements, even without exercising the camera's inherent injection inhibit mode, seem adequate to address all moonlight illumination levels down to at least quarter moon. For lower light levels, *i.e.* starlight only, additional technique development will be required, and may entail more extensive hardware modification.

Based on night-time sky and terrain radiance measurements (Duntley, 1970), there is good evidence that the

spectral nature of the night-time, moonlit sky is similar to that of the daytime sky down to about quarter-moon illumination levels. As this is readily verifiable using the radiometrically and geometrically calibrated whole sky imager itself with only minor optical modification, the extension of our blue/red ratio technique into much of the night-time regime is straightforward. Computational validations using the Hering FASCAT code, (Hering & Johnson, 1984), in a manner similar to that used for the daytime case, but substituting lunar irradiances rather than solar as input will provide additional insights particularly with respect to the influence of subtle shifts in the night sky spectral radiance distributions.

7.1.2 Night-Time Visibility Determination

Extending visibility determinations into the night-time regime provides a broad spectrum of potential techniques each with its share of challenging research opportunities. For the most part, the choices are divided primarily into using either passive or active systems. In this context, we would restrict the definition of "active" to imply the use of an emitter as in a transmissometer light source, or an external probe as in a lidar. The term "passive" implies a staring or scanning system that acts only as a non-interrogating receiver of information from its surrounding environment.

To the extent that the directional nature of the path radiance, induced by either direct solar irradiance or lunar irradiance plays its proportionate part along any selected horizontal path of sight, then the basic tenents of image transmission through the atmosphere (Duntley, 1948) should hold true. It is our basic contention that this condition exists for all moonlit night skies, and that, therefore, contrast transmittance measurements, *i.e.* visibility determinations, derived from an intensified, passive imaging system are reasonable and practical to achieve even at the implied low light levels. Illuminance scaling to the night-time flux levels should be well behaved under conditions where target selections and horizon sky backgrounds can be located without contamination by uncontrolled light sources.

When near new moon illuminations drop below the levels required for contrast discernment by the camera system, the control computer will have to shift to transmissometer mode, using pre-selected fixed lights as radiance sources. Supplementary algorithm development will be necessary to allow the conversions relating atmospheric transmissivity, source intensity, illuminance threshold and visual range. An analysis of Allard's Law, its relation to the visual detection of fixed lights, and conversions to equivalent daytime/night-time visual ranges is provided by Douglas & Booker (1977).

7.2 Cloud Field Statistical Analysis and Model Development

With a built-in software capability for extraction of high resolution cloud information from the acquired imagery, the generation of the basic climatological statistics can and should progress in concert with the WSI data acquisition program. A parallel and continuing program of synoptic climatological analysis is essential to help ensure that the observing and processing system provides a data base of sufficient accuracy and completeness to handle the intended objectives. Keeping pace with the data acquisition and archival program, the analysis phase should develop specialized statistical summaries of observed sky cover, cloud-free paths of sight, and cloud-free viewing intervals for each observing site. As a prime objective, the climatological summaries, conditional probability analyses, and space-time correlation studies among sites should be carried out as required to help validate and extend empirical and analytical models for estimating the expected frequency of cloud-free viewing paths and intervals using conventional meteorological data.

The WSI (Whole Sky Imagery) data analysis effort could readily consist of a variety of studies designed to help assess GBL (Ground Based Laser) performance as achieved through multiple site operations as well as multiple lines of sight at one GBL location. The basic statistical summaries should begin simultaneously with the WSI installation at each designated site. As the data base grows Cloud Free Line of Sight (CFLOS) and Cloud Free Arc (CFARC) probability distributions would be calculated with respect to total sky cover, arc length, arc position and orientation, season, time of day, etc. The statistical summaries should be designed to follow a general purpose format to ensure the widest possible application to analytical model development and validation.

Of unique interest and importance is the high resolution of the WSI data base in both time and space. The data acquisition schedule will provide simultaneous imagery at multiple sites on a time scale as short as one minute at reduced grid resolutions throughout the day. Thus, it will be possible to determine joint frequency distributions of initial and final CFLOS and CFARC conditions at a single station or between multiple sites over very short time intervals. Appropriate conditional probability summaries can be constructed to be directly applicable to the evaluation and refinement of simulation models, such as the AFGL/ETAC Sawtooth model which pro-

vides the joint frequency estimates from more generally available climatic information. For example, the comprehensive WSI data base may be used to determine the efficacy of the analytical models to estimate the probability of a CFARC of length l, at aim point (θ, ϕ) being observed for at least one site from a combination of N sites taken n at a time. Model evaluations might extend corollary questions including for example: If the CFARC condition does not exist now for the given site configuration, what is the probability of a CFARC of the designated length and aim point at later Δt (minutes or hours) at at least one site?

The statistical summaries and model evaluation studies should be continually updated to keep pace with the ever increasing WSI data base. Since the basic data requirements are somewhat less demanding, analyses of the more basic single-station models (AFGL, SRI) which estimate CFLOS and CFARC from total sky cover and zenith observation angle, can reach an effective level of validation and analysis much earlier than a similar resolution of the reliability of joint probability multi-station estimates from the more complex simulation models.

In the realm of cloud model development, emphasis should be placed on the extension and evaluation of a purely analytical model for estimating the joint occurrence frequency and persistence of CFLOS from multiple ground sites to points in space. Of special interest and importance is the validation of 0-U Markov process for estimating the joint occurrence statistics of CFLOS in space as well as in time. The success of the approach is also dependent on the efficacy of the Kielson-Ross procedure (Gringorten 1982) to model the climatic probabilities of the duration of cloud obscured line of sight episodes. The ever increasing WSI data base will provide a firm basis to examine closely these concepts as well as other modeling approximations required to assess the impact of clouds on ground to space system performance.

8.0 ACKNOWLEDGEMENTS

This final report has been prepared for the Air Force Geophysics Laboratory under Contract No. F19628-84-K-0047. The authors wish to thank the members of the Marine Physical Laboratory staff for their assistance in developing and building the automatic systems described herein, and the members of the Atmospheric Structures Branch of the Air Force Geophysics Laboratory for their technical support and council.

We particularly thank Mr. John Fox, our systems programmer, Mr. Jack Varah and Ms. Monette Karr, members of our collaborating engineering staff, for the many diligent hours they devoted to the development and fielding of these systems.

It should not pass without notice that the fabrication, modification and final assembly of these sophisticated systems could not have been accomplished without the outstanding attention to technical detail maintained by Mr. Bill Davy and Mr. George Trekas who built the sensor assemblies, and Mr. Harry Sprink who wired and assembled the electronic controls.

The preparation of this Final Report has been accomplished by our specialists in computer assisted publications, Mr. Phil Rapp and Ms. Carole Robb and Mr. J. C. Brown

The authors are greatly pleased to acknowledge the outstanding technical contributions provided by these esteemed colleagues.

9.0 REFERENCES

Allen, J. H. and J. D. Mahlick, (1983). *The frequency of cloud-free viewing intervals*, Preprint 21st Aerospace Science Meeting, 10-13 Jan. 1983, Reno, Nev.

Boehm, Albert, Irving A. Gringorten and Charles F. Burger, (1986). Private communication.

Burger, Charles F. and Irving I. Gringorten, (1984). *Two-dimensional modeling for lineal and areal probability of weather conditions*, AFGL-TR-84-0126, Environmental Research Papers No. 875, 1984. ADA 147 970.

Douglas, C. A. and R. L. Booker (1977). *Visual Range: Concepts, Instrumental Determination and Aviation Applications*, U. S. Department of Transportation, Federal Aviation Administration, Systems Research and Development Service, Report No. FAA-RD-77-8, Washington, D. C. 20590

Duntley, S. Q. (1948). *The Reduction of Apparent Contrast by the Atmosphere*, J. Opt. Soc. Am., **38**, 179-191.

Duntley, S. Q., A. R. Boileau, and R. W. Preisendorfer (1957). *Image Transmission by the Troposphere I*, J. Opt. Soc. Am., 47, 499-506.

Duntley, S. Q., R. W. Johnson, J. I. Gordon, and A. R. Boileau, (1970). *Airborne Measurements of Optical Atmospheric Properties at Night*, University of California, Scripps Institution of Oceanography, Visibility Laboratory, SIO Ref 70-7, AFCRL-70-0137, NTIS No AD 870 734.

Federal Meteorological Handbook No. 1 (1988). *Surface Observations*. Office of the Federal Coordinator for Meteorological Services, Rockville, MD. FCM-H1-1988.

Gringorten, Irving I., (1966). *A stochastic model of the frequency and duration of weather events*, J. Appl. Meteorol. **5**: 606-624

Gringorten, Irving I., (1968). *Estimating Finite-Time Maxima and Minima of a Stationary Gaussian Ornstein-Uhlenbeck Process by Monte Carlo Simulators*, J. Amer. Statistical Assoc., **63**: 1517-1521

Gringorten, Irving I., (1972). *Conditional probability for an exact noncategorized initial condition*, Monthly Weather Review, Vol. **100**, No. 11, 796-798.

Gringorten, Irving I., (1982). *The Kielson Ross Procedure for Estimating Climatic Probabilities of Duration of Weather Conditions*, AFGL-TR-82-0116, Environmental Research Papers No. 775, Air Force Cambridge Research Laboratories. ADA 119 860.

Hering, W. S. and R. W. Johnson, (1984). *The FASCAT Model Performance Under Fractional Cloud Conditions, and Related Studies*, University of California, San Diego, Scripps Institution of Oceanography, Visibility Laboratory, SIO Ref. 85-7, AFGL-TR-84-0168, NTIS No ADA 085 451.

Koschmieder, II. (1924). *Theorie der Horizontalen Sichtweit*, Beitr. Phys. freien Atm., **12**, 33-53, 171-181.

Lund, I. A., (1973). *Persistence and recurrence probabilities of cloud-free and cloudy lines-of-sight through the atmosphere*, J. Appl. Meteor., **12**, 1222-1228.

Lund, I.A., and D. D. Grantham, (1980). *Estimating the joint probability of a weather event at more than two locations*, J. Appl. Meteor., **19**, 1091-1100.

Lund, I. A., D. D. Grantham, and R. E. Davis, (1980). *Estimating probabilities of cloud-free-fields-of-view from the earth through the atmosphere*, J. Appl. Meteor., **19**, 452-463.

Lund, I. A., and M. D. Shanklin, (1973). *Universal methods for estimating probabilities of cloud-free-line-of-sight through the atmosphere*, J. of Appl. Meteor, **12**, 28-35.

World Meteorological Organization, (1971). *Guide to Meteorological Instrument and Observing Practices*. Fourth Ed. Secretariat of the World Meteorological Organization, Geneva, Switzerland WMO-No 8. TP. 3.

ATMOSPHERIC VISIBILITY
TECHNICAL NOTE NO. 200

MAY 1986

IMAGERY ASSESSMENT FOR THE DETERMINATION OF CLOUD FREE INTERVALS

R.W. Johnson
W.S. Hering
J.E. Shields

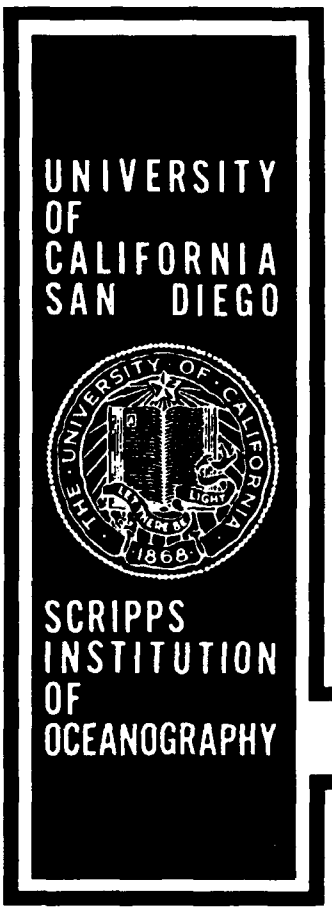

Contract Monitor, Donald D. Grantham
Atmospheric Sciences Division

Prepared for
Air Force Geophysics Laboratory, Air Force Systems Command
United States Air Force, Hanscom AFB, Massachusetts 01731

VISIBILITY LABORATORY La Jolla, California 92093

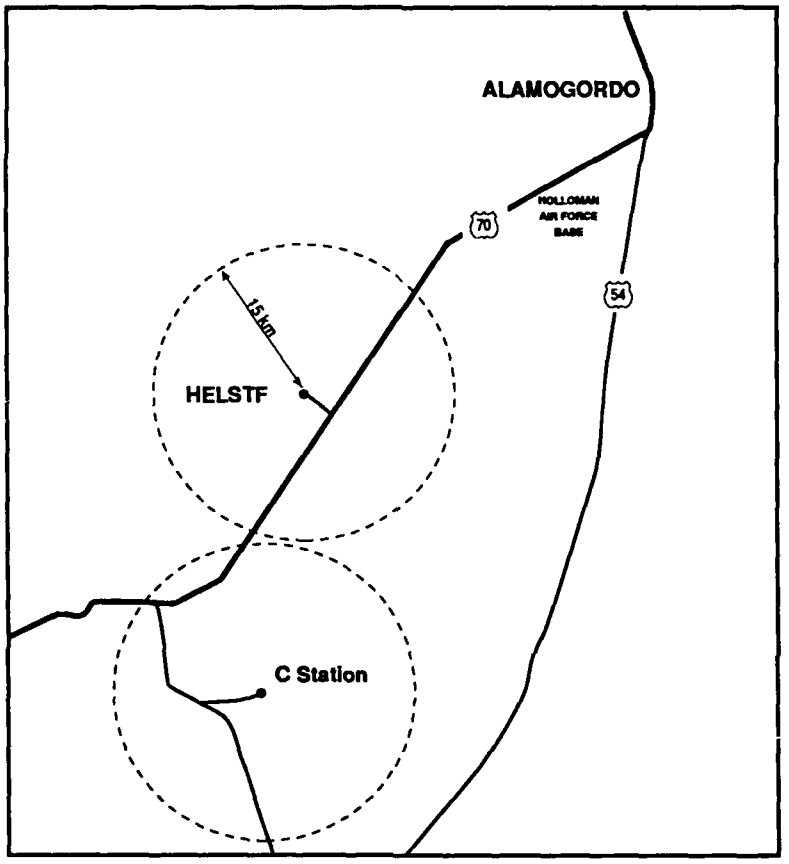

WHOLE SKY CAMERA TEST SITE
WSMR/C-STATION

TABLE OF CONTENTS

LIST OF TABLES AND ILLUSTRATIONS

IMAGERY ASSESSMENT FOR THE DETERMINATION OF CLOUD FREE INTERVALS

R.W. Johnson, W.S. Hering, & J. E. Shields

1.0 INTRODUCTION

This report describes the activities of the Visibility Laboratory in support of a multi-team system performance and site characterization exercise which occurred at the White Sands Missile Range, New Mexico, during the months of August and September, 1984. The goal of this demonstration was to illustrate the functional utility of an electro-optic camera system as a reliable data acquisition device for operations and research requiring automatic specification of cloud cover: its amount and distribution, both temporal and spatial.

More specifically the initial goal, for the Visibility Laboratory effort, was to deploy a prototype hardware system for the timely assessment of local cloud cover. This system was designed to acquire visible spectrum, whole-sky images in specific wavelength bands, in a digital format suitable for automated cloud analysis. A related and in the long term a more demanding task, was the initial development of the algorithms necessary to use this class of data for the real-time specification of cloud-free interval statistics and their related probabilities.

Since the test exercise schedule was relatively firm, and hardware deliveries were somewhat uncertain, several combinations of on-hand and on-loan composite instrument systems were prepared for deployment to New Mexico. Two electro-optical cameras and two 35mm photographic cameras with their associated control and recording electronics were provided. These systems are discussed in Section 2.

A two-person field team and the equipment were initially on-site Monday 27 August 1984, and began data collection on Wednesday, 29 August. Imagery was collected daily through Friday, 21 September, for a total of 24 days. A discussion of the collection procedures and a summary of the acquired data is given in Section 3.

Samples of the acquired imagery are given in Section 4. The quality of the digital images is compared with that of the photographic images. This is followed by a discussion of preliminary techniques for the interpretation of these images using a mainframe computer with an image processing system. For this prototype system, in-house processing followed the field deployment, however the eventual goal is the derivation of algorithms which could be applied in real time.

The techniques developed on the image processing system were applied to the full New Mexico data base of one of the electro-optical cameras, to yield initial statistical descriptions of the cloud cover. These results are given in Section 5. Finally, in Section 6, the current directions in hardware, algorithm, and software development are briefly discussed.

2.0 INSTRUMENTATION

A number of systems were deployed to New Mexico by the Visibility Laboratory, in order both to obtain the desired sky images and to fully evaluate the character of these images in relation to the cloud characteristics. The most important of the systems were two EO (electro-optic) camera systems in somewhat different stages of development. In addition, two photographic cameras were deployed, one color and one black and white. These two cameras provided a more traditional data source for comparison with the digital imagery acquired by the EO systems.

2.1 Electro-optic Camera Systems

Both EO camera systems consisted primarily of a standard GE solid state camera, with Visibility Laboratory optical and filter assemblies attached. In each case, the camera contained a CID (charge injection device) sensor. The external optics were designed to allow the use of a fisheye lens, for nearly full hemisphere cover-

age, as well as smaller field of view lenses. The filter assembly, which physically contained part of the optics mentioned above, allowed the spectral filtering of the light, as well as the control of light levels through use of neutral density filters. Finally, each system included control electronics as well as data archival electronics and systems. The components of these cameras are listed in Appendix A.

There were several important design considerations affecting the development of these instruments. Some of these are given below.

a) In the analysis of the images, it may be necessary to know the absolute radiance of each point in the image, in order to compare this radiance with a model or standard value. Even if knowledge of absolute radiance is not required, many of the potential techniques for cloud identification require knowledge of relative radiance within the image. In either case, this implies the use of a fixed gain system, that is one which does not change the electronic amplification as a function of the image itself. This was a major reason for choice of a CID imager with fixed gain.

b) It is convenient to obtain data for the whole sky in one image. In this particular application, it was deemed adequate to obtain all but near-horizon look angles. Consequently an upward looking fish eye lens was used. A related consideration, however, is that optical resolution must be adequate to image sufficiently small clouds. Whereas the backup system, EO Camera I, has a 128 x 128 picture element (pixel) array, with a resulting resolution of approximately 1.5° (zenith angle) per pixel, the prototype system, EO Camera II, has approximately 256 x 256 pixels, with a resolution of approximately 0.7° per pixel.

c) In order to obtain maximum radiometric resolution between clouds and sky, a filter changer was utilized which would allow data to be collected through a red filter. In this wavelength regime, the sky is relatively dark in comparison with the clouds. In addition, as backup, it is desirable to obtain data through a blue filter, so that clouds may be potentially identified through analysis of the measured spectral radiance ratios. For this deployment, the backup EO Camera I was fitted with a blue filter in addition to the red, whereas the prototype EO Camera II had only a red filter.

d) Since the range of the CID cameras was rather limited in comparison with observed sky and cloud radiances (just over 1 log of radiometric sensitivity), a number of neutral density filters were included in the filter changer in order to allow the input flux level to be changed in a controlled way. The use of the f-stops on the fisheye lens offered additional ranging capability.

Figure 2.1(a) illustrates the optical layout of the EO Camera I. The filters mounted in the filter assembly are listed in Table 2.1. EO Camera I could be run with either the 425nm filter or the 605nm filter, either with or without a .3 log neutral density filter. Additional control of flux level was obtained through the use of the various f-stops on the fisheye lens. Also, a 555nm filter was included in this system for acquiring pseudo-photopic test data.

The system block diagram for EO Camera I is illustrated in Fig. 2.2(a). The camera was a GE solid state CID camera, Model 2200. Camera control and data logging were accomplished through an HP mini-computer in conjunction with a Chieftan frame grabber. The data were recorded digitally on magnetic tape, and viewed simultaneously on a monitor. Digital tapes were returned to the laboratory for analysis. In this system, the iris assembly was manually controlled, as was the occultor assembly. The occultor assembly consisted of a shading device placed external to the fisheye lens to shade it from sunlight, thus reducing stray light within the system.

The optical layout for EO Camera II is illustrated in Fig. 2.1(b), with the filters listed in Table 2.1. This system is similar to EO Camera I, with a somewhat more compact optical assembly and a higher resolution sensor array. The sensor was a GE Model 2505 CID Camera. Data could be obtained either with a 650nm filter or spectrally unfiltered, and with any of four neutral density filters (or none) superimposed in the path.

Table 2.1. Filter assembly assignments

Camera Ident	Filter Position	Filter
EO CAM I	2	2-450 nm
	3	6-605 nm
	4	3-555 nm
	5	open hole
	6	open hole
	D/N	0.6 log ND
EO CAM 11	2	1.3 log ND
	3	0.9 log ND
	4	0.7 log ND
	5	0.4 log ND
	6	open hole
	D/N	5-650 nm

Figure 2.2(b) illustrates the system block diagram for EO Camera II. Figure 2.2(c), showing the "Proposed" system, illustrates the Zenith-driven system which was originally intended for this deployment, but not deployed. Third party delivery delays resulted in the deployment of the "As-built" system in Fig. 2.2(b). In this system,the video signal was routed through a time/date generator to a video recorder and a monitor. The primary disadvantage of the prototype system was the variable gain inherent in the VCR. The video tapes of data from this system were transported to the laboratory where they could be digitized and read into the mainframe computer for analysis. With this system, the iris assembly and occultor assembly were controlled remotely.

2.2 Photographic Cameras

In addition to the two electro-optic camera systems, two 35mm photographic camera systems were deployed. Each of these systems utilized a fisheye lens, as well as an occultor assembly similar to that utilized with the EO cameras. Both were Automax Model GI, 35mm systems.

The primary photographic camera system utilized black and white film, with a red filter in the optical path. The data from this camera may be used for comparison with the EO camera data. The back-up photographic camera system utilized color film. The primary purpose of this camera was to generally document the scene. These photographs are also useful as visual back-up by the analyst working with the EO camera images. The components of these photographic cameras are listed in Appendix A.

2.3 Hardware Organization

The four camera systems were mounted, for this deployment, on an expandable van as illustrated in Fig. 2.3. The van was provided as GFE by the ASL host organization through their DELAS-AT-O group as coordinated by Mr. R. W. Endlich. The van provided both the protective enclosure for the camera support electronics, as well as the elevated platform for the instrumentation hut containing the actual cameras.

The cameras are shown on the instrumentation hut in Fig. 2.4. In this illustration, the fisheye lenses are partially visible, as are the occultor assemblies shading each of the four cameras. The filter-control and camera assemblies are inside the hut, and thus not visible in this illustration.

The support electronics are shown in Fig. 2.5. The taller rack to the left contains the computer and control panels for the EO Camera I, while the darker blue rack to the right, and the shorter middle rack contain the equivalent controls for the prototype EO Camera II. The tape drive beneath the table and the plotter to the left of the scene support the archival and real-time display of the EO Camera I system.

2.4 Summary

In summary, there were four data acquisition cameras deployed to the test site.

I. The back-up system, EO Cam I, 128 x 128 array
II. The prototype system, EO Cam II, 256 x 256 array
III. The primary 35mm camera, black & white film
IV. The secondary 35mm camera, color film

The back-up system, EO Camera I, included all the peripherals required to obtain fixed-gain digital data. The prototype EO Camera II, with its higher pixel resolution, yielded potentially superior data to that of EO Camera I, but was for this deployment limited to recorded VCR data. The two 35mm cameras were included for site documentation and to provide data quality standards.

3.0 EXPERIMENTAL PROCEDURES

3.1 Data Collection

The data collection plan involved the capture of a preselected sequence of images from each of the four camera systems in close temporal proximity. The data collection procedure was designed to support the experimental procedure illustrated in Fig. 3.1. This figure shows the proposed application of the data, as briefly discussed in the previous section. In order to support this scenario, the minimum data required were as follows:

A. On an hourly basis, during daylight, coordinated with Met observations:
   1. One 128x128 image in each of two spectral bands, 450nm, and 605nm.
   2. One 256x256 image at 650nm.
   3. One black and white photograph.
   4. One color photograph.

B. During periods of dynamic cloud changes, (Optional)
   1. Sequence A above, at 5-minute intervals for 30-minute period.
   2. Special sequences at the discretion of the scientist in the field, for example shorter intervals for a shorter period, substitute small FOV for short samples, etc.

A sample data log is shown in Fig. 3.2. Items A 1 through 4 in the above list are included as events 5

through 9 in this data log. In addition, the data log includes space for several optional events: measurements of downwelling irradiance; measurements both before and after the EO Camera II with the other systems; and measurements with more than one neutral density filter setting if desired.

Thus the normal procedure was the collection of the following data:

1. EO Camera I, Downwelling Irradiance: 450nm, 605nm, 555nm.
2. EO Camera II, Downwelling Iradiance: 650nm.
3. Automax 1, black and white (Pre EO II)
4. Automax 2, color (Pre EO II)
5. EO Camera I, fisheye: 450nm, 605nm (Pre EO II)
6. EO Camera II, fisheye: 650nm
7. EO Camera I, fisheye: 450nm, 605nm (Post EO II)
8. Automax 1, black and white (Post EO II)
9. Automax 2, color (Post EO II)

In the above sequence, an Automax measurement consists of generally 2-3 photographic frames. A measurement by the EO Camera I consists of one data file, which contains four images taken one second apart. These four images are essentially duplicates, giving a means to check system noise. An EO Camera II measurement consists of 15 seconds of data collection on the VCR, and thus approximately 450 images. Only one image for each of these measurements would generally be extracted from each camera during post-deployment processing.

3.2 Data Base Summary

A summary of the data base obtained during the twenty-four day deployment interval is listed in Table 1. On a typical ten hour data day, one would complete events 5 through 15 on the data log (Fig 3.2) 10 times, and events 1 through 4 somewhat less often.

Appendix B contains a listing of those data from EO Camera II which were subsequently digitized and extracted for analysis. This digitization and the subsequent analysis are discussed in the next sections.

4.0 ANALYSIS OF ACQUIRED IMAGES

Following the field deployment, the camera data were shipped back to the Visibility Laboratory for analysis. The EO Camera I data consisted of tapes of computer compatible 128 x 128 images. The EO Camera II data were stored on video tape, in 15 second blocks of images recorded at roughly thirty 256 x 256 images per second. After these analog video data arrived in-house, one image for each 15 second block of fisheye data was digitized, yielding a computer compatible image which was then stored on tape.

In this section, sample images from EO Camera II are illustrated and described. They are then compared with images from EO Camera I and from the photographic camera, Automax I. Finally, the work done with the image processing system on these images to develop a preliminary cloud detection algorithm is described.

4.1 Description of Sample EO Camera Images

Sample images for EO Camera II are shown in Fig's. 4.1 (a-d). These figures illustrate a clear sky, scattered cumulus, broken altocumulus, and high broken cirrus conditions respectively.

Although the sensor array was rectangular, the image placed on this array by the optics was round. In these fisheye images, the center of the image is the zenith, and the edges represent the horizon. (The actual field of view extends to about 7 degrees above the horizon.) Various structures may be seen near the horizon, such as the small line near the top of the image, which is a telephone pole tohe south of the van. The black rectangular object is the sun occultor, used to shade the lens. The occultor was an opaque frame supporting a 3-log neutral density filter. The attenuated solar radiance appears as a bright spot. A small grey scale attached to the underside of the occultor may also be seen. The time and date inserted by a time-date generator on the recorded image appears near the bottom of the scene.

Although EO Camera II is referred to as having 256 x 256 resolution, the actual situation was somewhat more complicated. The original CID array had a 388 x 248 array, which was partially filled by the circular image. The image was recorded in video format, at which point the signal was analog. When the signal was redigitized, it was digitized into a 512 x 512 array. Thus the actual images manipulated on the computer were 512 x 512, however the original resolution was close to 256 x 256.

The images in Fig. 4.1 qualitatively look quite reasonable for our purposes. In the clear image, one can see the higher radiance near the horizon and in the upsun direction, especially near the aureole. The cumulus cloud case shown in Fig. 4.1(b) shows a number of clouds of various sizes and brightnesses. Both the angular resolution and radiometric resolution are adequate for these clouds to be quite obvious. The somewhat more difficult cases of smaller clouds and thinner clouds are shown in Fig. 4.1(c & d). In each of these scenes the clouds are apparent to the eye. It should be noted that the quality of the images as stored in the computer and viewed on the image

processing display is somewhat higher than viewed in these reproductions due to the degradations inherent in converting the images to hard copy.

4.2 Comparison of Camera System Images

An image from EO Camera II is compared with the images from EO Camera I and from the black and white Automax I in Fig. 4.2. The EO Camera I image is 128 x 128. The Automax image which was originally recorded through a red filter, was created by digitizing the film image. The digitizing was done with a 100 μm spot size, in order to duplicate the pixel size of the EO Camera II as closely as possible. With the spot size, the resulting image was 256 x 256 pixels.

In Fig. 4.2, one can see that for reasons discussed in Section II the EO Camera I image is significantly inferior to the other images. The clouds may be seen, however cloud edges are not clearly defined, and cloud identification is difficult, even for subjective viewer analysis. The EO Camera II images are sufficiently superior to offset the disadvantage of video recording, and for this reason the remaining analysis in this report is based on the EO Camera II data.

The Automax images shown in Fig. 4.2 are slightly superior to those of the EO Camera II. This is primarily due to the limited dynamic range of the electro-optic camera. Use of the Automax for the accumulation of real time results or extended data bases is not practical, for two reasons. One is the difficulty associated with converting the photographic images to digital images which could be utilized with a computer. The second is the difficulty in maintaining radiometric control with the photographic images, thus making absolute calibration and comparison with model clear day skies very difficult. The use of the electro-optic camera overcomes these shortcomings. From comparison with the Automax I it is apparent that it does so with only limited loss of digitized image clarity.

Figure 4.3 illustrates a line grab from the images shown in Fig's. 4.1(b), 4.2(a) and 4.2(b). The signal level for a row just below the center of the image is shown for all three systems. In this figure, one can see that the cloud edges are reasonably sharp for both EO Camera II and the Automax I, and somewhat more diffuse for EO Camera I.

4.3 Development of Cloud Identification Techniques

For the images illustrated in the beginning of this section, it is apparent that the information necessary for cloud discrimination is inherent in the image. That is, a subjective viewer of the image can readily identify which sky sections are clear, and which are obscured by clouds. At this point then, the problem is to determine a quick and reliable procedure by which a computer may make objective identification of the cloud cover.

An immediately obvious feature of these measured images is that the clouds tend to be brighter than the background sky. An illustration of this is shown in Fig. 4.4, which is a composite plot of relative radiance values extracted along identical sky arcs from electro-optical images recorded on two successive days at approximately the same local time on each day. The first day, 3 September, was cloudy and the second day, 4 September, was clear. The surface weather observation for 3 September at 1258 LST shows 6/10 cumulus clouds with bases of 6500 ft. and a prevailing surface visibility of 55 miles. For the corresponding time on the following day, the sky was clear except for a few isolated cumulus clouds on the NE horizon, and the estimated visibility was 50 miles. The prescribed arc is a straight-line path on the recorded image, extending from west to east and passing near the zenith. In this case, a simple instantaneous comparison of the relative signal profile at 650nm on the cloudy day versus the expected clear sky radiance profile at 650nm yields good discrimination of the 3 September cloud field along the designated arc segment. In the future we plan to have images which are radiometrically calibrated, and make a direct comparison with modeled partly cloudy skies and spectral radiance ratios. An algorithm could then be based on the comparison of measured data to model calculations derived from inherent image information.

For this deployment, the lack of absolute calibration precluded the use of algorithms based on model vs measured radiances. It should also be noted that algorithms based on the use of the blue/red radiance ratio could not be applied, since EO Camera II data were acquired only with a red filter. However, for purposes of preliminary analysis, the development of alternate algorithms has been approached. This development helps give the analyst experience with the quality of the images, and the results may be useful in the later development of algorithms for application to calibrated imagery.

Identification by Threshold

The application of several test algorithms to one image is illustrated in the next several figures. Figure 4.5(a) illustrates the sample test image. The simplest test was the definition of any point with a radiance over a given

threshold as cloud. Figure 4.5(b) illustrates this test. In this case, the threshold chosen was 50 (where the recorded digitized signal may vary from 0 to 255, and is monotonically related to radiance). For this illustration, all points with signal less than 50 are coded blue, and those with signal greater than 50 retain their original black and white color from the display screen. This threshold worked reasonably well, as a first approximation. Most of the clouds are correctly identified. The two main areas not correctly identified are the overhead sky between the two bright clouds, which is shown in grey and thus erroneously identified as cloud, and a small patch of cloud near the west horizon (the left edge of the image) which is identified as sky. Thus one trouble spot is near the sun between clouds, where the sky becomes quite bright. Another is in clouds near the horizon, where the radiance may become less than the sky radiance over most of the image.

Measured Gradient

Another source of information is the positional rate of change of the radiance. In general, the cloud edges in these images represent large abrupt changes in radiance. Figure 4.6 shows an application of this information. Figure 4.6(a) shows a pseudo gradient derived from the cloud field image. This image is the difference between adjacent x pixel values, rectified and added to the rectified difference between adjacent pixel values. Cloud edges may be clearly seen, even on the small clouds in the lower half of the image. Near the horizon the edges may be seen, however definition of cloud vs hole becomes more difficult. A mask based on the gradient image is superimposed on the threshold image in Fig. 4.6(b). Here one can see that where the threshold detection fails, overhead, the gradient provides the additional needed information. Development of a simple algorithm to make use of the gradient information is not trivial however, due to the complexity of the gradient field.

Identification using Image Ratios

One problem with the radiance threshold detection scheme is that the radiance of a clear sky varies with look angle. Thus a threshold low enough to correctly identify downsun clouds near the horizon will incorrectly identify the upsun clear sky, particularly near the aureole. One way around this problem is to ratio the image with a clear day image with comparable sun elevation and turbidity conditions, thus normalizing out the clear sky radiance changes.

Figure 4.7 illustrates the ratio of the test image signal with the clear sky image signal taken the following day near the same time. In this image, any ratio less than or equal to 1 has been color coded blue, while any ratio between 1 and 1.4 has been coded pink. Ratios higher that 1.4 have been left black and white. In this image, the holes between clouds have ratios very close to 1 for most of the sky, as expected. The cloud edges themselves have higher ratios, as does the region directly overhead where there is a hole between two bright clouds close to the solar aureole. These pink-coded regions most probably represent the enhanced path radiance which is expected near cloud edges.

From Fig. 4.7(a), it is apparent that for this test case, identification of the clouds based on a signal ratio threshold of 1.4 would be quite accurate. That is, if the ratio of test image to the clear image taken at the same time is greater than or equal to 1.4, that point would be characterized as cloud. This procedure was applied to the image, with the binary result given in Fig. 4.7(b). In this figure, points identified as clear or cloud are assigned values of 0 or 1 respectively. Comparison with the original image indicates that this result is reasonably accurate.

One problem with applying this particular identification algorithm to the general case would be that the clear sky radiance itself depends on the aerosol load in the atmosphere. One advantage of comparison with a model rather than a measured clear day image is that this variation could potentially be allowed for.

Variable Gain Effects

For the example given in the previous paragraphs, the cloudy and clear day images were taken with the same f-stop and neutral density on the camera system, and comparison of the uncalibrated radiances yielded reasonable results. For most of this deployment however, the images were recorded with a variety of f-stop settings and neutral density filters interposed in the path. Unfortunately, although a change of neutral density filter or f-stop causes a fixed ratio change of input radiance, it does not cause a fixed change in signal level, partly because the VCR which was used to record the data had a variable gain which could not be controlled.

To analyze the magnitude of the problem caused by the variable gain in conjunction with the changing f-stops and neutral density filters, two images were extracted from 11 September. These two images were recorded approximately one minute apart, first with a 0.7 log neutral density filter in place, and then with the 1.3 log neutral density These values differ by 0.6 logs. At the actual wavelength of 650nm, the measured filter re-

sponses differed by 0.69 logs. Thus the radiance reaching the sensor changed by a factor of 4.9 (or $10^{.69}$). These cameras are reasonably linear with radiance (not with log of radiance), so the signal should have changed by an approximately constant factor of about 4.9. Taking the ratio of the actual images, it was found that the signal ratio varied from about 1.1 over much of the downsun sky to about 2.4 in the upsun clouds. Figure 4.8 illustrates the ratio of the two images. Checking other similar cases revealed that the signal level change caused by changing f-stops or neutral density filters was in general not close to the expected value, nor similar from one case to the next, and as illustrated in Fig. 4.8, not even constant within one image.

The result of this unfortunate variance caused presumably by the variable gain, is that two images recorded with different set-ups cannot be compared accurately, for this deployment. Even if one image were normalized to the other at some point, the within-image variance caused by this problem is too large. Thus, for this data set it is not possible to use the ratio of "test" to "clear" image algorithm except in those limited cases where the cloudy image is taken with the same setup as the clear image.

Difference Image

Since comparison of signal levels between images was a problem for this data set, it was decided to try to develop a technique which would identify the clouds within an image based on the signals in that image alone. For this reason, another look at the gradient field seemed in order. There are various techniques for looking at closed contours, however we needed an algorithm which could be applied to one line from an image after it had been extracted. For this reason, the difference between the signal in adjacent x pixels was investigated. Figure 4.9 shows this difference image, color coded by magnitude. Points which appear blue show little change between adjacent x pixels. Points which are yellow, red, and black show correspondingly greater differences between x pixels.

Several features may be noted in this illustration. First, not all of the clouds have particularly large differences at the edges. In fact, some of the within-cloud edges show more difference than the cloud edges. The line to the left of point "a" in the illustration is one such within-cloud variance. Point "b" points out one of the actual cloud edges which shows less difference than observed at point "a". Thus the simple technique of looking for a large positive change followed eventually by a large negative change, and identifying the points between as cloud, would be ineffective. Second, the clouds in general are characterized by higher x differences than seen in the clear sky sections of the image. However, the centers of large clouds in several cases (such as point"a") show low differences; thus identifying a cloud by a threshold in the x-difference would be ineffective.

Hybrid Difference and Threshold Algorithm

Although neither clouds nor cloud edges are characterized by a given gradient in Fig. 4.9 (not all cloud pixels have high gradient), it is noticeable that all pixels with high gradient are cloud. This was utilized in the following test.

First, all points with a difference in x of more than 3 were identified as cloud. Next, all those points which passed this test (and were within a center section of the row) were averaged, to yield an approximate value for cloud radiance within this image. Last, any additional points on that row which had signals greater than or equal to .85 times this average were identified as cloud also. Thus an average cloud signal was determined based on those points with a large x difference; then, any points with a signal close to or higher than this average were also identified as clouds.

This hybrid difference and threshold algorithm worked very well for the test images. Two sample images are shown in Fig. 4.10, in which the row to be extracted is color coded blue if the algorithm identifies the point as clear, and red if it is identified as cloud. The technique was tested on one row extracted for each image in the data base (as discussed in the next section), and found to be reasonably accurate except in a few cases. The algorithm has the advantage that it is not highly affected by radiance level or signal gain and thus can be easily extended from a test case to all the images. The main source of error is in the case when the extracted row covers a range from upsun to downsun (near dawn or sunset), as will be discussed in the next section.

The procedures for extracting one row for the entire data base and applying the algorithm are discussed in the next section, along with the results of this processing.

5.0 CLOUD STATISTICS: EXTRACTION AND RESULTS

One of the goals of this deployment was the demonstration of a system which could be used to automatically determine a variety of cloud statistics for a given region. As discussed in previous sections, the EO Camera system was successfully deployed, yielding sky images in which the clouds could be readily seen. This prototype system was limited in that data were acquired using a

video recorder with variable gain. As shown in the previous section, this limits the type of cloud identification algorithms which can be applied.

The data were however adequate to generate a reasonably accurate algorithm, which may be applied to the data for demonstration purposes. Accordingly, a computer program was developed which could extract the desired data and apply the prototype cloud algorithm, and extract illustrative statistical data.

In addition, cloud/no-cloud results were manually extracted from the acquired imagery, and resulting statistics were determined. This section includes a brief description of the automated extraction. This is followed by an analysis of the resulting statistics, and a comparison with the manually extracted data.

5.1 Automated Extraction of Cloud Statistics from Images

The automated extraction procedure makes use of EO Camera II data extracted from the video tapes and converted to digital format. These data are processed using a mainframe computer. A conceptualized flowchart of the processing program is illustrated in Fig. 5.1. The program extracts one row or column from each desired image, and associates it with the appropriate time/date information. A system such as illustrated in Fig. 2.2(c) could automatically record time, date, and filter information. With this prototype system utilizing the video recorder, the time and date were extracted from the manual field logs for input to the program, and verified using the time/date superimposed on each image by the time/date generator.

An algorithm is then applied to the line of data extracted for each image, to convert it to a line of 0 or 1 values, corresponding to a no cloud or cloud decision respectively at each pixel along the line. This decision algorithm takes the form described in Section 4. That is, those points with high variance along the line are assigned a value of 1, or identified as cloud. An average of the signal values for certain of these points is computed. Then other points with signal greater than .85 times this average are also assigned 1 values. The program allows one to determine one average based on the central portion of the line, or determine separate averages for several segments of the line. Test runs have been made which determine the sensitivity of the results to the various constants used in the algorithm. The constants derived on the basis of the figures shown in Section 4 also yield the best cumulative results in comparison with the manual data.

Next, the zenith angle associated with each pixel is computed. This computation takes the form

$$\theta = \theta_{max} \frac{\left[(x - x_o)^2 + (y - y_o)^2\right]}{\left[a^2(x - x_o)^2 + b^2(y - y_o)^2\right]^{1/2}}$$

where

θ_{max} = max θ at edge of lens
x_o, y_o = center of elliptical image
a,b = axes of elliptical image

The geometric calibration was derived using images such as illustrated in Fig. 5.2. This image was acquired in a large hemispherical room, with the camera lens mounted level with the base of the hemisphere. The angles associated with the edges of the various lit panels are known. The pixel positions of these panel edges were extracted and used to derive the above geometric calibration equation. The results were found to be linear within 2 degrees in zenith angle, and within less than one pixel uncertainty in azimuth angle.

After the program applies the geometric calibration to the data, the line for each image is printed, yielding a listing of 0's and 1's as a function of zenith angle along the line. When the azimuthal angle exceeds 180 degrees (left half of image), the value of $-\theta$ is printed as a code in place of θ.

The program then combines the results from all images to yield certain statistics. The first extracted statistic is the percentage of cases which were cloudy at each angle, as a function of angle. Next, the longest cloud-free interval along the line is determined for each image (here longest is defined as the largest zenith angle change, not necessarily the largest pixel count along the line). These values are then combined to yield the cumulative frequency of cloud free arc length. These results will be discussed later in this section.

5.2 Evaluation of Automated Extraction Accuracy

Sample output from the cloud extraction program are shown in Fig's. 5.3 and 5.4. Fig. 5.3 gives the frequency of cloud free line of sight as a function of zenith angle for the extracted row. That is, at each angle, which in turn corresponds to a pixel location in the image, the percentage of cases in the data base which were cloud free at that angle is given. Figure 5.4 gives the cumulative frequency for cloud free arc length. For each image, the longest segment which is cloud free is identified, and these

results for all of the images were combined to yield the cumulative frequency. The statistical summary includes data extracted from 233 images at 1-hour intervals for the hours of 0700-1600 LST inclusive for the 23-day period ending 20 September 1984. The prescribed arc extends west-east and passes near the zenith.

In each plot two curves are given: the program output, created using the program discussed in Section 5.1, and the manual output, created from the data pulled manually from the video images. The third curve in Fig. 5.3 will be discussed in the next section. Given the expected uncertainties inherent in the current algorithm, (resulting from the use of the uncalibrated data), the computed and manual results are surprisingly close. In Fig. 5.3, both curves indicate clear skies overhead in 80-90% of the cases, with a lesser probability of cloud free sky at the horizon. This drop near the horizon is to be expected partly because a layer of clouds overhead with even linear spacing in the horizontal direction will have decreasing angular spacing as the path of sight becomes more slanted away from the vertical.

In Fig. 5.3, although the computed and manual results compare quite well for zenith angles near -80 through +50 (west horizon through overhead partway to east horizon), the computed results drop lower than manual for zenith angles near +80. Thus near the east horizon the algorithm tends to identify too many cases as cloud.

Although the cumulative statistics in Fig's. 5.3 and 5.4 look quite good, this interim algorithm is subject to uncertainty. The algorithm essentially identifies cloud signal on the basis of edges and any other points with considerable variance, and then finds the rest of the clouds by comparison with this signal. It is to be expected that problems will occur if the cloud signal itself varies in certain ways, or if the sky signal is too close to the cloud signal.

Several individual cases were examined to determine the extent of these problems. In most cases, the identification of the cloud locations for the extracted line compared quite well with the manual identification. Probably the most common inaccuracy occurred near sunrise or sunset, when the extracted line represents look angles quite near the sun. In these cases, the upsun sky signals were sometimes identified as cloud.

Another example of a case in which the algorithm did less well was a case in which the cloud edges were very bright relative to the rest of the cloud. In this case the center of the cloud was identified as sky, and only the proverbial silver lining was identified as cloud.

The current algorithm is good enough to identify many cases correctly, and can be used to demonstrate the types of computations which may be made with a system of this type. However, the statistical results must be taken as approximate, and the results for individual images cannot be trusted in every case. The future availability of EO Camera data with fixed gain and radiometric calibration will give us the ability to apply potentially much more accurate algorithms based on comparison with clear day images and models, and comparison of blue/red ratios with model ratios.

5.3 Evaluation of Extracted Statistics

The field site for the electro-optical (EO) system experiments was established adjacent to C Station, White Sands Missile Range, where a complete program of surface weather observations is maintained in accordance with prescribed standard procedures. Sky condition observations from C Station provide a basis for general assessment of cloud cover during the course of the experiments relative to climatological expectancy. Shown in Fig. 5.5, is a comparison between the relative frequency of cloud cover by category as recorded at C Station for (1) the specific time period of EO system operation which included the daylight hours from 0700 LST to 1600 LST from 29 August to 20 September 1984, and (2) the long term average for all hours in September for the period 1951 to 1973. Making some allowance for an expected enhanced frequency of small scale convective clouds during the daylight hours (1/10-5/10 category), the cloud conditions during the experimental period appear to be about normal for late August and September at White Sands, New Mexico.

Systematic extraction of cloud/no-cloud data from the digital EO camera imagery along prescribed arcs yields the information required for the objective determination of the observed frequency of cloud-free intervals of varying lengths along the track over selected periods of time. An example is the observed cumulative frequency of arc length for a pre-selected arc over the period of EO observations at White Sands Missile Range, as shown in Fig. 5.4. Note, for example, that the frequency of cloud-free arc length greater than or equal to 90 degrees was 75 percent for the White Sands location for the specified period of time.

The cumulative frequency of the longest arc length should, of course, reflect the observed frequency of clear skies for this period, which as calculated from Station C surface weather observations was 37.8 percent. The manually extracted results fall close to this value, however, the automatically extracted results are somewhat

lower. The 38% cumulative frequency occurs at an arc length of 139 degrees, rather than at the maximum, 148 degrees. Thus, the current algorithm yields clear day cloud free arcs which are often too short, indicating incorrect identification of near-horizon pixels.

Another stochastic feature of the observed sky conditions easily derived from the archived digital imagery is frequency distribution of cloud-free-line-of-sight, CFLOS, as shown previously in Fig. 5.3. For the prescribed arc, the observed frequency of CFLOS for all zenith viewing angles less than 40 degrees ranged between 85 and 92%. Proceeding with the knowledge that observed average sky conditions during the experimental program did not differ markedly from normal, it is of interest to compare the observed CFLOS frequency along the single designated path with model calculations. With the assumption that the average cloud amount for all sky condition observations designated clear on the Surface Observation Form MFI-10 is 0.25, the calculated average percent sky cover over the specific period of 233 observations was 0.248. The probability of CFLOS corresponding to this average cloud cover as calculated by the geometric model of Allen and Malic (1983) is given by the dashed line in Fig. 5.3. Their model, which fits the Lund and Shanklin (1973) cloud data base reasonably well, represents the probability of CFLOS by the relationship

$$PCFLOS = P_o^{(1 + b\tan\theta)}$$

where θ is zenith viewing angle,

$$P_o = 1 - n\,(1+3n)/4,$$

and

$$b = 0.55 - n/2$$

where n is sky cover in tenths.

The close correspondence in the simplified model calculations and the observed CFLOS frequency for this very limited example is undoubtedly fortuitous. Furthermore, application of the modeling approximation to the "average" cloud cover is not necessarily commensurate with the approach used in its development. However, the important point is that the EO camera system can be used to help establish a reliable and comprehensive cloud data base in a form that can be used readily to validate existing models and to modify, adapt and extend these techniques. A radiometrically calibrated EO system offers the advantages of economical and reliable performance for systematic field use and, with appropriate algorithm development, the resultant data can be tailored to provide specific and objective determinations of sky condition and its statistical behavior as required for a variety of applications.

6.0 SUMMARY AND ONGOING DEVELOPMENTS

A preliminary data base has been obtained, which demonstrates the feasibility of acquiring sky images suitable for evaluation of cloud field characteristics. The imaging system consists of a solid state camera with various optics for control of radiance levels and spectral content, with associated electronics for controlling data acquisition and storage.

Data were acquired hourly for 24 days, and subsequently digitized in-house. The resulting images show the clouds clearly, in a variety of meteorological conditions. The primary system evaluated in this report, designated EO Camera II, is superior to the prototype EO Camera I, which has lower resolution. Comparison with photographic camera images demonstrates the excellent resolution and enhanced utility of the EO Camera II images.

As a result of delivery problems, the primary system was deployed uncalibrated. This limits the types of cloud decision algorithms which may be applied to this preliminary data base. However, an algorithm has been developed which gives reasonable representation for most images. Using this algorithm as a demonstration, sample statistics characterizing the observed cloud fields have been extracted.

Following the deployment of the camera system in the field, a number of modifications have taken place or are being developed at this time. These may be briefly summarized here. Perhaps the most important modification from the analyst's point of view is the change from video recording to straight digital output, with the frame grab performed electronically and controlled by computer in the field. This allows the recording of fixed gain, well controlled data. As a result radiometric calibration of the instrument becomes feasible. This in turn makes comparison with radiative transfer model calculations more practical.

In the realm of recent advances, the electronics control function has been considerably enhanced with the addition of computer control of the filter mechanism. This filter mechanism includes both a spectral wheel and a neutral density wheel, allowing independent variation of the two filter types. As a result, both blue filtered and red filtered images may be acquired routinely at a variety of

neutral density settings. Additional microcomputer control functions include writing of identifying header information to tape preceding the image data, and writing of embedded time, date, and filter information in each image.

Simultaneously with these mechanical developments, software and analysis developments have occurred. A version of the FASCAT atmospheric model Hering 1985) has been implemented on the microcomputer. As a result of parametric studies using this model, it has been determined that, given fixed gain and calibrated imagery from the EO camera system, the blue-red spectral ratio technique is potentially the most promising candidate method of cloud discrimination. Radiative model calculations clearly indicate that a ratio of simultaneous images made with narrow-band red and blue filters will provide good cloud recognition over a broad range of meteorological conditions. Problems center primarily on cloud analysis in the upsun direction, near the horizon at sunrise and sunset, and of course the identification of thin cirrus. For the latter problem, analysis of the spatial variations in the measured radiance field in the solar aureole region appears to be the most promising approach.

In summary, as the continuing mechanical improvements proceed, evaluation of images and development of algorithms is continuing, utilizing both the mainframe computer (primarily for evaluation), and the minicomputer. The goal is, as before, the development of accurate techniques which may be implemented on a minicomputer and deployed in the field for real time assessment of the cloud information inherent in the acquired imagery. Using the results of the White Sands field demonstration of the prototype system, and utilizing the improved capabilities of the current hardware and software systems, we feel this goal to be fully realizeable.

7.0 REFERENCES

Allen, J.H. and J.D. Malick (1983), "The Frequency of Cloud-Free Viewing Intervals", AIAA 21st Aerospace Sciences Meeting Paper, AIAA-83-0441, 5, Reno, Nevada.

Hering, W.S. and R.W. Johnson (1985), "The FASCAT Model Performance Under Fractional Cloud Conditions and Related Studies", University of California, San Diego, Scripps Institution of Oceanography, Visibility Laboratory, SIO Ref. 85-7, AFGL-TR-84-0168.

Lund, I.A. and M.D. Shanklin (1973), "Universal Methods for Estimating Probabilities of Cloud-Free Lines-of-Sight Through the Atmosphere", J.Appl.Met., 12, pp 28-35.

8.0 ACKNOWLEDGEMENTS

This work is performed under contract to Air Force Geophysics Laboratory, Contract No. F19628-84-K-0047. The authors are grateful to Mr. D. Grantham of AFGL for his valuable suggestions and guidance. We wish to thank Mr. R.W. Endlich and the host for the field test, Atmospheric Sciences Laboratory, for their coordination and assistance. Finally we wish to thank Mr. J.C. Brown, Mr. J. Rodriquez and Mr. J.S. Fox of the Visibility Laboratory for their support.

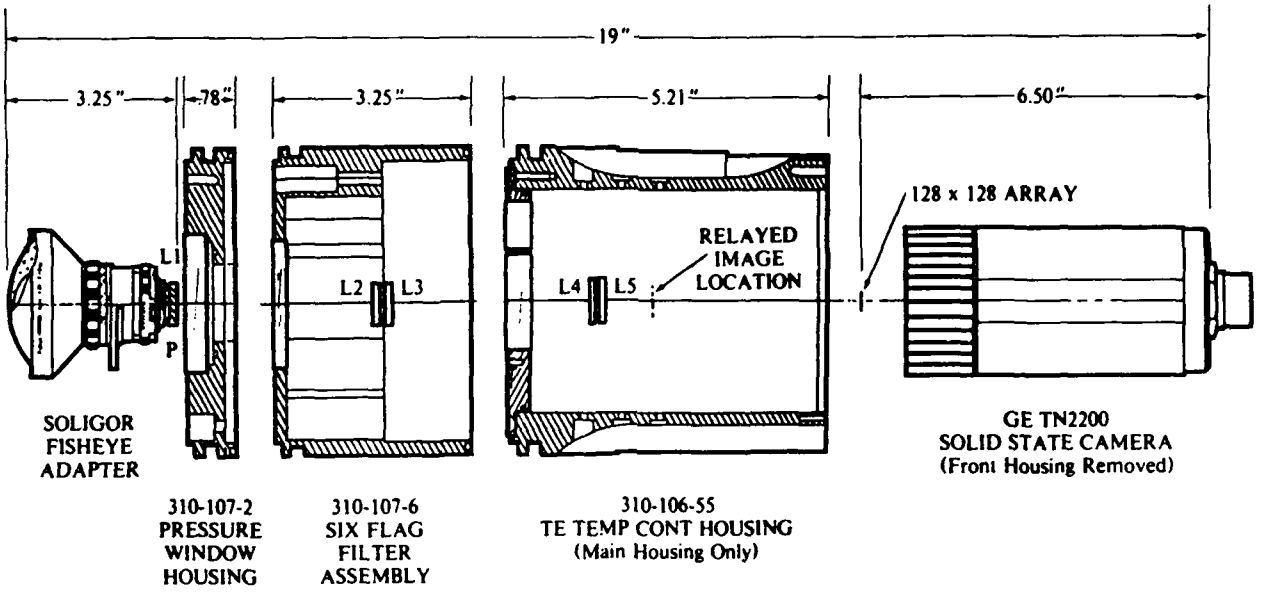

(a) Multi-spectral imaging fisheye scanner (EO Camera I)

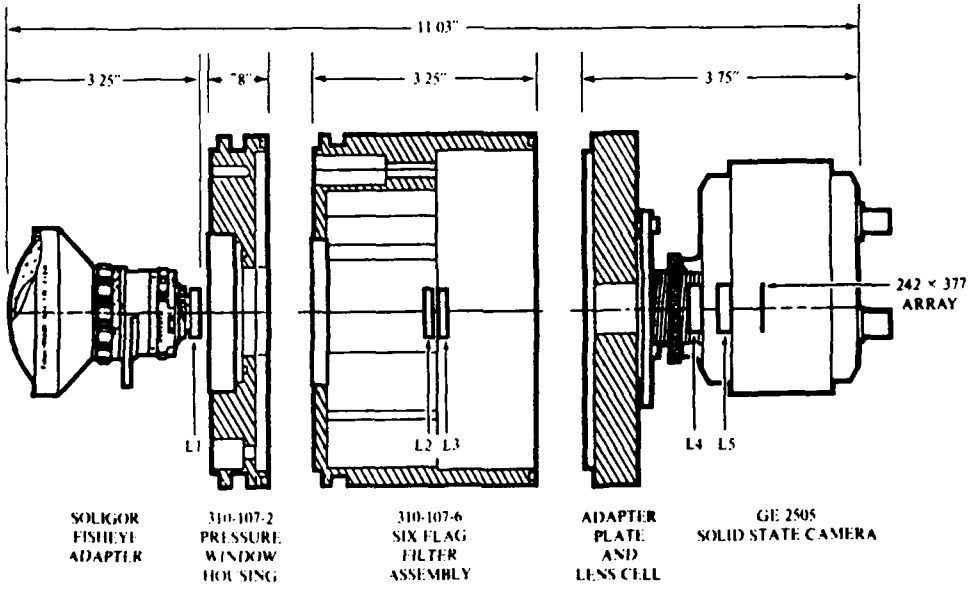

(b) Multi-spectral whole sky imager (EO Camera II)

Fig. 2-1. EO Camera optical layout.

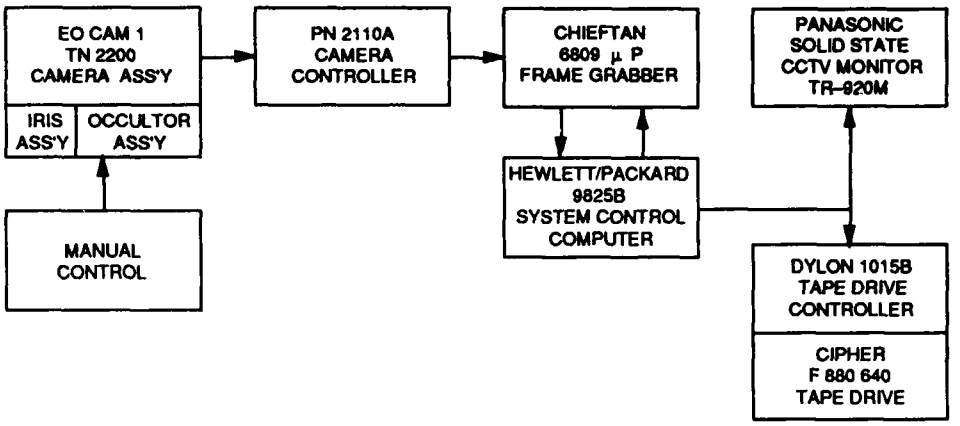

(a) Back-up system as-built for AUG '84 deployment. (EO Camera I)

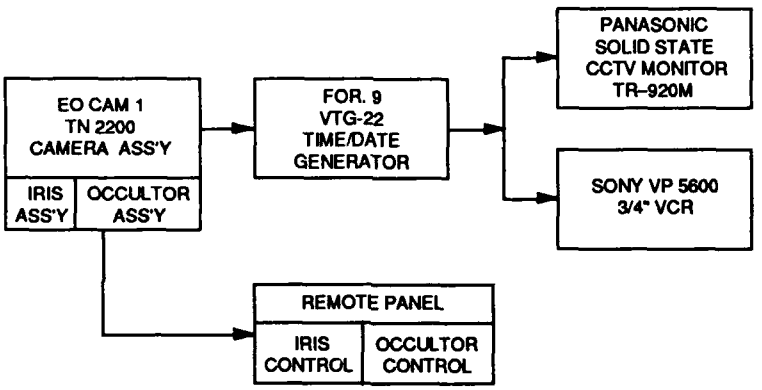

(b) Prototype system as-built for AUG '84 deployment. (EO Camera II)

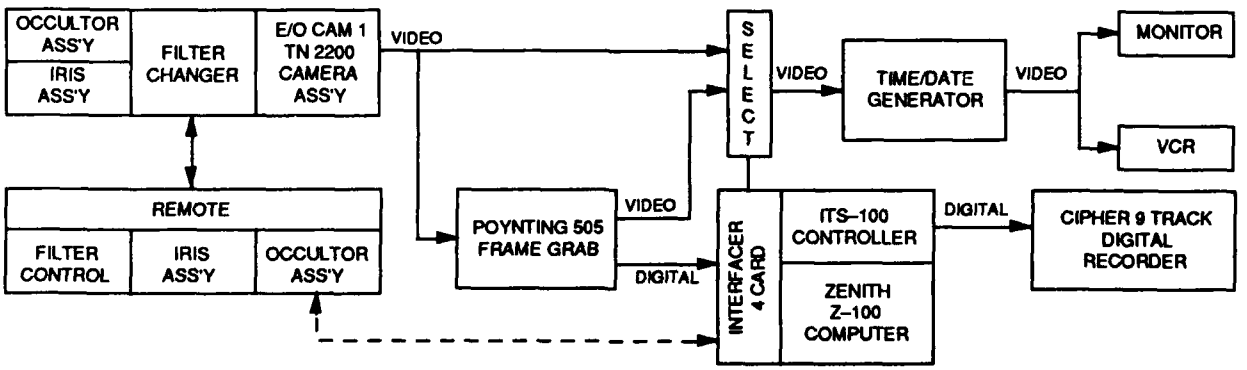

(c) Composite system proposed for CFLOS Algorithm development.

Fig. 2-2. Equipment organization schematic.

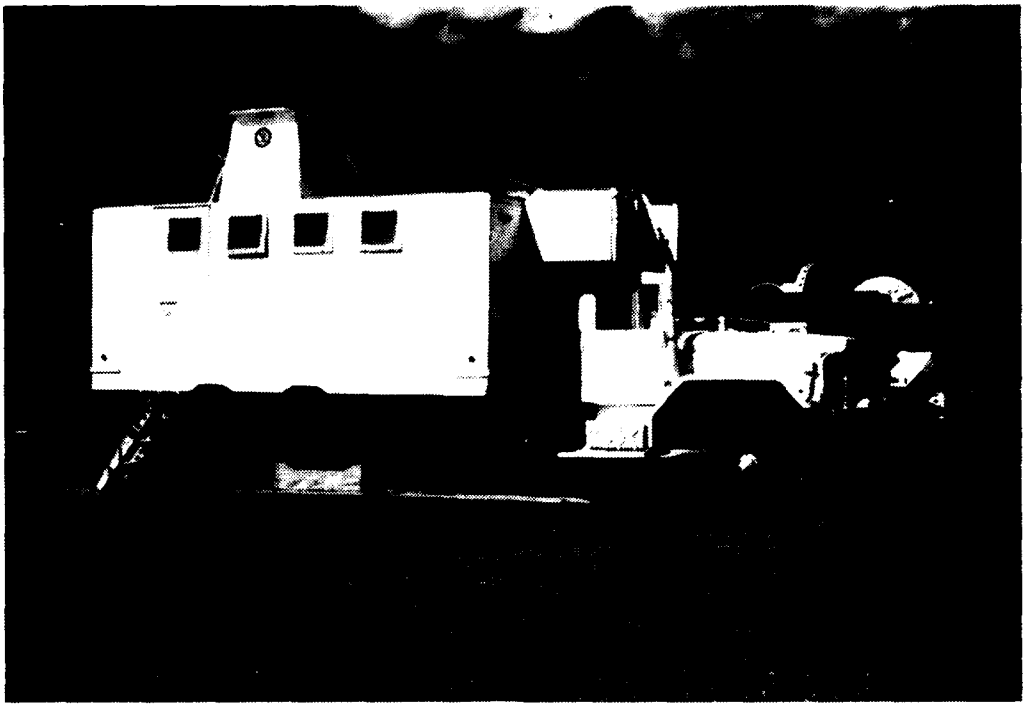

Fig. 2-3. External equipment layout.

Fig. 2-4. Instrumentation hut on van.

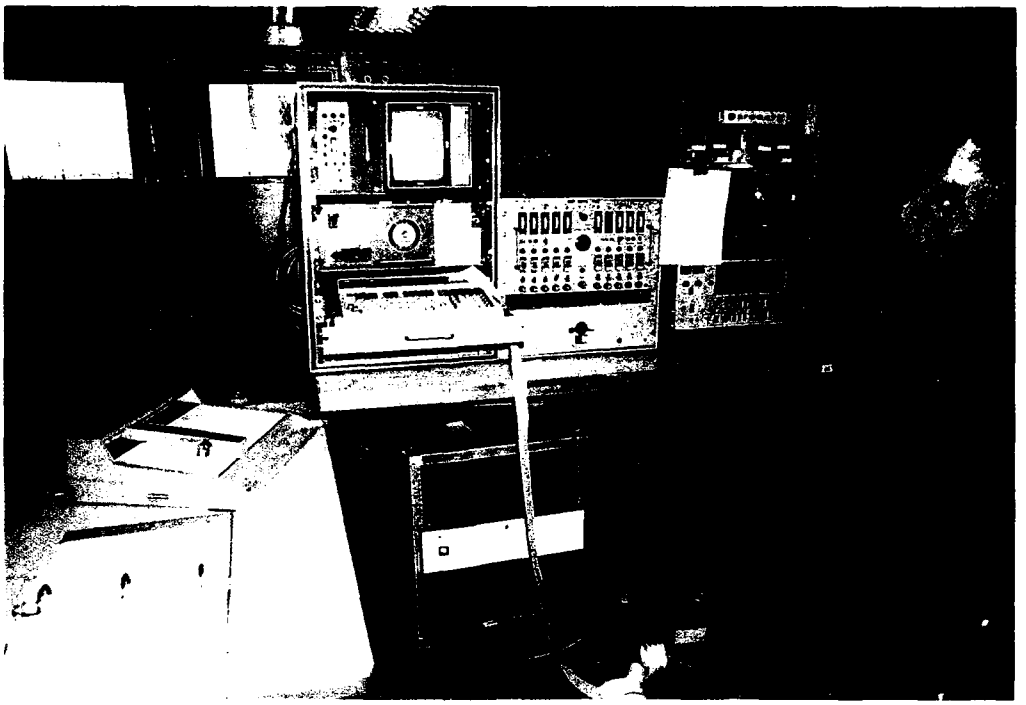

Fig. 2-5 (a). Internal equipment layout. Full complement instrumentation

Fig. 2-5 (b). Internal equipment layout. Dual console operator station.

Table 3.1. Data base summary.

Data Date	E/O CAMERA I					E/O CAMERA II			AUTOMAX 1 & 2	
	Tape Ident Number	Number of 4-Image Files				Cassette Number	Number of 15-sec Image Sets		Number of Film Sets	
		Fisheye		Irrad.	Total		Fisheye	Irrad.	B & W	Color
		Filter 2	Filter 3							
29 AUG	1	20	21	0	41	1	10	0	19	19
30 AUG	2	12	12	0	28	1	6	0	12	12
31 AUG	4	25	24	0	49	2	14	0	22	19
1 SEP	5	22	22	3	48	2	13	0	21	21
2 SEP	6	24	22	3	49	2	12	0	23	23
3 SEP	7	23	23	0	46	2	12	0	20	20
4 SEP	8/9	33	33	12	79	2	11	3	22	22
5 SEP	10	21	21	15	57	3	7	3	14	14
6 SEP	11/12	27	27	24	79	3	10	8	18	18
7 SEP	13	30	30	30	95	3	15	6	20	20
8 SEP	14	17	17	12	46	3	14	2	10	10
9 SEP	15	6	6	6	22	4	2	2	4	4
10 SEP	16	34	34	30	105	4	31	9	24	24
11 SEP	17	36	36	30	107	4/5	23	10	24	24
12 SEP	18	26	26	24	76	5	12	8	17	17
13 SEP	19	32	32	30	94	5	22	9	20	20
14 SEP	20	21	21	20	63	6	8	7	14	14
15 SEP	21	33	33	34	105	6	11	11	22	22
16 SEP	22	27	27	27	82	6	9	9	18	18
17 SEP	23	27	27	27	84	6	9	9	18	18
18 SEP	24	27	27	27	85	7	9	9	18	18
19 SEP	25	27	27	27	82	7	10	9	18	18
20 SEP	26	18	18	18	55	7	6	6	12	12
21 SEP	27	27	27	27	82	7	9	9	18	18

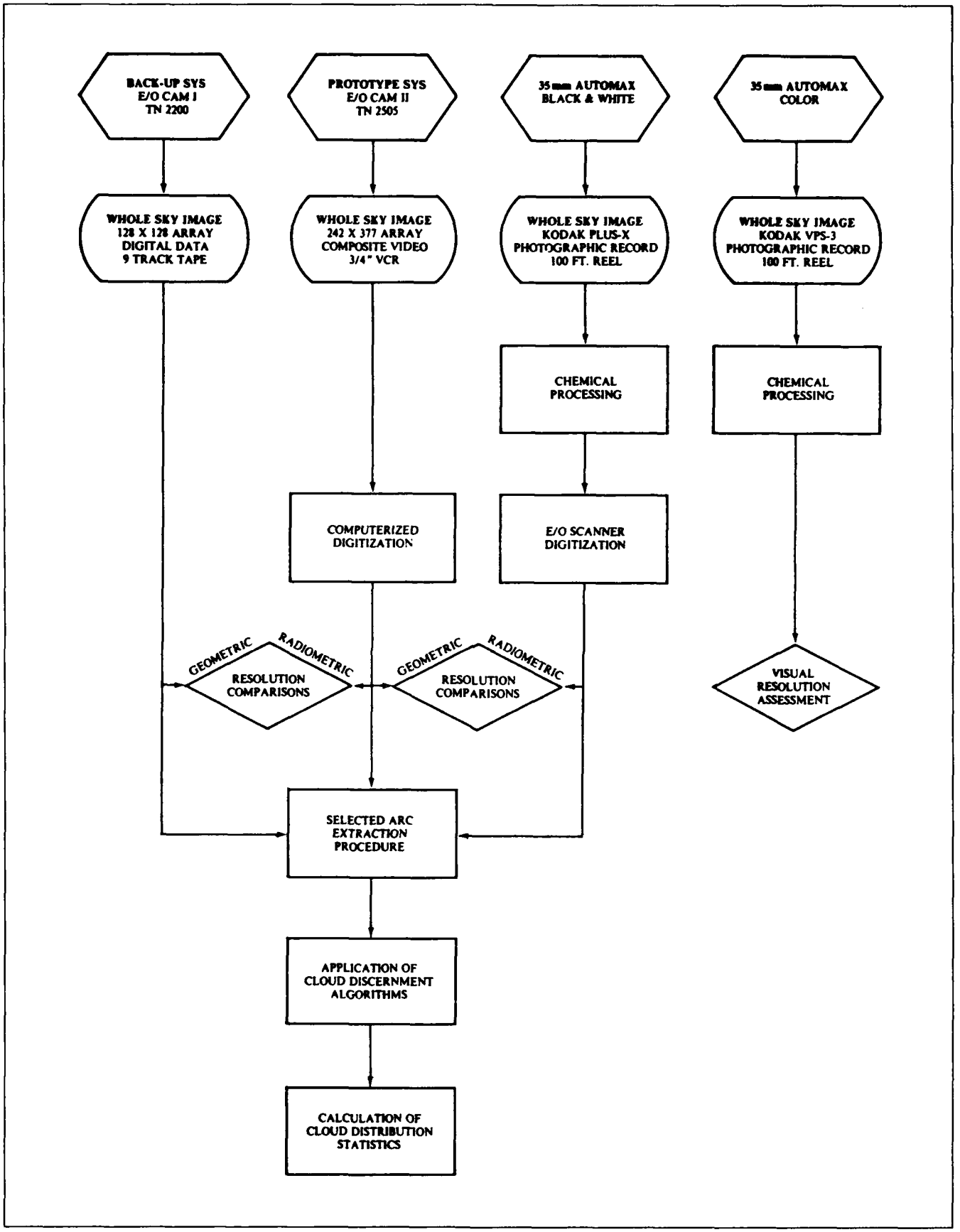

Fig. 3-1. Experimental procedure - whole sky camera system.

E/O CAM FIELD DATA LOG
Standard Hourly Set

DATA SITE	WSMR	DATA DATE	15 Sep 84	LOG # FOR THIS DATE	5	START TIME	1141

CHANGES SINCE LOG #1 OF THIS DATE (SET-UP):

CLOUD CONDITIONS: 60% cirrus – looks like a single layer

Event No.	System (Hdr.)	Time	IDENT: Frame, File, or Count:	f/stop	Filter Flag	D/N	Comments
1	E/O CAM-1 (I)	1141	file 37	11	2	0	Irrad.
2	E/O CAM-1 (I)	1142	file 38	11	3	0	Irrad.
3	E/O CAM-1 (I)	1142	file 39,40	11	4	0	Irrad. Sun came out
4	E/O CAM-2 Beg. / End	114245 / 114300	139 ft. / 144 ft.	16	5	in	Irrad
5	Automax 1	1145	1957-8	–	–	–	
6	Automax 2	1145	1959-60	–	–	–	
7	E/O CAM-1 (G)	1148	file 41	11	2	0	Sky onscale
8	E/O CAM-1 (G)	1148	file 42	11	3	0	
9	E/O CAM-2 Beg. / End	114845 / 114930	144 ft. / 148 ft.	16	3	in	
10	E/O CAM-1 (G)	1149	file 43	11	2	0	
11	E/O CAM-1 (G)	1149	file 44	11	3	0	
12	E/O CAM-1 (G)	1151	file 45	11	2	.6	Clds onscale
13	E/O CAM-1 (G)	1151	file 46	11	3	.6	
14	Automax 1	1152	1961	–	–	–	
15	Automax 2	1152	1962	–	–	–	

Fig. 3-2. Field data log.

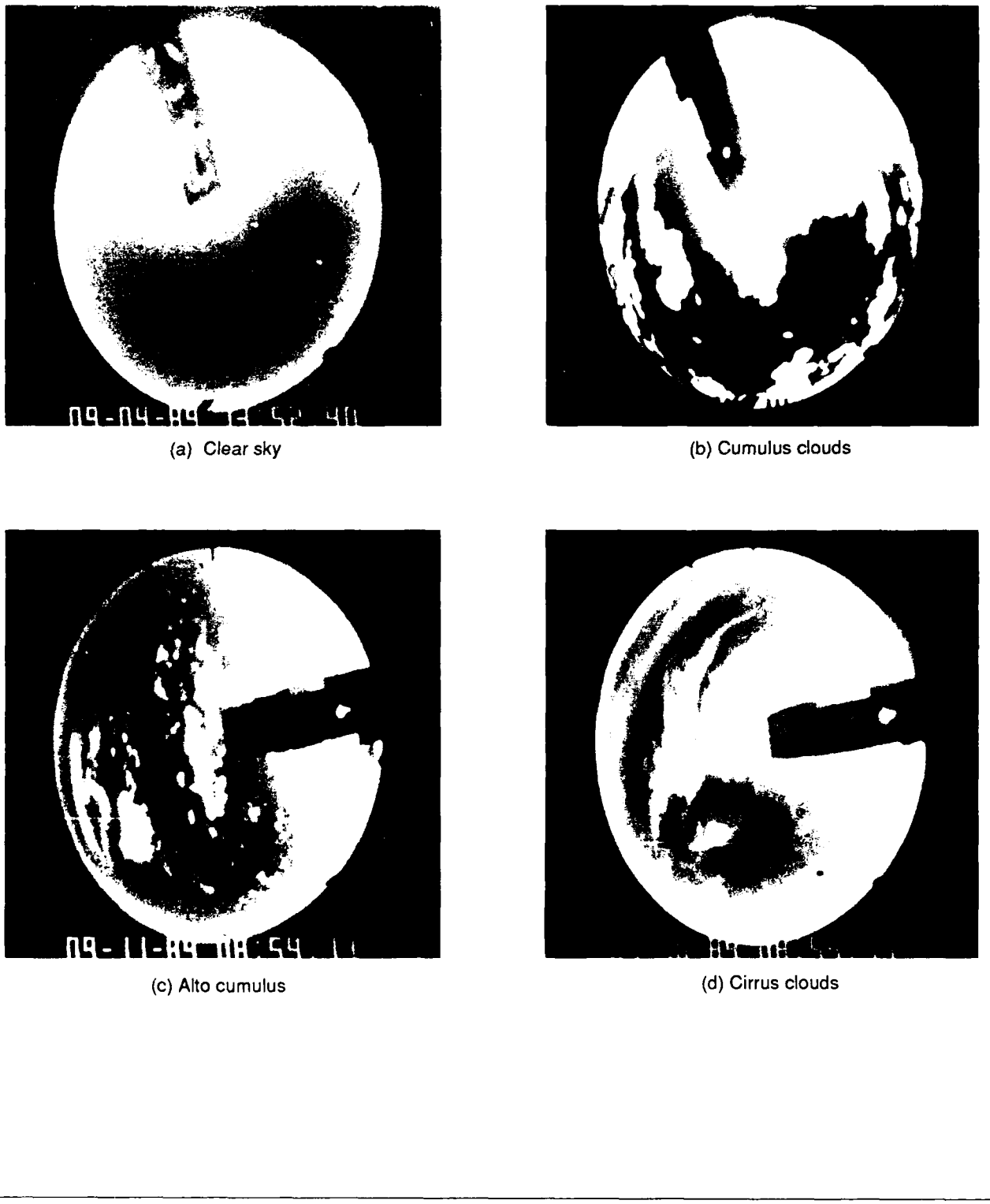

(a) Clear sky

(b) Cumulus clouds

(c) Alto cumulus

(d) Cirrus clouds

Fig. 4-1. Imagery from EO Camera II for a variety of sky conditions. Images were digitized from video, piped through image processing, displayed into matrix camera.

(a) EO Camera I expanded to 256 x 256

(b) Automax I digitized at approximately 256 x 256

Fig. 4-2. Imagery from EO Camera I and Automax I for comparison with EO Camera II images. Images acquired on 3 SEP 84 near 1401 hours.

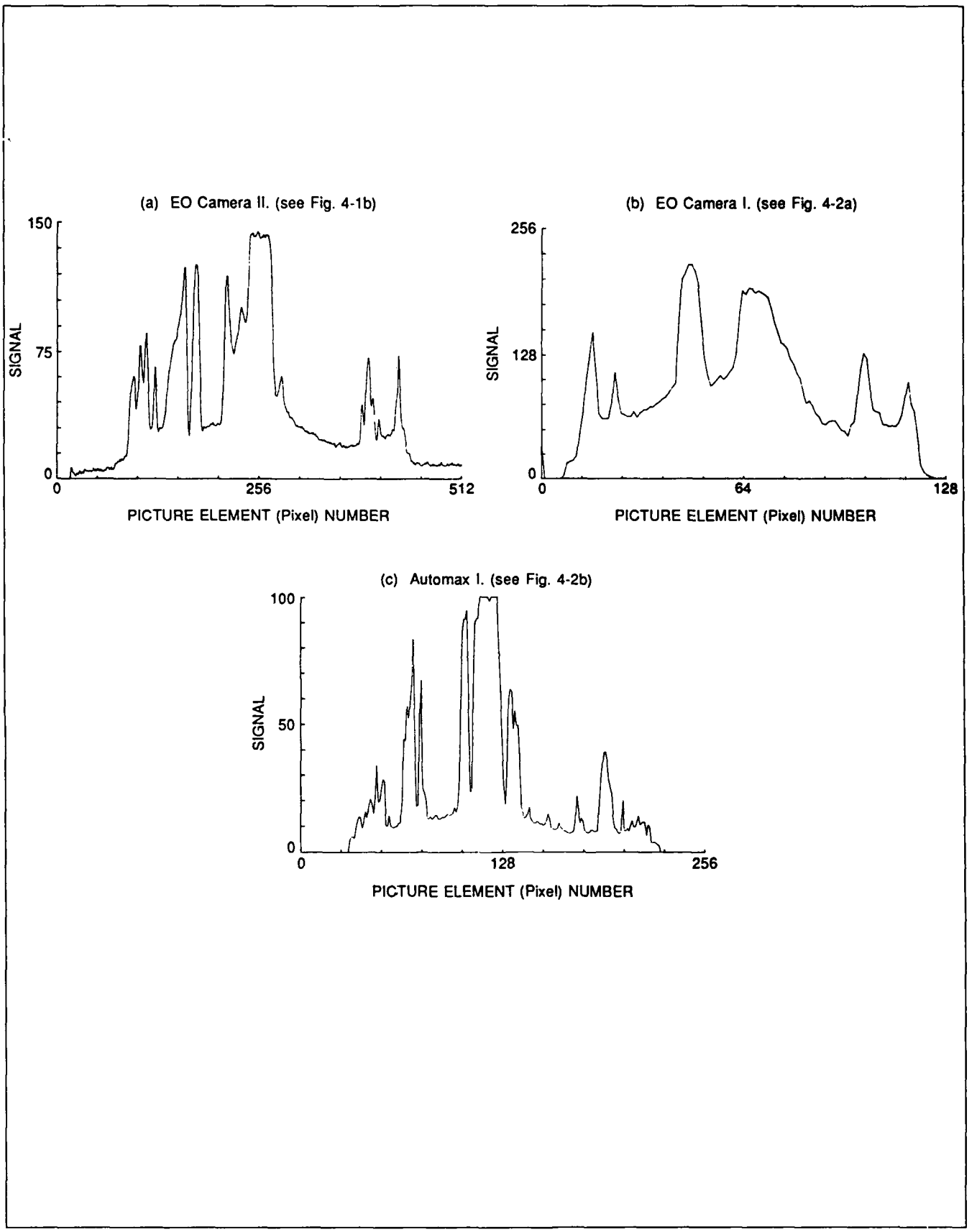

Fig. 4-3. Line plot of cumulus cloud image for EO Camera II, EO Camera I and Automax I. The data were acquired 3 SEP 84 near 1401 hours. Row 282 from EO Camera II and corresponding rows of EO Camera I and Automax I were extracted.

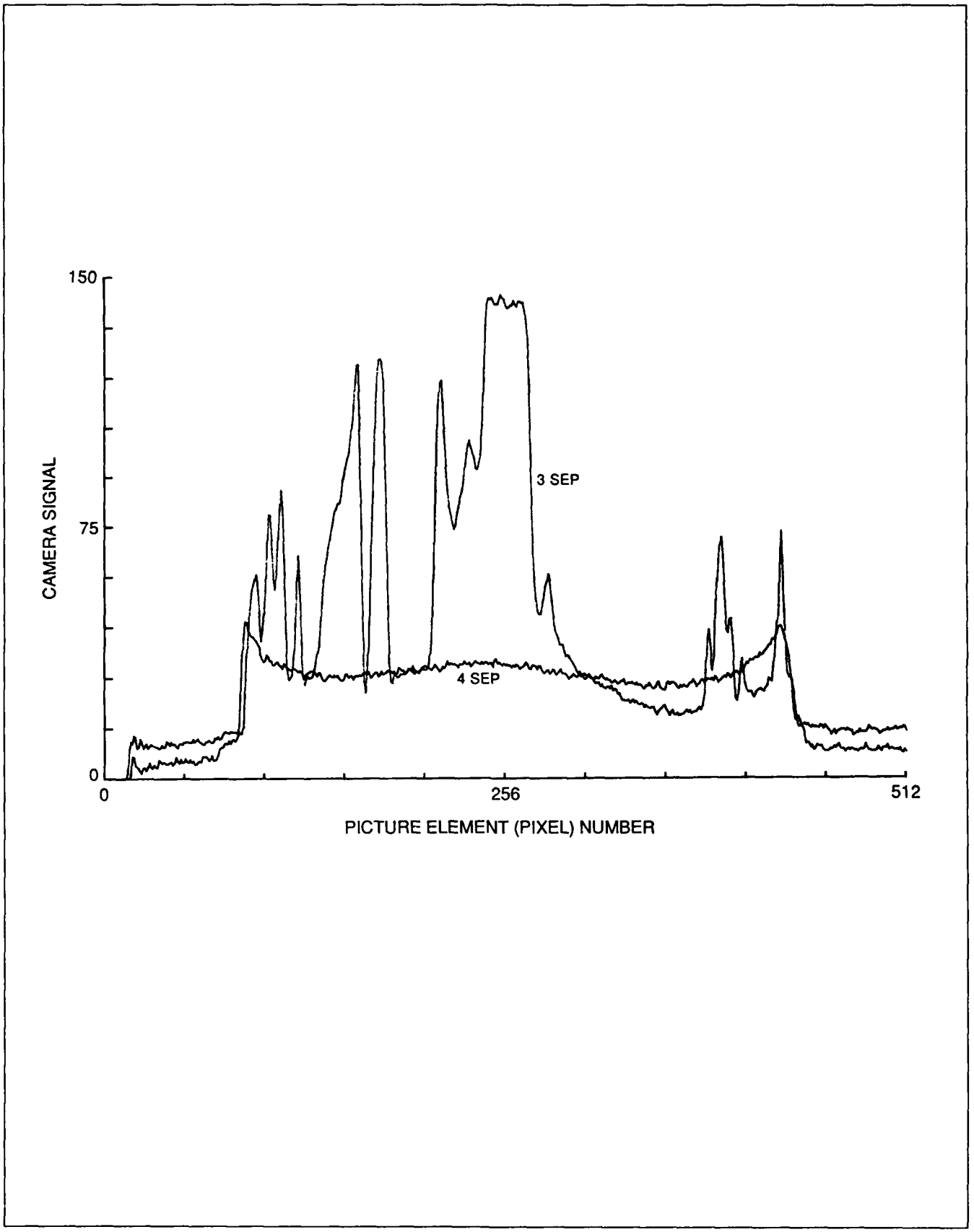

Fig. 4-4. Measured signal (from radiance at 650nm) as measured by the EO system on 3 SEP and 4 SEP 1984 at 1400 LST along an east-west arc passing near zenith. 3 SEP had broken cumulus, 4 SEP was clear.

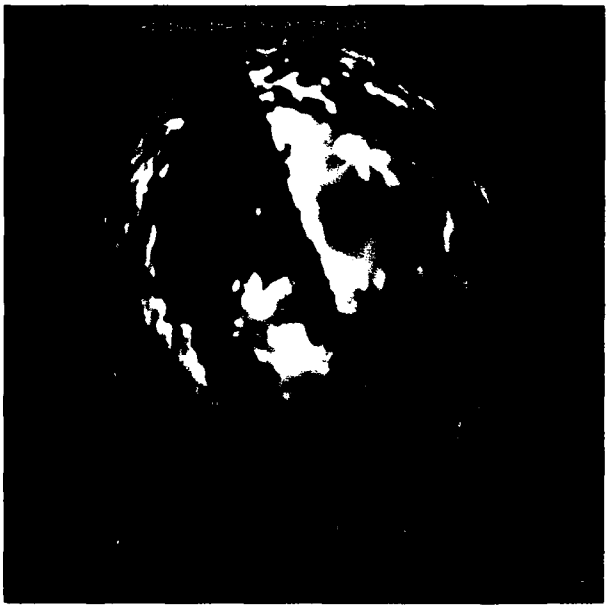

(a) Original image.

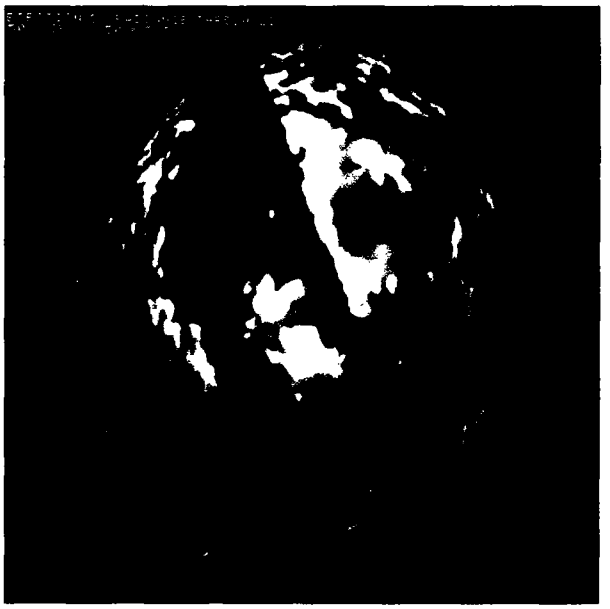

(b) Image with all signal levels less than 50 color-coded blue.

Fig. 4-5. Test of radiance thresholding for cloud detection.

(a) Pseudo gradient derived from image.

(b). Pseudo gradient color-coded red, superimposed on threshold color-coded image.

Fig. 4-6. Gradient information in cloud detection test image. 3 SEP 84 - 1401 hours.

(a) Ratio image. Ratios <1 coded blue, ratios <1.4 coded pink, ratios >1.4 coded grey.

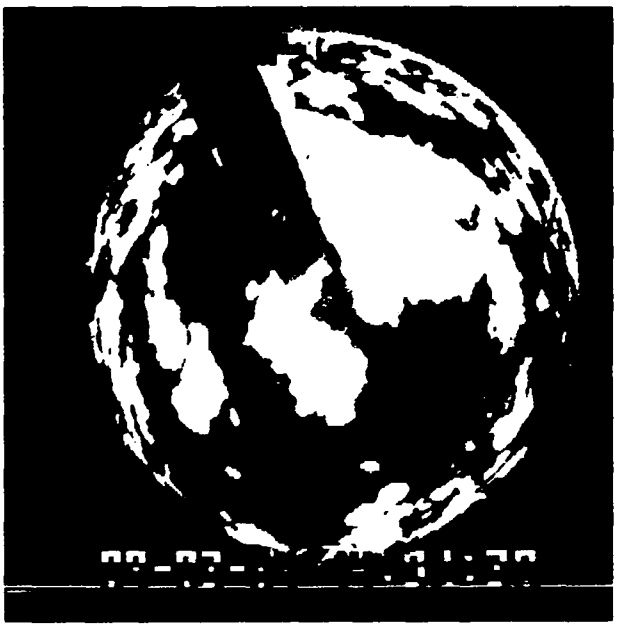

(b) Cloud discrimination result using a ratio threshold of 1.4.

Fig. 4-7. Test of cloud discrimination using ratio of test image to clear image data.

Fig. 4-8. Ratio of images taken with 0.7 log filter and 1.39 log filter, both acquired 11 SEP 84 - 1055.

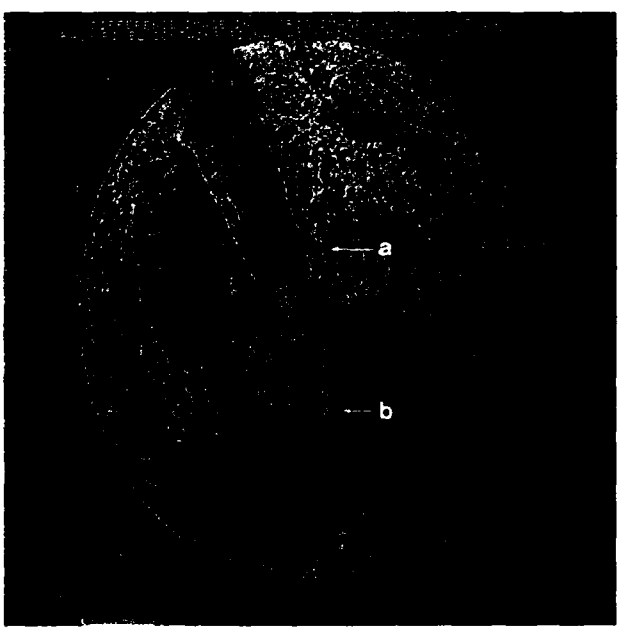

Fig. 4-9. Difference image, shows |signal (x) – signal (x+1)| 3 SEP 84 - 1401.

(a) Cross-sun case. 3 SEP 84 - 1401.

(b) Upsun case. 3 SEP 84 - 1657.

Fig. 4-10. Cloud discrimination for 1 row with hybrid algorithm, utilizing difference information as well as signal level.

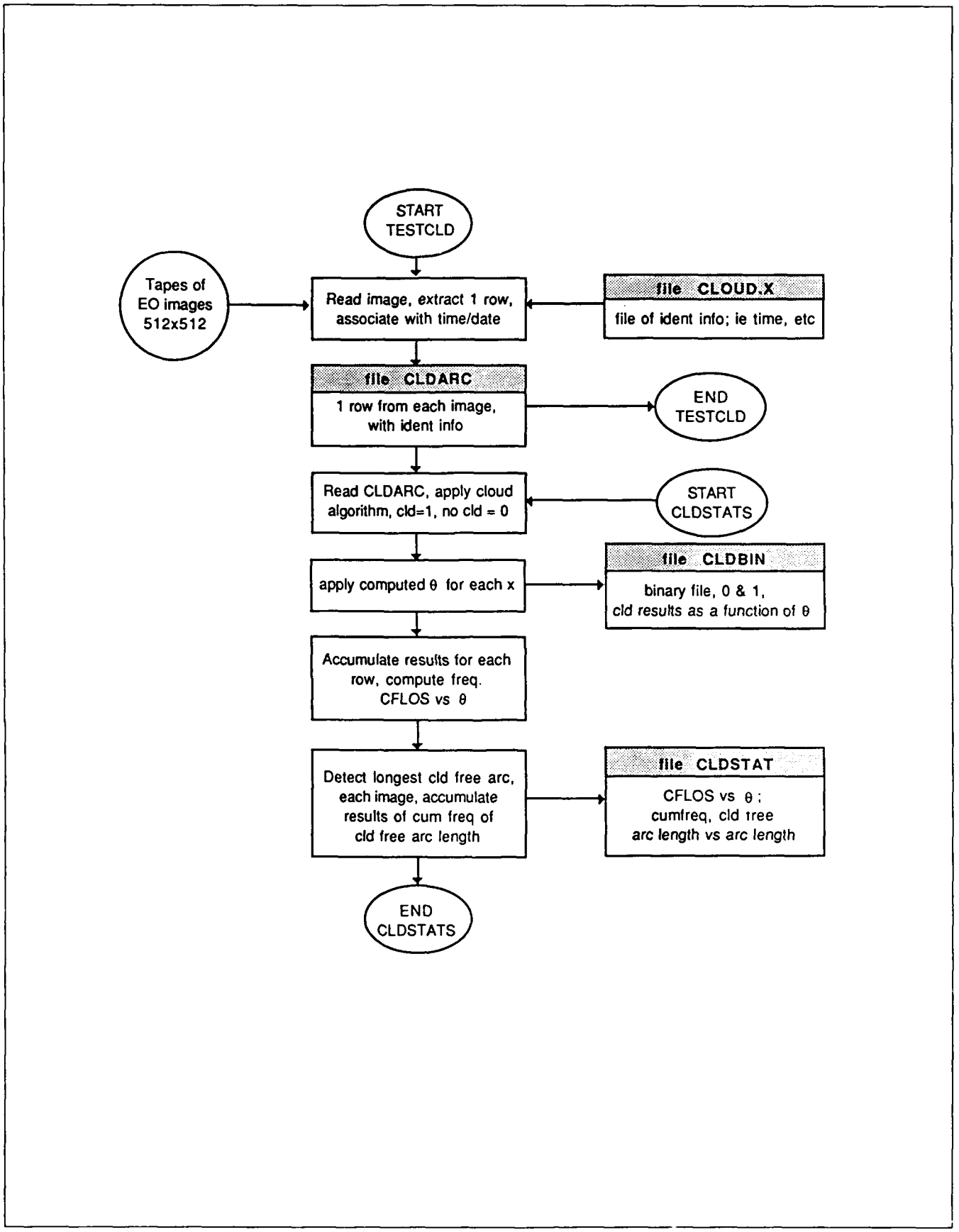

Fig. 5-1. Conceptualized chart of EO Camera data processing program.

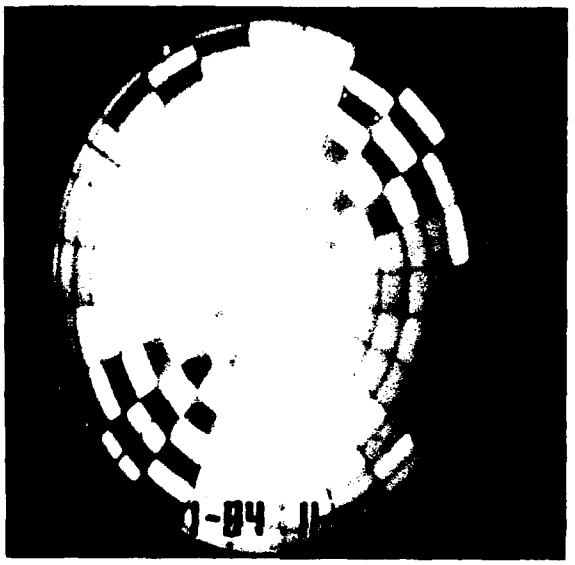

Fig. 5-2. Sample imagery utilized for geometric calibration.

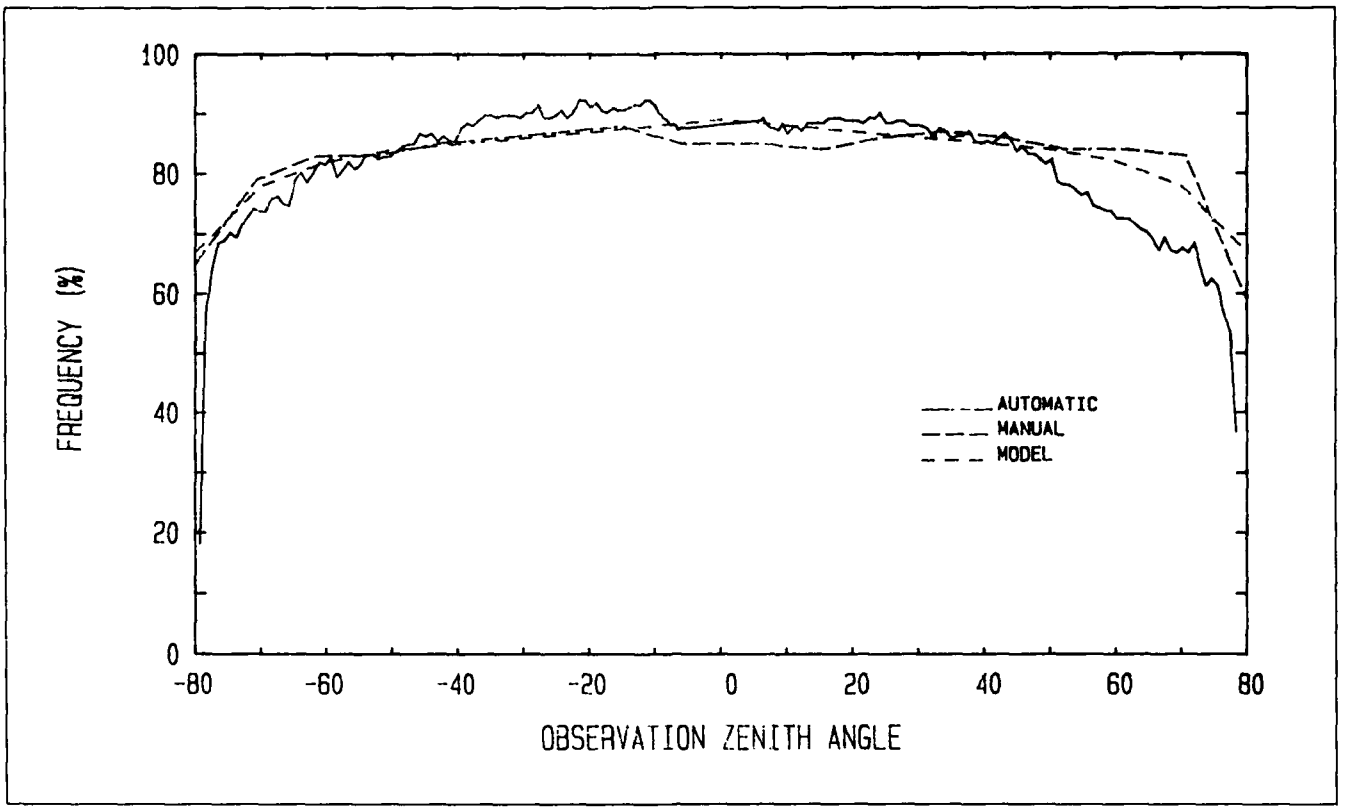

Fig. 5-3. Cloud free line of sight, frequency of occurrence vs zenith angle.

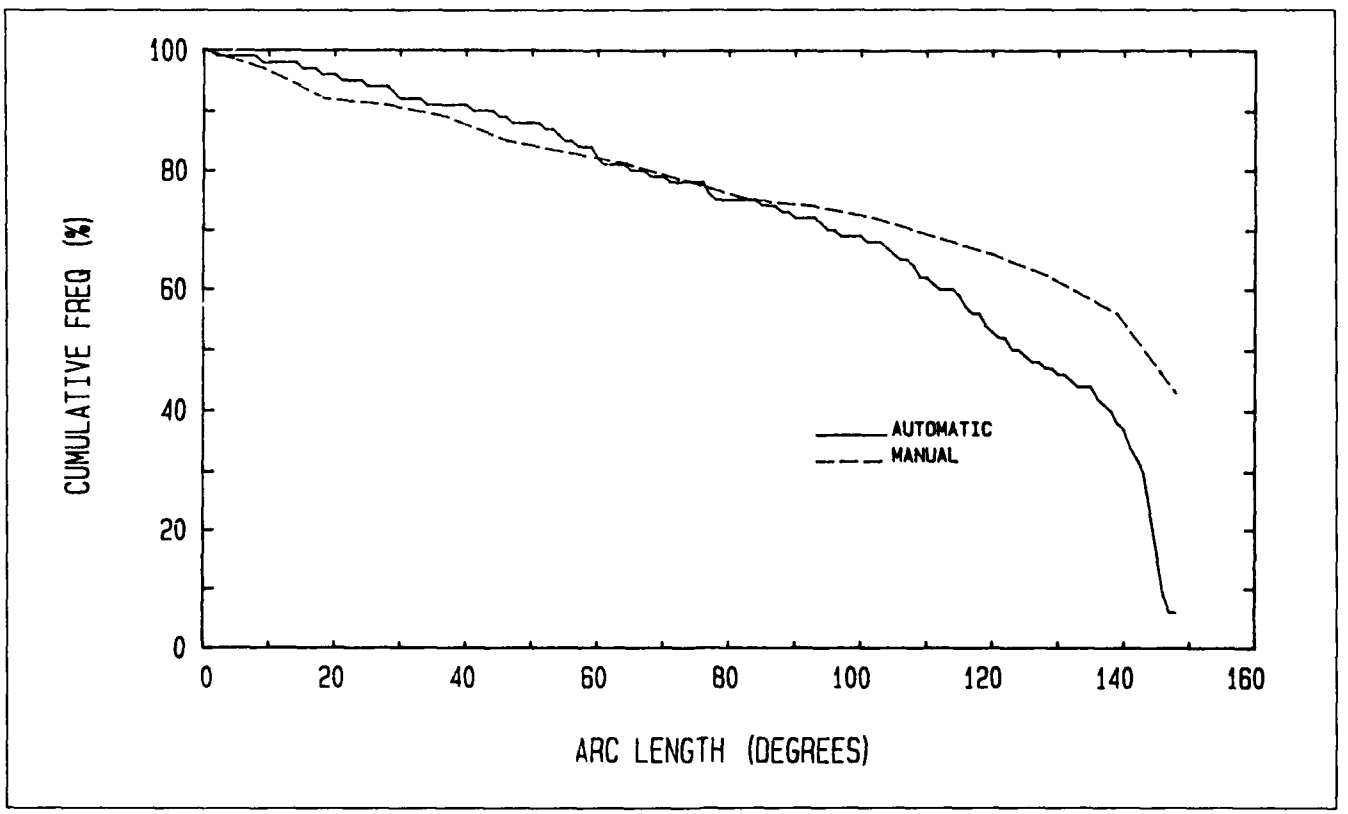

Fig. 5-4. Cloud free arc length, cumulative frequency of occurrence vs arc length.

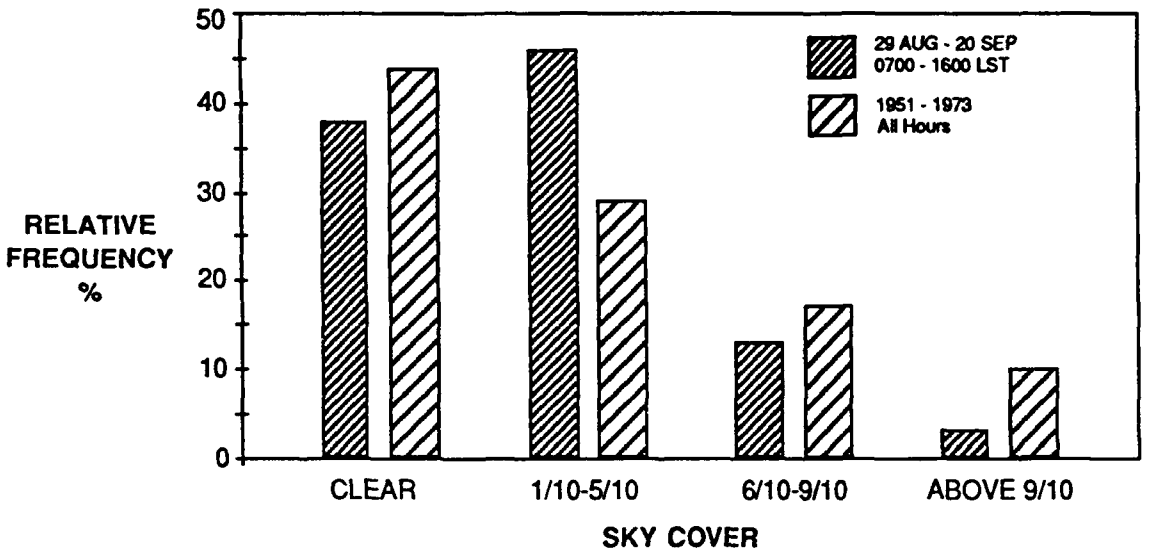

Fig. 5-5. Relative frequency of cloud cover at C station, White Sands Missile Range.

TN 200 Appendix A — Table A. WSMR demonstration/equipment list.

I. BACK-UP SYSTEM, EO CAM I

A. Detector Assembly

1. GE TN2200, 128X128 Solid State Camera, w/Controller.
2. C-130 Filter Assy. #8, (450nm, 605nm) – see AV84-063t (23 AUG 84).
3. Bicar Fisheye Lens Assembly, manual Iris acontrol.
4. Manual Solar Disc Occultor.
5. Prototype Irradiometer attachment (Cosmicor 19• FOV Back-up).

B. Monitor and Control Assemblies

1. C–130 Filter Control Panel.
2. Panasonic, model TR-920M Solid State T.V.
3. Dylon, model 1015B, Magnetic Tape Controller.
4. Cipher, model F880640-90-1025U, Magnetic Tape Drive.
5. Hewlett-Packard 9825 Computer.
6. Computerware 5809-based Computer/Controller.

C. Inter-connecting Cabling

II. PROTOTYPE SYSTEM, EO CAM II

A. Detector Assembly

1. GE TN2505, 242x370 Solid State Camera, w/power supply.
2. C–130 Filter Assy. #12, (650nm) – see AV84-063t (23 AUG 84).
3. Bicar Fisheye Lens Assembly, prototype remote control Iris.
4. Protype remote control Solar Disc Occultor.

B. Monitor and Control Assemblies

1. CRM Filter Control Panel.
2. Panasonic, model TR-920M Solid State TR.V.
3. Sony, model V05600, 3/4" VCR.
4. Inter-connecting Cabling.

III. PHOTOGRAPHIC CAMERA SYSTEMS (see AV84-052t/18 July 84)

A. Primary Camera, Automax, Model G1

1. Traid model 735, 180• Lens.
2. 100 ft. magazine.
3. Black and White Film, Kodak Plus-X.

B. Secondary Camera, Automax, Model G1

1. Traid model 735, 180• Lens.
2. 100 ft. magazine.
3. Color Film, Kodak VPS-3

C. Back-up Camera, 35mm SLR Hand-held

1. Bicar Fisheye Adaper.
2. 36 exposure individual roll film.
3. Black & White – Color.

D. Support Equipment

1. Autor..ax Remote Control Panel.
2. Time/Date Bracket for Automax.
3. Automax control Cables.

IV. PERIPHERAL SUPPLIES

A. Wratten N.D. Filters
B. Filter Cutters
C. Clear Cover Plates
D. Minor Repair Tool Kit
E. Optical Cleaning Kit
F. Magnetic Tape, 2400 ft. reels, 30
G. Tape Mailer Case
H. Data Logs
I. Procedural Check List

TN 200 Appendix B This section lists those EO Camera II images which have been extracted for data analysis. Whereas all of the fisheye images have been digitized and may be computer accessed, some of the fisheye images were special purpose images, such as extra data taken under certain cloud conditions. For the statistical analysis, one image for each hour has been extracted and included in the computations. The following table lists these images. In addition, on certain days when the sky was clear for several hours continuously, data were acquired every second hour. In these cases, the statistics program has treated the times with no data as having a clear sky. Those cases with clear sky but no data are listed in the second table.

In the first table, the date, time, F-stop, and neutral density filter were extracted from manual data logs. The tape file refers to the location on tape of the digitized image. The last column indicates the clear data image number which is closest in time, where 1 represents the image near 0800, 2 is 0900, and so on through clear image number 12 near 1900 hours.

EO Camera II Images Extracted for Analysis

CLOUD IMAGE#	DATE	TIME	F-STOP	N.D. FILTER	TAPE FILE	CLEAR COMP#
1	082984	0902	16	4	1	2
2	082984	1010	16	4	2	3
3	082984	1100	16	4	3	4
4	082984	1201	16	5	4	5
5	082984	1300	16	5	5	6
6	082984	1401	16	5	6	7
7	082984	1500	16	4	7	8
8	082984	1607	16	4	8	9
9	082984	1702	16	4	9	10
10	082984	1802	16	4	10	11
11	083084	0804	16	5	11	1
12	083084	0901	16	5	12	2
13	083084	1001	16	4	13	3
14	083084	1105	16	4	14	4
15	083084	1203	16	3	15	5
16	083084	1302	16	3	16	6
17	083184	0808	11	5	17	1
18	083184	0904	11	4	18	2
19	083184	1000	11	5	19	3
20	083184	1112	11	4	20	4
21	083184	1202	11	4	21	5
22	083184	1259	11	4	22	6
23	083184	1411	11	4	23	6
24	083184	1507	11	4	24	8
25	083184	1607	11	4	25	9
26	083184	1701	11	4	26	10
27	083184	1753	11	5	27	11
28	083184	1902	11	4	28	12
29	083184	1927	11	6	1	12
30	090184	0816	11	4	2	1
31	090184	0901	11	4	3	2
32	090184	0952	11	4	4	3
33	090184	1054	11	4	5	4
34	090184	1156	11	4	6	5
35	090184	1301	11	4	7	6
36	090184	1358	11	3	8	7
37	090184	1512	11	4	9	8
38	090184	1602	11	3	10	9
39	090184	1656	16	3	11	10
40	090184	1754	16	5	12	11
41	090284	0753	11	4	13	1
42	090284	0900	16	3	14	2
43	090284	1002	11	3	1	3
44	090284	1115	11	4	2	4

APPENDIX A

CLOUD IMAGE#	DATE	TIME	F-STOP	N.D. FILTER	TAPE FILE	CLEAR COMP#
45	090284	1159	11	3	3	5
46	090284	1302	11	4	4	6
47	090284	1356	11	4	5	7
48	090284	1458	11	3	6	8
49	090284	1549	11	3	7	9
50	090283	1655	11	3	8	10
51	090284	1757	11	4	9	11
52	090384	0757	16	4	10	1
53	090384	0855	16	4	11	2
54	090384	1001	16	4	12	3
55	090384	1057	11	4	13	4
56	090384	1151	11	3	14	5
57	090384	1255	11	3	15	6
58	090384	1401	11	3	16	7
59	090384	1453	11	3	17	8
60	090384	1556	11	3	18	9
61	090384	1657	11	3	19	10
62	090384	1756	11	4	20	11
63	090484	0750	11	4	21	1
64	090484	0853	11	4	22	2
65	090484	0950	11	3	23	3
66	090484	1100	11	3	24	4
67	090484	1153	11	4	25	5
68	090484	1248	11	3	26	6
69	090484	1352	11	4	27	7
70	090484	1503	11	4	28	8
71	090484	1558	11	3	1	9
72	090484	1654	11	4	2	10
73	090484	1748	11	4	3	11
74	090584	0814	11	4	4	1
75	090584	0853	11	4	5	2
76	090584	0954	11	4	6	3
77	090584	1053	11	3	7	4
78	090584	1204	11	3	8	5
79	090584	1259	11	4	9	6
80	090584	1356	11	3	10	7
81	090684	0756	11	4	11	1
82	090684	0858	11	3	12	2
83	090684	1011	11	3	13	3
84	090684	1150	11	3	14	5
85	090684	1257	11	3	15	6
86	090684	1359	11	3	17	7
87	090684	1458	11	3	18	8
88	090684	1555	11	3	19	9
89	090684	1657	11	4	20	10
90	090784	0815	11	4	21	1
91	090784	0900	11	3	22	2
92	090784	0958	11	4	23	3
93	090784	1054	11	4	24	4
94	090784	1156	11	4	25	5
95	090784	1257	11	4	26	6
96	090784	1359	11	4	27	7
97	090784	1455	11	4	28	8
98	090784	1551	11	3	1	9
99	090784	1655	11	4	2	10
100	090884	0856	11	4	3	2
101	090884	1000	11	4	4	3
102	090884	1056	11	4	5	4

CLOUD IMAGE#	DATE	TIME	F-STOP	N.D. FILTER	TAPE FILE	CLEAR COMP#
104	090884	1259	11	4	6	6
105	090884	1356	11	2	7	7
106	090884	1429	11	2	8	8
107	090884	1551	11	3	9	9
108	090884	1701	11	4	10	10
109	090984	0857	11	4	11	2
111	090984	1054	11	4	12	4
115	091084	0820	11	2	13	1
116	091084	0849	11	4	17	2
117	091084	0951	11	4	18	3
118	091084	1052	11	4	19	4
119	091084	1155	11	5	20	5
120	091084	1257	11	4	21	6
121	091084	1404	11	4	22	7
122	091084	1453	11	4	23	8
123	091084	1607	11	3	24	9
124	091084	1702	11	4	26	10
125	091084	1758	11	4	1	11
126	091084	1850	11	5	3	12
127	091184	0754	11	3	6	1
128	091184	0854	11	3	9	2
129	091184	1000	11	3	11	3
130	091184	1055	11	4	12	4
131	091184	1154	11	2	14	5
132	091184	1300	11	4	15	6
133	091184	1355	11	2	19	7
134	091184	1457	11	2	21	8
135	091184	1551	11	2	24	9
136	091184	1654	11	2	26	10
137	091184	1752	11	3	1	11
138	091284	0801	11	5	3	1
139	091284	0855	11	4	4	2
140	091284	0951	11	4	5	3
141	091284	1058	11	3	6	4
142	091284	1155	11	4	7	5
143	091284	1252	11	2	8	6
144	091284	1353	11	2	9	7
145	091284	1450	11	2	11	8
146	091284	1555	11	2	12	9
147	091384	0754	11	4	14	1
148	091384	0851	11	4	15	2
149	091384	0952	11	3	16	3
150	091384	1054	11	3	17	4
151	091384	1153	11	3	18	5
152	091384	1306	11	3	19	6
153	091384	1354	11	3	20	7
154	091384	1548	11	2	21	9
155	091384	1700	11	2	24	10
156	091384	1759	11	5	27	11
157	091484	0806	11	2	1	1
158	091484	0852	11	4	3	2
159	091484	0953	11	4	4	3
160	091484	1043	11	4	5	4
161	091484	1150	11	3	6	5
162	091484	1248	11	4	7	6
163	091484	1346	11	4	8	7
164	091584	0758	5.6	4	9	1
165	091584	0850	16	4	10	2

APPENDIX A

CLOUD IMAGE#	DATE	TIME	F-STOP	N.D. FILTER	TAPE FILE	CLEAR COMP#
166	091584	0948	16	4	11	3
167	091584	1050	16	3	12	4
168	091584	1148	16	3	13	5
169	091584	1300	16	2	14	6
170	091584	1346	16	2	15	7
171	091584	1454	16	3	16	8
172	091584	1547	16	3	17	9
173	091584	1647	16	3	18	10
174	091584	1747	11	3	19	11
175	091684	0754	11	3	20	1
176	091684	0851	16	3	21	2
177	091684	0955	16	2	22	3
179	091684	1154	16	2	23	5
181	091684	1351	16	3	24	7
182	091684	1450	16	2	25	8
183	091684	1552	16	3	26	9
184	091684	1649	16	3	27	10
185	091684	1747	11	2	28	11
186	091784	0755	8	2	1	1
187	091784	0852	11	3	2	2
189	091784	1049	16	3	3	4
191	091784	1251	16	3	4	6
192	091784	1353	16	3	5	7
193	091784	1449	16	3	6	8
194	091784	1554	16	3	7	9
195	091784	1652	16	3	8	10
196	091784	1754	16	3	9	11
197	091884	0750	8	3	10	1
199	091884	0953	16	4	11	3
201	091884	1156	16	4	12	5
202	091884	1254	16	3	13	6
203	091884	1350	16	2	14	7
204	091884	1456	16	3	15	8
205	091884	1550	16	3	16	9
206	091884	1653	16	3	17	10
207	091884	1746	5.6	3	18	11
208	091984	0753	5.6	3	19	1
209	091984	0849	5.6	3	20	2
211	091984	1053	16	4	21	4
213	091984	1248	16	4	22	6
214	091984	1351	16	4	24	7
215	091984	1449	16	3	25	8
216	091984	1552	16	4	26	9
217	091984	1658	16	4	27	10
218	091984	1757	16	4	28	11
219	092084	1252	8	2	1	6
220	092084	1355	16	3	2	7
221	092084	1452	16	3	3	8
222	092084	1551	16	3	4	9
223	092084	1651	16	4	5	10
224	092084	1754	11	3	6	11
225	092184	0752	4	3	7	1
226	092184	0854	11	3	8	2
227	092184	0954	16	4	9	3
228	092184	1049	16	4	10	4
229	092184	1144	16	4	11	5
230	092184	1248	16	4	12	6
231	092184	1350	16	4	13	7

CLOUD IMAGE#	DATE	TIME	F-STOP	N.D. FILTER	TAPE FILE	CLEAR COMP#
232	092184	1450	16	5	14	8
233	092184	1552	16	5	15	9

Clear Sky Incidents without recorded data

CLOUD IMAGE#	DATE	TIME
103	090884	1200
110	090984	1000
112	090984	1200
113	090984	1300
114	090984	1400
178	091684	1100
180	091684	1300
188	091784	1000
190	091784	1200
198	091884	0900
200	091884	1100
210	091984	1000
212	091984	1200

ATMOSPHERIC VISIBILITY
TECHNICAL NOTE NO. 201

MAY 1986

A MULTI-SPECTRAL IMAGER FOR THE AUTOMATIC DETERMINATION OF SECTOR VISIBILITIES AND THE CONCURRENT OPTICAL STATE OF THE ATMOSPHERE

R.W. Johnson
W.S. Hering

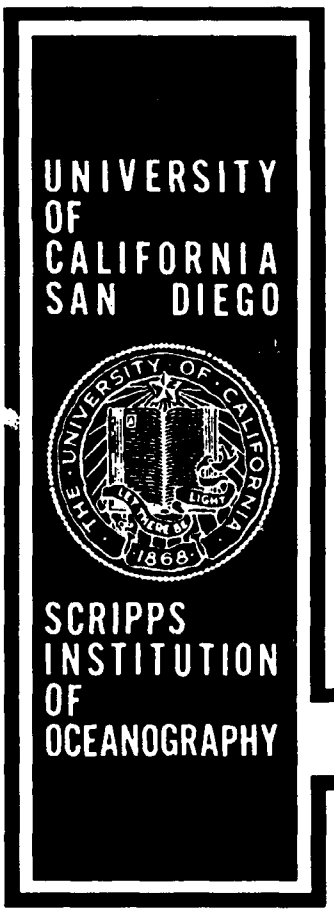

Contract Monitor, Donald D. Grantham
Atmospheric Sciences Division

Prepared for
Air Force Geophysics Laboratory, Air Force Systems Command
United States Air Force, Hanscom AFB, Massachusetts 01731

VISIBILITY LABORATORY La Jolla, California 92093

APPENDIX B

TABLE OF CONTENTS

LIST OF TABLES AND ILLUSTRATIONS

A MULTI-SPECTRAL IMAGER FOR THE AUTOMATIC DETERMINATION OF SECTOR VISIBILITIES AND THE CONCURRENT OPTICAL STATE OF THE ATMOSPHERE

Richard W. Johnson and Wayne S. Hering

Visibility Laboratory
University of California, San Diego
Scripps Institution of Oceanography
La Jolla, California 92093

INTRODUCTION

The proliferation of advanced military electro-optical (E/O) systems that are designed for visible spectrum operations within the troposphere has greatly increased the need for a compact automatic system designed to assess and predict the optical and meteorological properties of this operational medium.

The Visibility Laboratory, under the sponsorship of the Air Force Geophysics Laboratory, is developing a family of small, solid state imaging systems to address this need. Several existing and developing versions of these devices and their proposed uses are described briefly in the following paragraphs and illustrations.

In its most basic form, each of these devices consists of a computer controlled solid state video system that provides calibrated multi-spectral imagery suitable for the automatic extraction of local image transmission and cloud cover information. Imbedded within the control computer are prototype and proprietary extraction algorithms necessary to provide these numerical products. In addition to radiometrically calibrated imagery, advanced algorithm development is currently underway to provide near real-time products of the data acquisition, processing, and display system in the form of continuously updated digital presentations of selected operational quantities. The quantities most desired for describing the optical state of the atmosphere in which this sensor system operates are of course task dependent, but current algorithm development is slanted toward cloud detection, cloud free arc determinations, sector visibilities and total cloud cover. The multi-spectral imagery is equally applicable in more generalized search, detect and identify scenarios.

FIRST GENERATION INSTRUMENTATION

The system block diagram shown in Fig. A is intended to illustrate configurational relationships common to all systems described herein, and is not necessarily an as-built drawing. For example, the "select" function linking the Z-100 computer and the Time/Date Generator is conceptual only. Both the video and digital data are routed through the system simultaneously and independently. The parallelism is an operator convenience, not a necessity. Most of the operational characteristics illustrated in Fig. A are included in each of the currently evolving hardware configurations.

Several versions of the basic computer controlled system designed for the semi-automatic acquisition and archival of calibrated imagery are illustrated in Figs. B thru E. Their component sub-assemblies are listed in Table A.

The schematic drawing of the multi-spectral imager shown in Fig. B illustrates two important features of the camera system that contribute to its general utility.

First, the Filter Changer Assembly is shown to contain two independently controlled filter locations on the optical axis. In actuality, this assembly contains two filter wheels, each holding four separate filters in addition to the five lens optical relay. Each wheel can position any one of its four filters into the optical path under either manual or computer control. In its present configuration, the forward wheel contains four glass absorption neutral density filters, while the rear wheel contains four spectrally different interference filters. Thus, both spectral band and flux level can be controlled either manually or by predetermined computer program.

Second, the multi-lens Turret Assembly (shown pictorially, not as built), provides an efficient method of modifying the overall optical path to meet task specific requirements. In the prototype systems currently in use, the two lens assemblies require manual substitution into a fixed adapter. The remotely controlled turret assembly is still under development, as are the remote control of the Iris and Occultor sub-assemblies. However, it is important to note that the system lends itself well to task specific changes in turret design.

The composite, as-built system shown in Fig. C is the currently operating Z-100 system. Both the video and digital options previously illustrated are contained in the two instrument racks. The camera, filter changer, and fisheye lens assembly, are supported on the temporary camera pedestal. This successfully deployed operational system is designed primarily for image acquisition and archival only. The computer does not contain the programmed algorithms necessary for sophisticated image manipulation and analysis, although relatively simple data extractions and numerical computations are readily available. The system can reliably acquire an image every two seconds and store it on the internal hard disk. Identifying time/date and filter information is imbedded within each image data array for subsequent processing and analysis control. At the present time 360 images are stored on disc prior to their batch mode downloading to magnetic tape. A simplified version of this system, similar to that in Fig. C only without the VCR mode, is illustrated in Fig. D.

The fundamental shortcoming of this computer system is its limitation to eight bit I/O, and lack of image-oriented, third party software/firmware support. The first generation systems shown in Figs. C and D both use the GE2505A2 solid-state CID video camera as the primary detector. This camera outputs a standard RS170 composite video signal which is grabbed and digitized by the Poynting 505 frame grabber. The resultant 8-bit 256x256 data array is subsequently operated upon to yield an image that is radiometrically calibrated in absolute radiance units traceable to the National Bureau of Standards. Geometric calibrations are performed on the array such that with the 174(degree) Fisheye adapter lens in place the system yields an angular resolution of approximately 0.7 deg/pixel, and with the 30(degree) small FOV lens in place yields approximately 0.1 deg/pixel resolution.

SYSTEM CALIBRATION

Whereas many useful algorithms for the determination of atmospheric properties can be devised to require only the input of the relative values of radiant flux fields, it is generally true that far more redundant and reliable methodologies are available when absolute values of radiance are available. Thus, to enable an optimum selection of techniques for analytic applications, the camera systems described in this note are all calibrated against standards of radiant intensity traceable to N.B.S. The general calibration procedures are outlined in Fig. F.

The step-by-step sequences required to accomplish the procedures outlined in Fig. F, are discussed in detail within several separate notes and will not be addressed herein. The key feature underlying all of the calibration sequences is, of course, the stability and reproducibility of the system radiometric linearity. Two examples of the Linearity Calibration conducted on the systems illustrated in Fig. C are shown in Fig. G.

SECOND GENERATION INSTRUMENTATION

Having satisfactorily demonstrated the ability to rapidly and reliably acquire and archive calibrated whole sky imagery with the Z-100 based systems described above, there was an immediate recognition that an even more powerful tool was clearly within our grasp. By increasing the image manipulation capabilities within the host computer, and by further customizing the optical collection optics, it seemed possible to create an acquisition and computational environment suitable for advanced, automatic determinations of the optical state of the atmosphere. The following paragraphs describe the cogent electro-optical and computational characteristics of this emerging system.

The evolution of the second generation system is defined by two basic changes. First to an enhanced host computer, and second to a more exotic optical turret". Other than that the system concept remains the same, calibrated imagery is manipulated to mimic the observational skills of a human observer.

With regard to the first change, it was felt that a true 16-bit machine was necessary to handle the data flows and computational techniques anticipated. Since the early Z-100 systems had performed well, it was decided to stay within the Zenith environment, but to upgrade to their IBM clone, the Z-200 series, in order to avail ourselves of the rapidly expanding IBM support within the third party vendor market. Following this plan, the second generation system outlined in Table A has been partially acquired and exercised. Most of the algorithm development and preliminary computations discussed later in this note have been performed in the Z-200 environment. Other than some minor inconveniences in fully exploit-

ing the computer's enhanced RAM (1.2 MB) via the LOTUS 1-2-3 code, the computer system has performed well. It is anticipated that both the second and third generation systems will continue to use the Z-200 family computer. Only the tenant IP systems will change, in association with future task specific I/O and display requirements.

The revision of the system to incorporate a second generation "turret" has required several iterations of optical mock-up and evaluation. The sensor assembly currently proposed for use is illustrated in Fig. E. In this semi-exploded pictorial, the essential features of this emerging system are clearly illustrated.

The "turret" has become a rotating stage assembly upon which are mounted a telephoto lens for scanning the local horizon, a prismatic beam splitter, and a mechanical two aperture shutter assembly. Rotation of the shutter about the optical axis of the beam splitter controls which of two image sets are transmitted through the filter changer to the fixed camera. In one position the optical path of sight is through the fisheye lens, and whole sky images are acquired for the determination of local cloud cover, cloud-free paths of sight, etc. In the second position, the optical path of sight is through the telephoto lens, and small field of view images containing the local horizon are acquired for the determination of sector visibilities.

The entire electro-optical assembly is contained within an insulated weatherproof housing. The remaining design problems relate to the inevitable problems associated with maintaining optically clean windows through which the lenses must collect their imagery. While the solution of these problems will involve some severe aggravation, the fundamental concept of the device should remain uncompromised.

The third generation system summarized in Table A represents two refinements to the basic Z-200 system. The first is a change to the more powerful Image Technology FG-100 Frame Grabber, and the second is a change to the 2710 camera. Both changes are directed toward improving the precision and accuracy of the radiometric calibrations and do not imply a change in the basic philosophy underlying the systems performance.

SYSTEM PERFORMANCE CAPABILITIES

The dedicated system which combines solid-state image sensing capability with microcomputer technology is ideal for the acquisition, processing, and analysis of background sky, cloud and terrain radiance fields. Measurement accuracy and operational efficiency are achieved through:

(a) excellent control over both the spatial resolution and the relative brightness accuracy. Since each pixel element has exact placement in the solid-state sensor array, the geometry is fixed. Thus, any imperfection in discrete element performance can be diagnosed and specific corrections applied. The responses tend to be highly linear and stable so that the corrections for individual pixels are easily made and tend to be valid for extended time periods.

(b) the rapid response of the solid state detectors with no memory problems. Thus, once the brightness field is read out, it is immediately set for renewed data acquisition and provides excellent temporal resolution.

(c) the digital data format, which allows quick and easy computer conversion of the relative brightness field into the absolute radiance field for direct determination of the optical properties of the atmosphere.

BASIC EXPRESSIONS FOR VISIBILITY DETERMINATION

Each pixel value in the resultant computer processed image is the calibrated apparent radiance of the corresponding line of sight. Let us now consider the application of these data for quantitative determination of atmospheric clarity as represented by specific estimates of the prevailing visibility or the visual range for designated lines of sight.

Neglecting turbulence effects, the apparent spectral radiance of a distant object t at range r along a path of sight specified by zenith angle θ and azimuthal angle ϕ, can be written (see Duntley *et al.*, 1957)

where

$$ {}_tL_r(z, \theta, \phi) = T_r(z, \theta)\, {}_tL_o(z_t, \theta, \phi) + L_r^*(z, \theta, \phi) \qquad (1) $$

${}_tL_o$ is the inherent target radiance at altitude z_t corresponding to a measurement at zero range on the path of sight.

T_r is the radiance transmittance or the fraction of the inherent radiance remaining after traversing the optical path of length r.

L_r^* is the path radiance generated by the light reaching the path of sight from the sun and the surrounding sky and terrain and in turn is scattered by the air molecules and aerosol particles along the path in the direction of the sensor located at altitude z.

Similarly, the apparent radiance of the background b, immediately adjacent to the target is given by

$$ {}_bL_r(z, \theta, \phi) = {}_bL_o(z_t, \theta, \phi)\, T_r(z, \theta) + L_r^*(z, \theta, \phi) \qquad (2) $$

where

${}_bL_o$ is the inherent radiance of the background at range zero (target position).

The radiance transmittance is given by

$$ T_r = \exp = \int \alpha(r)\, dr \qquad (3) $$

where

α is the volume attenuation coefficient and is equal to the sum of the scattering (α_s) and absorption (α_a) extinction coefficients.

The inherent spectral contrast is defined

$$ C_o(z_t, \theta, \phi) = [{}_tL_o(z_t, \theta, \phi) - {}_bL_o(z_t, \theta, \phi)] / {}_bL_o(z_t, \theta, \phi) \qquad (4) $$

and the corresponding definition for apparent spectral contrast at range r is

$$ C_r(z, \theta, \phi) = [{}_tL_r(z, \theta, \phi) - {}_bL_r(z, \theta, \phi)] / {}_bL_r(z, \theta, \phi). \qquad (5) $$

Subtracting Eqs. (1) and (2) and combining with Eqs. (4) and (5), it follows that

$$ C_r(z, \theta, \phi) / C_o(z_t, \theta, \phi) = T_r(z, \theta, \phi)\, {}_bL_o(z_t, \theta, \phi) / {}_bL_r(z, \theta, \phi). \qquad (6) $$

As emphasized by Duntley *et al.*, (1957) the above expression for the contrast transmittance of the path of sight is the law of contrast reduction in its most general form. It applies to any path of sight regardless of the extent that the ambient light or the optical scattering properties of the atmosphere vary from point to point.

DETERMINATION OF DAYTIME VISIBILITY

The process of daytime visibility determination either instrumentally or by a human observer ultimately involves the resolution of the distance from pre-selected targets that the apparent contrast, C_r, reduces to some minimum (threshold) value needed for detection. The threshold contrast is dependent on a number of factors including the visual acuity of the observer as well as the angular subtense of the target, its shape and its location with respect to background features. Human estimates of visibility result from adaptive integration by the eye in time and space of all scene features. However, for official observations the World Meteorological Organization (WMO) and the Federal Meteorological Handbook (FMH) recommend that daytime visibility targets be black or very dark targets viewed against the background sky. However, in order to achieve adequate areal coverage, objects pre-selected for visibility markers for routine meteorological observations often are less than ideal both in angular size and inherent optical properties.

With these problems in mind, let us consider the general approach involved in the application of the solid-state, EO camera system to visibility measurement. The goal is to develop a completely automated system to provide objective quantitative estimates that are consistent regardless of time and location. The degree of visual modeling required to provide, for example, the visual range along specific pre-selected horizontal or slant paths depends upon the accuracy needed to satisfy the individual user requirements. In the following discussion, we limit attention to the more general problem of determining prevailing visibility, which is defined by Douglas and Booker (1977) as the greatest visibility equal or excluded through at least half of the horizon circle which need not be continuous, *i.e.* the median visibility around the horizon circle. The EO camera system provides a continuously updated representation of the detailed radiance scene for the discrimination of prevailing visibility and its sector variations. The objective is to use effectively the measured apparent radiance contrast for all suitable objects in the scene, adjusting the resultant visibility estimates as necessary to compensate for the non-standard nature of individual targets.

We note that for the common situation where an object is viewed against the clear horizon sky, the inherent background radiance, ${}_bL_o$, as measured at the target position and the apparent background radiance at the measuring point, ${}_bL_r$, tend to be equal. To a good first approximation, the horizon sky brightness does not change appreciably as one approaches or backs away from the target. Thus, Eq. (6) for the contrast transmittance reduces to

(Note: henceforth for convenience, the directional notation will be omitted in most cases)

$$ C_r / C_o = T_r = e^{-\alpha} \qquad (7) $$

where

α is the average attenuation coefficient for path of sight of length r.

If the object is at the maximum range of detection

$$\varepsilon = C_o e^{-\alpha V_c} \quad (8)$$

where

ε is the threshold contrast. A value of .05 is recommended by the WMO.

V_c is the corresponding object range and is the visibility as determined from the measured apparent contrast of the object.

From Eq. (4) we see that the for the special case of a black target, ${}_bL_o=0$, the inherent contrast, C_o is always -1. Since the contrast cannot change sign with distance along the path of sight, the negative sign can be ignored. So, for the black target viewed against the horizon sky Eq. (7) may be written simply as

$$C_r = T_r \quad (9)$$

and if the object is just visible

$$\varepsilon = e^{-\alpha V_N} \quad (10)$$

where

V_N is the visibility as determined for a black target with horizon sky background which we define as standard conditions or the "normalized visibility".

If we solve for V_c and V_N and divide Eq. (10) by Eq. (8) we have

$$V_N = V_c \ln \varepsilon / (\ln \varepsilon - \ln C_o) . \quad (11)$$

Thus, for objects with horizon sky background, the normalization adjustment of the visibility as determined for objects other than black is independent of the transmittance and the directional scattering properties of the atmosphere, but is a function of the inherent contrast, C_o.

Additional modeling procedures are required to obtain reliable estimates of prevailing visibility from the measured apparent contrast of objects viewed against a terrestrial background. For the essentially horizontal paths of sight involved in visibility determinations, Eq. (2) for the apparent background radiance may be written with good approximation (Duntley, 1948)

$${}_bL_r = {}_bL_o T_r + L_q (1 - T_r) \quad (12)$$

and

$$L_q (z, \theta, \phi) = \int L (z, \theta', \phi') P (z, \beta) d\Omega \quad (13)$$

where

L_q is the point source function of the path radiance and is the radiance that must exist at each point such that the loss of radiance within that path segment is balanced by the gain

P is the single scattering phase function

β is the scattering angle between ambient source light direction and path of sight.

In effect, Eq. (12) assumes that L_q is spatially constant for the integration of the path function over range, r. Notice that, for the long path length associated with the horizon sky background, T_r tends to zero and the apparent clear-sky horizon radiance, ${}_bL_r$ is equal to the source function (equilibrium radiance), L_q, for the corresponding scattering angle with respect to the sun.

Substituting Eq. (12) in Eq. (6) and solving for the apparent contrast, C_r, we have,

$$C_r = C_o T_r / [S + T_r (1-S) \quad (14)$$

where

$S = L_q / {}_bL_o$ is the sky/ground radiance ratio (Duntley, 1948).

If the object is just visible, $C_r = \varepsilon$ and re-arranging terms we have

$$e^{-\alpha V_c} = \varepsilon S / [C_o - \varepsilon (1 - S)] . \quad (15)$$

Dividing Eq. (10) by Eq. (15), the expression for the normalization of the visibility, V_c, as determined for the general target to the visibility corresponding to the standard black target conditions, V_N, is given by

$$V_N = V_c \ln \varepsilon / \{\ln (\varepsilon S) - \ln [C_o - \varepsilon (1 - S)] \} \quad (16)$$

Thus, the adjustment needed to help ensure consistent determinations of visibility from this general class of targets, involves the specification of the inherent contrast, C_o, and the sky ground ratio, S, or its components L_q and ${}_bL_o$. These quantities are subject to significant variability depending upon such factors as sun angle, cloud cover and the relative amounts of direct sun and multiply scattered diffuse light incident on the target, the background, and the path of sight. The quantity L_q can be determined from the measured apparent horizon sky radiance where the sun scattering angle, β, is the same for the path of sight to the horizon and the path of sight to the object. However, the other parameters are not available direcuy from the calibrated radiance field as determined by the remote solid-state camera system. Appropriate analytic methods must be introduced to derive the information from the measured radiance distributions.

The analytic techniques inherent in computationally fast atmospheric radiance models such as FASCAT (Hering, 1984) can be used to extract diagnostic information from the observed radiance fields and continu-

ously update the adjustment factors for designated visibility targets in accordance with significant changes in background radiance. Sensitivity calculations with the FASCAT model serve to identify the responses of the sky/ground ratio and inherent target contrast to key factors such as the variations in the 3-dimensional target irradiance (direct sun and diffuse) and variations in the optical and meteorological properties of the atmosphere. The approach is to establish provisional algorithms for real-time calculations of the adjustment factors as required for pre-selected targets and then refine these algorithms as necessary on the basis of information acquired through operational use of the system. Ideally, the objective estimates of normalized visibility from individual targets should correspond closely during periods when boundary layer mixing is sufficient to result in a spatially uniform distribution of atmospheric attenuation coefficient, α, and source function, L_q. Careful monitoring of the system operation during periods of horizontal uniformity provides the data needed to help establish the uncertainties associated with the available target array as well as a basis for refinement and improvement in the daytime visibility determinations.

ACKNOWLEDGEMENTS

This research was funded by the Air Force Geophysics Laboratory under Contract F19628-84-K-0047.

REFERENCES

Douglas, C.A. and R.L. Booker, "Visual Range: Concepts, Instrumental Determination, and Aviation Applica-tions", Final Report No. FAA-RD-77-8, U.S. Department of Transportation, Federal Aviation Agency.

Duntley, S.Q. (1984), "The Reduction of Apparent Contrast by the Atmosphere", J.Opt.Soc.Am. **38**, 179-191.

Duntley, S.Q., A.R. Boileau, and R.W. Preisendorfer (1957), "Image Transmission by the Troposphere 1, J.Opt.Soc.Am. **47**, 499-506.

Hering, W.S. (1984), "Analytic Techniques for Estimating Visible Image Transmission Properties of the Atmos-phere", University of California, San Diego, Scripps Institution of Oceanography, Visibility Laboratory, SIO Ref. 84-6, AFGL-TR-83-0236.

Table A. Hierarchy of Prototype Imaging Systems

(Not Including Optical Accessories & Housings)

First Generation, Z-100 Based System

Item No.	Item Description
1	ZENITH Z-100 COMPUTER, 8088/8085 µP, enhancements, 40 MB hard disk
2	Poynting 505, Video Frame Grabber
3	Poynting 208, Digital Video Memory
4	Cipher F880640, Microstreamer Tape Drive
5	RCA TC1910 CCTV Monitors
6	GE2505A2 CID Video Camera
7	VisLab Dual Wheel Optical Filter Changer
8	VisLab Accessory Control Panel
	Archival Only, No Image Processing (i.e. I.P.) Software

Second Generation, Z-200 Based System

Item No.	Item Description
1	Zenith Z-200 Computer, 80286 µP, enhancements, 40 MB hard disk
2	ITI, PFG-8-1-U-XT Video Frame Grabber (Internal Board)
3	Zenith ZVM-135 Hi Resolution Monitor
4	Cipher 540 Streaming Cartridge Tape Drive (Proposed)
5	Sony PVM 1271(Q) Hi. Res. Video Monitor (Proposed)
6	GE2505A2 CID Video Camera
7	VisLab Dual Wheel Optical Filter Changer
8	VisLab Accessory Control Panel
9	Okidata µ83A MicroLine Printer
	Designed to run LOTUS 1-2-3 and PC Vision/Image Lab I.P. Software

Third Generation, Z-241 Based System

Item No.	Item Description
1	Zenith, Z-241 Computer, 80286 µP, enhancements, 40 MB hard disk
2	Imaging Technology FG-100 AT Frame Grabber
3	Zenith ZVM-133 RGB Video Display
4	Cipher 540 Streaming Cartridge Tape Drive
5	Sony PVM 1271(Q) Hi. Res. Video Monitor
6	GE 2710 CID Video Camera
7	VisLab Dual Wheel Optical Filter Changer
8	VisLab Accessory Control Panel
9	Epson FX85 Printer
	Designed to run LOTUS 1-2-3 and PC Vision/Image Lab I.P. Software

APPENDIX B

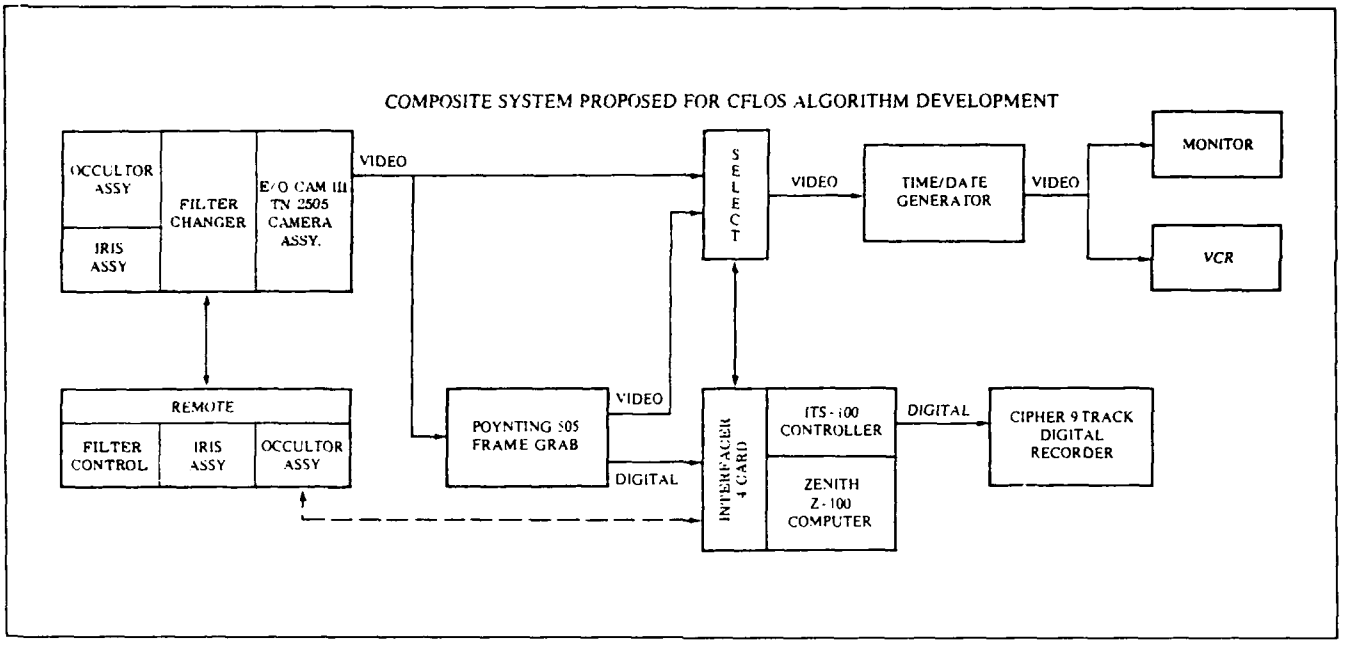

Fig. A

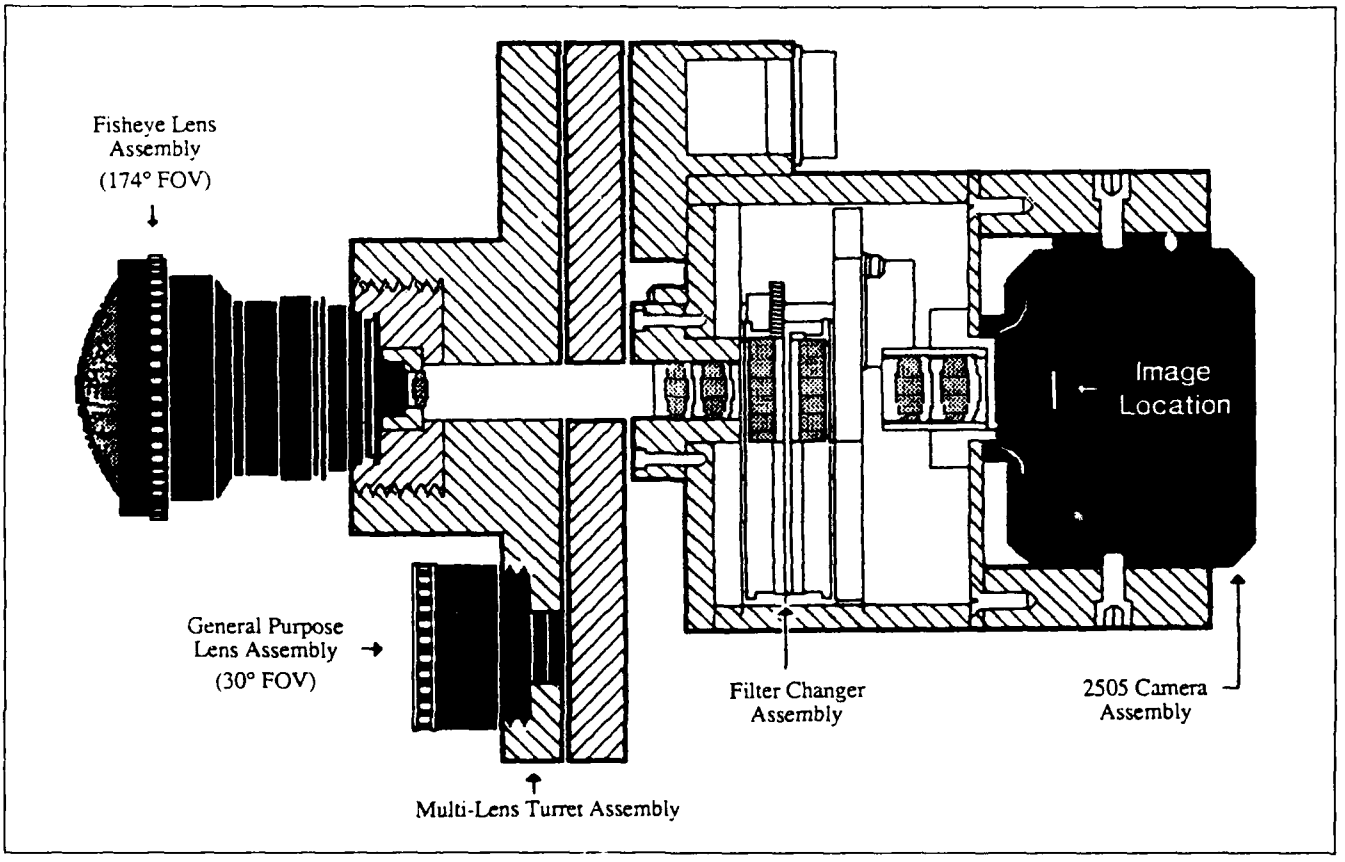

Fig. B

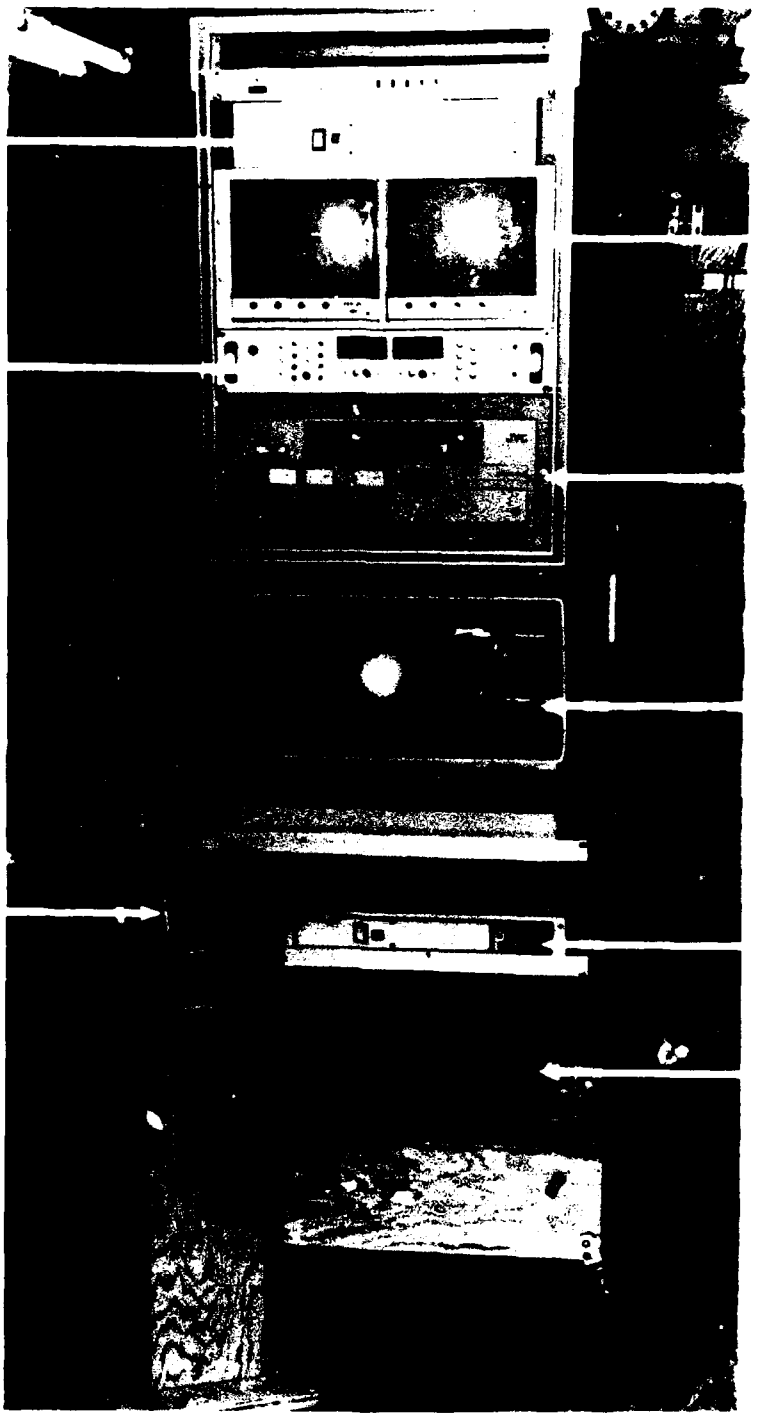

Fig. C. Composite system proposed for CFLOS algorithm development.

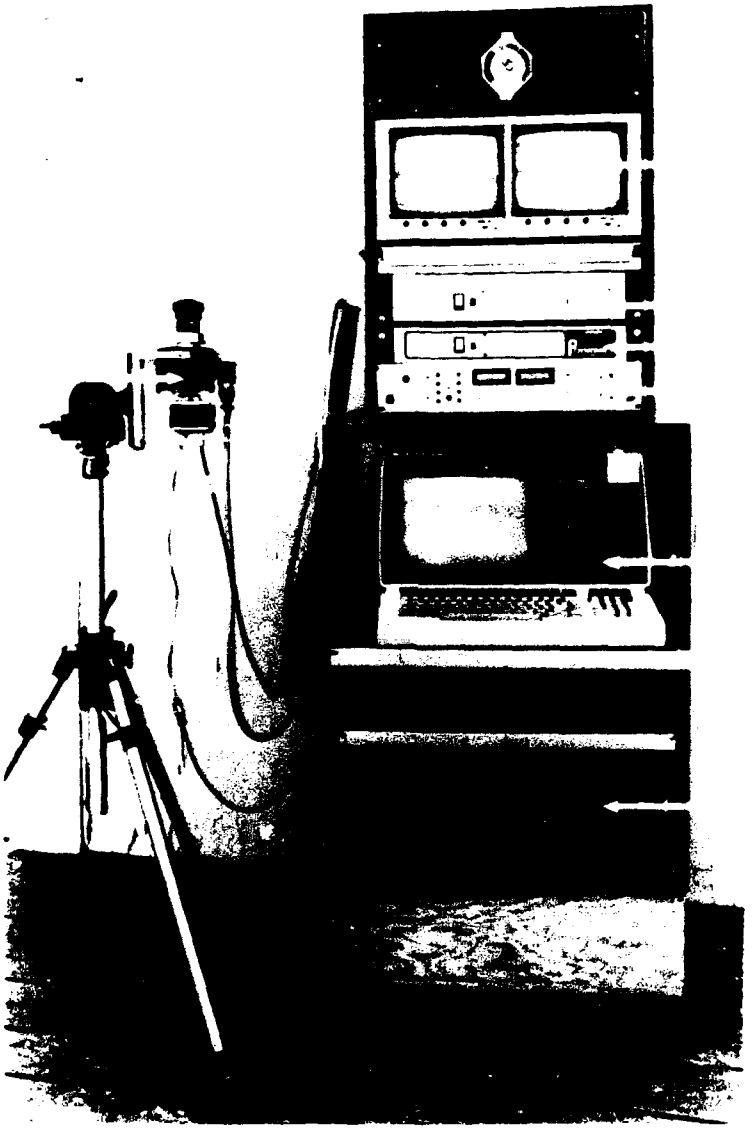

Fig. D. Z-100 system for Whole Sky Image Archival.

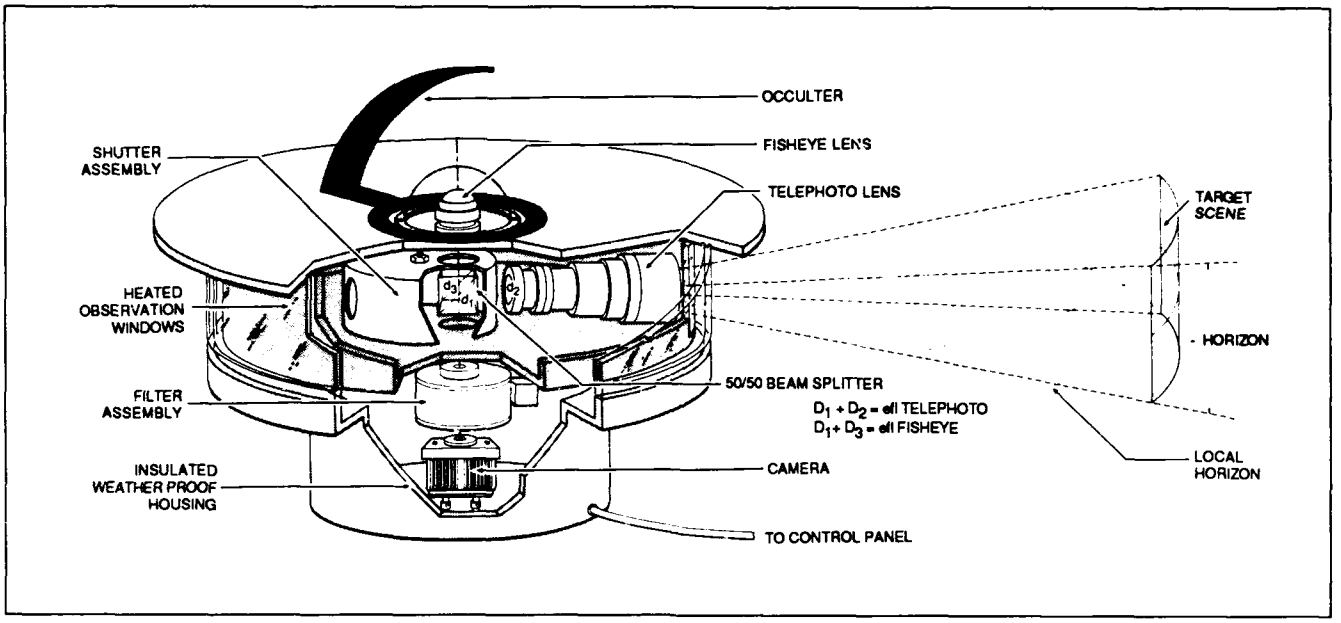

Fig. E. Automatic Observing System for whole sky and horizon imagery.

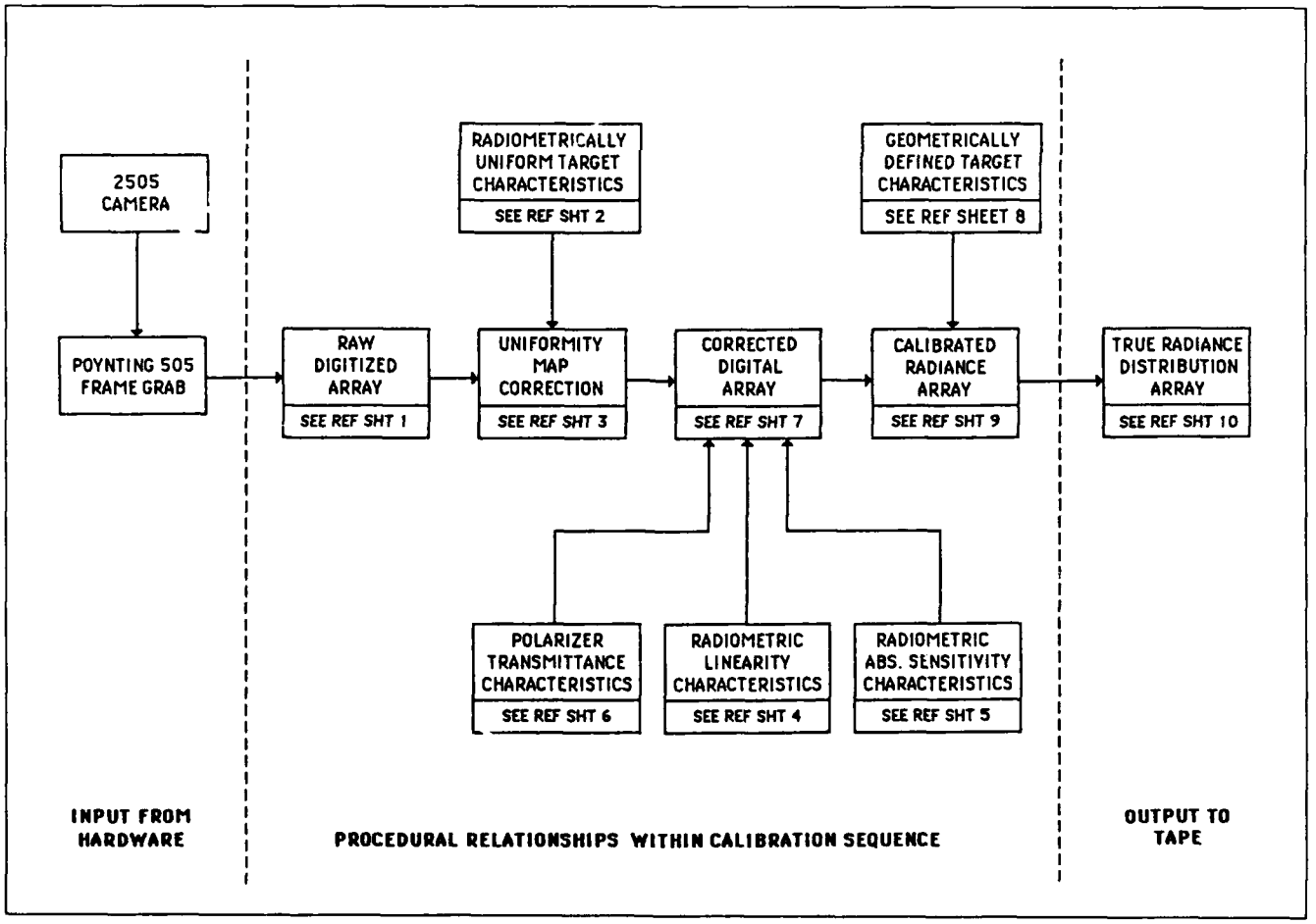

Fig. F. EO CAM III: System calibration procedures.

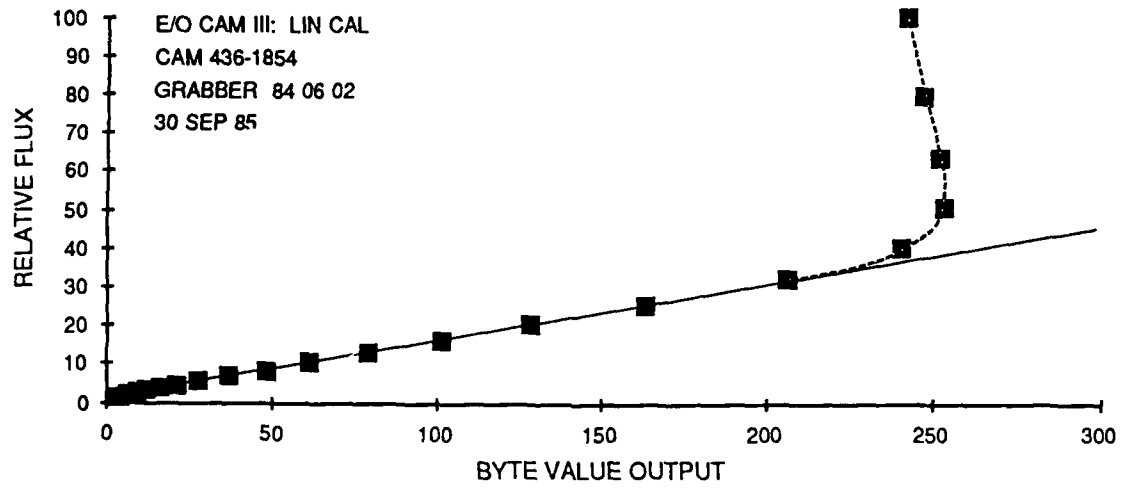
E/O CAM III: LIN CAL
CAM 436-1854
GRABBER 84 06 02
30 SEP 85
RELATIVE FLUX
100
90
80
70
60
50
40
30
20
10
0
0
50
100
150
200
250
300
BYTE VALUE OUTPUT

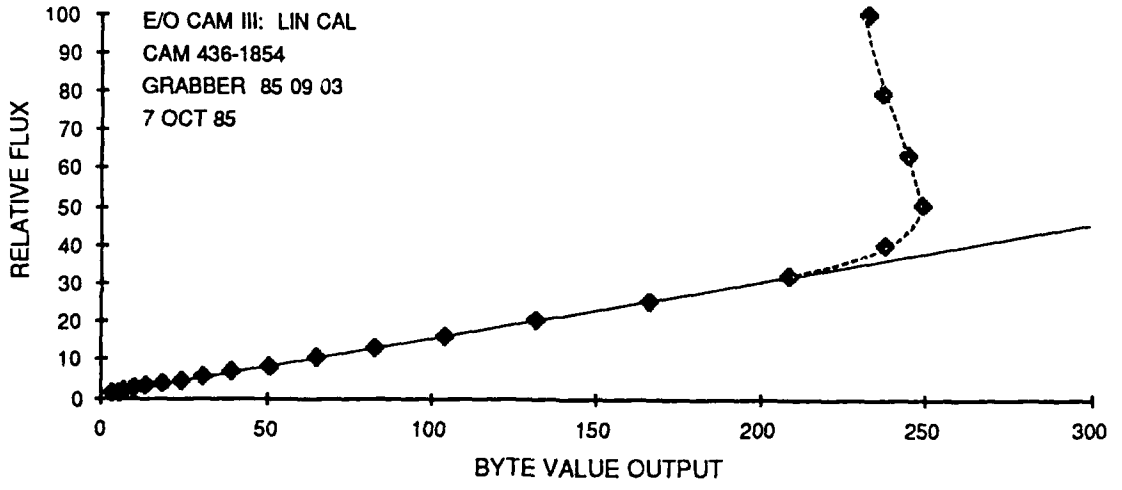
E/O CAM III: LIN CAL
CAM 436-1854
GRABBER 85 09 03
7 OCT 85
RELATIVE FLUX
100
90
80
70
60
50
40
30
20
10
0
0
50
100
150
200
250
300
BYTE VALUE OUTPUT

Fig. G.

The selection and use of the components discussed herein does not imply endorsement or recommendation of the tested products by the Marine Physical Laboratory or its sponsors to the exclusion of other products which may be suitable.

MAJOR VENDOR SPECIFICATION SHEETS

1. Texas Microsystems, Inc., Model 2001A Computer
2. Imaging Technology, Inc., PC Vision Frame Grabber
3. Imaging Technology, Inc., PC Vision, FG-100AT Frame Grabber
4. General Electric, Model 2505, Solid State Video Camera
5. General Electric, Model 2710, Solid State Video Camera
6. Sony, Model PVM-1271Q, Color Video Monitor
7. Daedal Corp. Series 20,000, Precision Rotary Table

Table A. EO Camera, System 5 as-built parts list. 12 October 87 (AV 87-036t)

Item No.	Model No.	Manufacturer or Vendor	Function
1	2001A	Texas Microsystems Inc.	Computer Base Unit
2	B286-I-AT	Texas Microsystems Inc.	CPU
3	80287-8	Texas Microsystems Inc.	Math Co-Processor
4	KBIAT	Texas Microsystems Inc.	Keyboard
5	BVC-1	Texas Microsystems Inc.	Color Video Card
6	ST-277R	Seagate	65 MB Hard Disc
7	HCRA2	Western Digital	Disc Controller
8	EXB-8200	Exabyte	2.2 GB Tape Streamer
9	ASC-88	Advanced Storage Concepts	SCSI Host
10	DIO-96	ICS Computer Products	TTL I/O Ports
11	FG-100-1024-U-AT-A	Imaging Technology Inc.	Video FG & IP
12	Hayes 2400B	Arrow Electronics Inc.	Smart Modem
13	Sony PVM1271Q	Voice & Video	Color Monitor
14	GE-2710	DRF Associates	Video Camera
15	GC-1000	Heath/Zenith	NBS Radio Clock
16	EO3-1200-01	MPL/UCSD	Opt. Filter Changer
17	EO3-3000-01	MPL/UCSD	Acc. Control Panel
18	EO3-3500-01	MPL/UCSD	WXP Camera Housing
19	EO3-3600-01	MPL/UCSD	WXP Lens Housing
20	EO3-2101-01	MPL/UCSD	Solar Attenuator
21	EO3-3700-01 & 3800-01	MPL/UCSD	Stand & Shroud
22	Cable Set	MPL/UCSD	CAM/ACP, etc.0
23	91F1697	BUD	19" Rack
24	SRI	TMI	Rack Slides
25	Pedestal	AFGL	Camera Pedestal
26	42BY 76055 C	Sears or equivalent	Pedestal Air Cond.
27	42HY 36502C	Sears or equivalent	Pedestal Heater

1. GENERAL DESCRIPTION

1.1 Introduction

The 2000 series of industrial computers are suited to a wide variety of applications where durability, and ruggedness are required from a powerful IBM PC XT/AT compatible computer system. Factory automation, machine control, process control and data acquisition systems are only a few of these applications.

Because the computers are completely IBM XT or AT compatible, they take advantage of hundreds of application software packages, translators, and operating systems. Hundreds, possibly thousands of compatible plug in cards ranging from sophisticated graphics cards to thermocouple sensors cards are also available.

This manual can be used in conjunction with the 2001A, 2003A and 2004A AT computers for configuration reference, setup and operating information, maintenance procedures, and specifications.

1.2 Computer Specifications

Each of the computers have the following features in common:

- IBM PC/AT Compatibility
- Shock mounted disk drives (in most configurations)
- Passive backplane (5,8 bit and 5,16 bit slots)
- Vertically removable CPU card for maintenance
- 150 Watt power supply

In addition, the 2001 computer is designed to be mounted in a 19" RETMA rack. It features positive pressure, filtered airflow, a separate compartment for circuit cards, and up to three shock mounted disk drives.

The 2003 computer is a smaller benchtop or wall mounted computer for more specialized applications. It typically has a hard disk and/or one floppy disk.

A portable, self contained floppy disk drive is sometimes used with this computer when it is installed in industrial environments not suitable for floppy diskettes.

The 2004 computer features NEMA 4 packaging and electronics contained in a sealed compartment cooled by a unique moving air heat exchanger.

1.3 B286 Specifications

The B286 CPU is a high performance IBM AT compatible 6 layer CPU card featuring the following:

- Up to 1 Megabyte of parity checked DRAM memory
- Switchable clock: 6 and 8 or optional 6 and 10 MHz
- On-board battery supports real time clock
- 80287 Co-processor socket
- Proprietary Bios with built-in "setup" program
- External reset switch and speaker jack

Rather than mount horizontally in the the bottom of the computer, (as with a typical motherboard computer) the B286 pluga into a passive horizontal motherboard. If replacement is required, the board can be removed and replaced as easily as any expansion card. There is no need to disconnect any cables or remove any other boards.

5. MODULES

5.1 Central Processing Units (CPUs)

Paragraphs of this section of the manual which pertain to all revision levels of the B286 CPU make no notation of revision level in their paragraph title. Those paragraphs which pertain only to specific revision levels of the B286 CPU card, designate this applicability and limitation in the paragraph title. Users should make note of the Revision Level of the CPU Card (referenced on the serial number tag). After noting the CPU card revision, users should utilize those sub-sections/paragraphs of this manual which pertain to their particular CPU revision.

5.1.1 B286 (AT) CPU

5.1.2 Description

The B286 is an IBM PC/AT compatible CPU board, designed for industrial applications. The PC/AT sized card plugs into a passive backplane (BP2 or BP3) and provides the central processing functions of an industrial computer.

The board contains an 80286 6Mhz (optional 8Mhz or 10Mhz) 16 bit microprocessor, optional 80287 numeric processor, 512KB or 1MB of parity checked random access memory (RAM), battery backed up clock, 50 bytes of battery backed up CMOS RAM, long life battery, 15 interrupt channels, 7 DMA channels, real-time-clock, keyboard interface microprocessor, audio generator and driver, external reset switch and 16 bit PC/AT bus interface electronics.

The board is implemented with CMOS and advanced low power shottky gate arrays for minimum power consumption. Interfaces to the board, other than the standard PC/AT bus are for keyboard and speaker connections, and an external audio jack. The PCB is implemented with 4 circuit layers, one power plane and 1 ground plane.

5.1.3 Specifications

Temperature range	0° to 60°C
Relative Humidity	95% Non-condensing
Supply requirements	+5V at 2.2A typical
Battery rating	3.5V 750mAH
Power OFF battery drain	.017mA typical
Dimensions	14.5" x 6.5" x .55"
Weight	1 lb.
Skirt Protrusion	.4"
Operating Speed	6Mhz Lo / 8Mhz Hi
or	6Mhz Lo / 10Mhz Hi
On Board Memory wait States	1
Bus Memory wait States	1 (optionally 2 at Hi Speed)
8 Bit I/O Wait states	4 Lo, 6 Hi
16 Bit I/O Wait States	1 Lo, 2 Hi
Standard 80287 Clock speed	2/3 of CPU Clock speed
Optional 80287 Speed	8 Mhz and 10 Mhz options

Imaging Technology, Inc., PC Vision Frame Grabber

PCVISION®
FRAME GRABBER

Real-Time Video Digitizer Module For IBM Personal Computers

IMAGING Imaging Technology Incorporated

Features

- Accepts RS-170/330 video
- Digitization of analog video to 8 bits of precision with a 10 MHz flash A/D converter
- Each pixel represents one of 256 possible gray or over 16 million pseudocolor levels
- Full support for gen-locking to an external video source
- 256K bytes on-board frame memory
- Graphic overlays under software control
- Frame memory is mapped into the IBM PC memory space in 64K byte blocks
- One or three 8-bit D/A converters
- RS-170 output
- Full color imaging to 24 bits per pixel with 3 PCVISION Frame Grabbers
- Occupies single slot
- Internal crystal generates sync if video source is lost
- Four programmable input lookup tables (256 × 8 bits each) (Optional)
- Three output channels, each with its own set of four programmable look-up tables (256 × 8 bits each) (Optional)
- Demonstration software package and cables included.

Typical Applications

- Graphic Arts
- Teleconferencing
- Robotic Vision
- Automated Factory Inspection
- Medical Imaging
- Microscopy
- X-ray Analysis
- Research and Education

Technical Description

The **PCVISION® Frame Grabber** is a board-level video digitizer and display module that is plug-compatible with the IBM Personal Computer. This module captures an RS-170 or RS-330 video signal (TV standard) at a rate of 30 frames per second, stores the image in an on-board 512 × 512 × 4- or 8-bit frame memory, and simultaneously displays the stored image on an external monitor. It is available with two optional plug-on sub-modules: Extended Memory and Pseudocolor. Both provide additional functionality without requiring an additional expansion slot in the backplane.

The **Extended Memory Module** contains four bit planes of frame memory, allowing all 8 bits from the A/D converter to be stored.

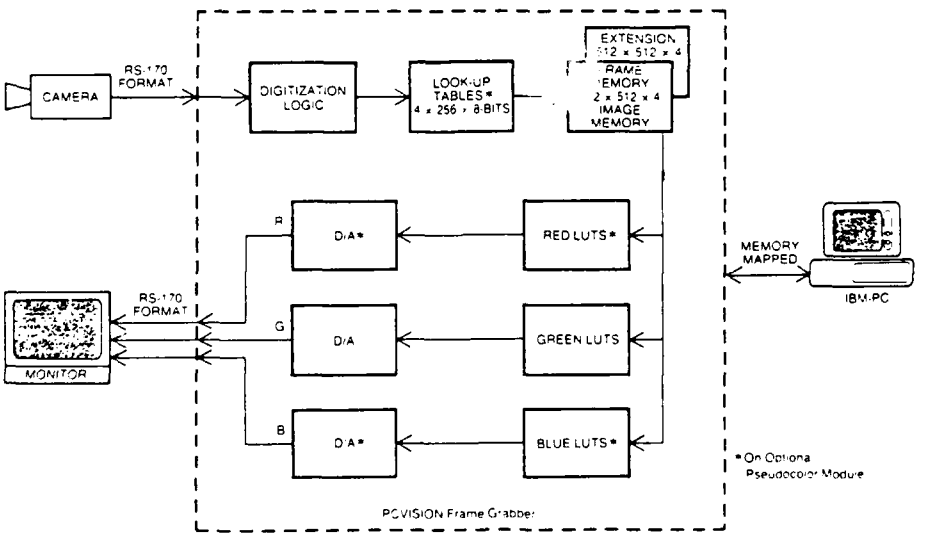

The **Pseudocolor Module** expands the number of output channels from one to three and provides each channel with its own set of four look-up tables. This gives the PCVISION Frame Grabber the ability to display monochrome input as pseudocolors, yielding greater image analysis possibilities.

The combination of the IBM Personal Computer and the PCVISION Frame Grabber is ideal for low-cost, high-performance image processing. The image stored in the frame memory can be accessed by the IBM PC to implement algorithms for image enhancement, feature extraction, pattern recognition, and image transmission and archiving.

A block diagram of the PCVISION Frame Grabber is shown in Figure 1. Each functional block is described in greater detail in the following sections.

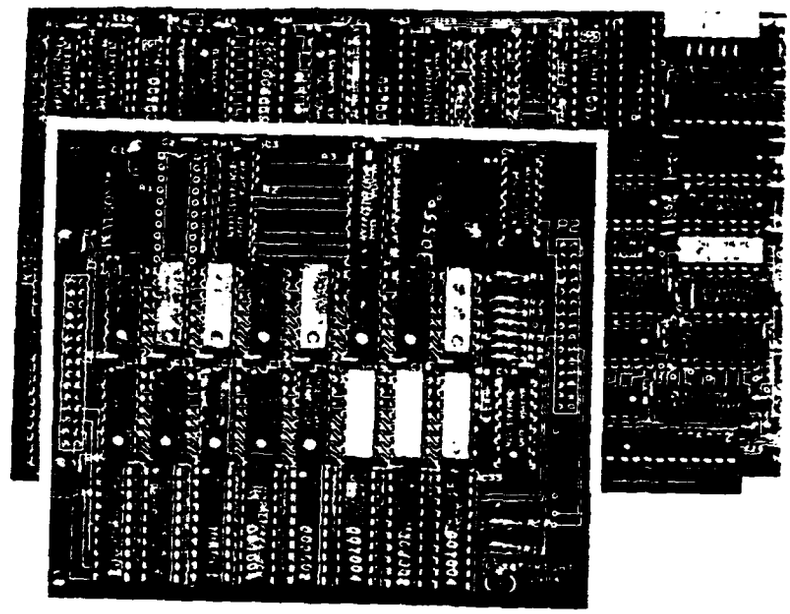

Digitization Logic

The PCVISION Frame Grabber accepts a standard RS-170/330 (CCIR at 50 Hz) signal. The analog video signal is digitized to 8 bits of accuracy at a rate of 30 frames per second with a flash A/D converter. The digitized pixel data stream is stored in a 512 × 480 frame memory window. (The full 512 × 512 frame memory is filled at the 50 Hz CCIR standard.) The 8 bit A/D provides a digitization range of 256 possible gray levels.

Four input look-up tables (256 × 8 bits each), available on the Pseudocolor Module, can be used to transform digitized data before it is stored.

Frame Memory

The basic PCVISION Frame Grabber contains a 512 × 512 × 4 bit frame memory which stores the four most significant bits of the digitized data. The entire frame memory can be expanded by four additional bit planes to a total of 8 bits per pixel with the installation of the Extended Memory Module.

The frame memory has been designed to allow simultaneous acquire, display, and CPU read/write access operations. The IBM Personal Computer can randomly access individual pixels in the frame memory at one microsecond per pixel (average). This capability allows the IBM PC to process the digitized data and generate graphic overlays.

The frame memory is divided into quadrants. At any given time, one quadrant is mapped directly into the memory space of the IBM PC. Therefore, users must reserve 64K bytes — the size of one quadrant — in the memory space of the IBM PC for frame memory access.

The frame memory base address is configurable to any 64K byte boundary in the memory space of the IBM PC. The quadrant to be mapped is selected under software control. This memory mapping scheme allows a high data transfer rate between the IBM Personal Computer and the PCVISION Frame Grabber.

Each frame memory bit plane can be protected under software control, facilitating the implementation of graphic overlays.

Display Logic

The display logic consists of four programmable transformation look-up tables and one D/A converter. Once the digitized or computer-generated data is stored in the frame memory, the LUTs can be used to perform linear, inverting, thresholding, or other transformation functions. The signal is then converted to an analog RS-170 signal for display on a standard TV monitor.

By adding the Pseudocolor Module, the number of output channels is increased to three. Each channel has its own set of four 256 × 8 bit RAM look-up tables which can be programmed to generate and display pseudocolor images.

After the image data is transformed by the LUT(s), high speed 8-bit Digital-to-Analog (D/A) converters simultaneously transform the digital image data to three RS-170 video signals for display.

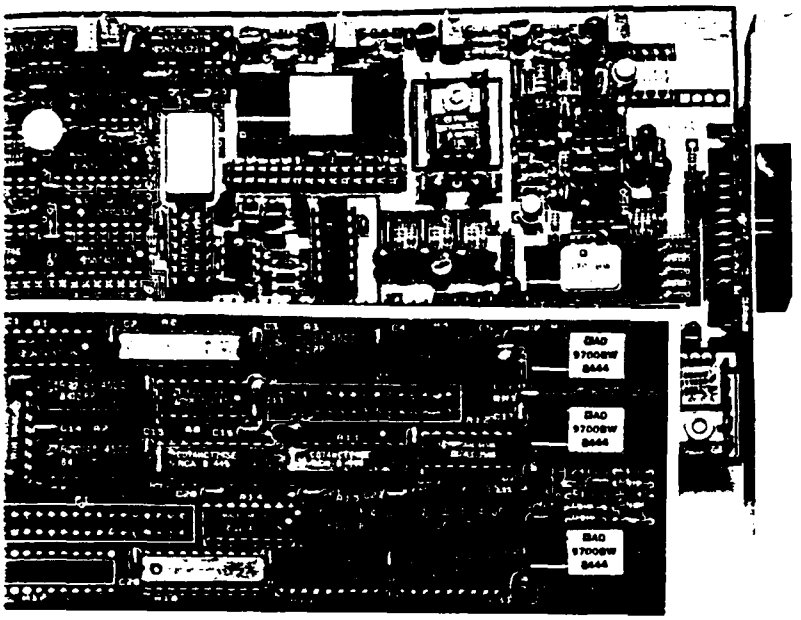

IBM PC Bus Interface

The IBM PC Bus Interface contains 7 registers for controlling the functions of the PCVISION Frame Grabber, and for transferring the status/control information to the IBM PC.

A block of 32 bytes must be set aside in either the memory space or the I/O space of the IBM PC for these registers. The register base address is configurable to any 32 byte boundary in the selected space.

The PCVISION Frame Grabber also supports a vertical blank interrupt. The interrupt is jumper-configurable to any of the 6 priority levels supported by the IBM PC.

Register Base Address +	
0	Control/Status Low
1	Control/Status High
2	Look-up Table Address
3	Look-up Table Data
4	Mask Register
5	Frame Memory Block Select
6	Reset Vertical Blank Interrupt
7-F	Reserved

Synchronization Modes

The PCVISION Frame Grabber works in a variety of synchronization modes. Most commonly, the module will lock itself to the video source by means of the on-board phase locked loop. If this is desired, the PCVISION Frame Grabber can:

- Gen-lock onto composite video.
- Accept separate video and composite sync signals.
- Accept separate video and horizontal and vertical sync signals.

Alternatively, the PCVISION Frame Grabber can use its internal crystal to generate composite sync, or horizontal and vertical syncs to drive the video source. The internal crystal also takes over if the video source is lost, assuring continuity and consistency of the image in frame memory.

Full Color Image Processing

Three PCVISION Frame Grabbers can be used for full color image processing. In this configuration, one module is designated a master and generates the system timing for the other two modules. Each board digitizes, stores, and displays one color primary; red, green, or blue. NTSC composite color is not supported.

The 3 PCVISION Frame Grabbers in a full color system must reside at different register base addresses. However, to limit the amount of memory space necessary for frame memory access, each module can be mapped into the same 64K byte segment in the IBM PC memory space. A "board select" enable bit in the Control/Status Register enables one of the PCVISION Frame Grabbers into the segment at any given time.

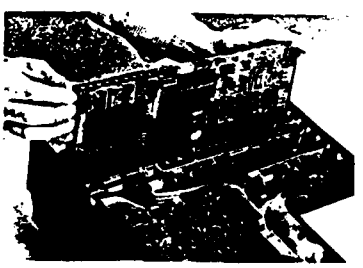

Software Support

Imaging Technology provides a demonstration software package that will enable you to use the PCVISION Frame Grabber the day you take delivery.

Included in this package are the basic drivers necessary to control the PCVISION Frame Grabber. These drivers are written in Basic and IBM PC MACRO assembly language; source code is provided. Also included is a complete diagnostic software package that checks each functional area on the board and verifies its operation.

Imaging Technology, Inc., PC Vision Frame Grabber

The supported commands are:

BORDER—write a border
CHARGEN—character generator
CLEAR—clear frame memory
DISABLE—disable PFG in color systems
ENABLE—enable PFG in color systems
FREEZE—stop continuous acquire
GRAB—initiate continuous acquire
HELP—display help menu
INIT—initialize PFG
LUTD—look-up table dump
MAP—display memory map
MENU—display main menu
QUIT—terminate session
READ—read frame memory
READR—read register
RESTORE—load an image stored on disk
RMAP—display register map
SAVE—write an image onto disk
SNAP—single frame acquire
STATUS—display status
TEST—run diagnostic
WEDGE—load gray scale into memory
WRITE—write frame memory
WRITER—write register

Power Requirements (Typical)

PCVISION Frame Grabber
+ 5 2.25 amps
+12 .20 amps
−12 .25 amps

With Extended Memory Module
+ 5 3.00 amps
+12 .20 amps
−12 .25 amps

With Pseudocolor and Extended Memory Modules
+ 5 3.80 amps
+12 .40 amps
−12 .25 amps

NOTE

The combination of the PCVISION Frame Grabber with other plug-in boards that consume significant power (e.g., additional memory) can strain the power supply within personal computers. Therefore, we recommend use of the IBM models XT or AT.

Be sure to consult the specifications for your personal computer and the boards you are using to determine whether sufficient power is available.

Ordering Information

Frame Grabber
PFG-M-D-Hz-A

M = 8 of 4 (bits of memory)
D = 1 (monochrome only) or 3 (RGB pseudocolor)
Hz = U (60 Hz) or E (50 Hz)
A = PC, XT, AT, or other.

Extended Memory Module
(if ordered separately)
PEM-4

Pseudocolor Module
(if ordered separately)
PPC-3

Notes:

1. Hz does not affect price.
2. All documentation, cables, and demo software are included.
3. When placing an order, please include a description of the typical configuration in which the boards will be used.

Imaging Technology Incorporated also designs and manufactures a complete line of image processing modules and accessories that are compatible with Multibus® and Q-Bus™ architectures. For additional information, please contact our Sales Department at (617) 938-8444.

IMAGING Imaging Technology Incorporated
600 West Cummings Park Woburn, MA 01801 (617) 938-8444 Telex: 948263 IMAGING WOBN

Printed in U.S.A. PH-7/85-10M

Imaging Technology, Inc., PC Vision, FG-100AT Frame Grabber

New Product

PCVISION®
FG-100-AT

Real-Time Video Digitizer Module for the IBM Personal Computer AT

IMAGING

Features

- Compatible with IBM Personal Computer AT bus architecture
- Occupies a single slot
- Digitizes analog video signal to 8 bits for 256 gray levels
- VCR lock capability
- 512 × 512 × 12-bit on-board frame memory
- Direct memory mapping with programmable window size
- Direct or indirect frame memory access
- Separate memory plane protection for CPU access and image acquisition
- Hardware zoom of 2, 4, 8
- Pixel-by-pixel pan and scroll
- Input look-up table (LUT: 4096 × 12 bits) accepts input from A/D converter, frame memory, or LUT Select Register, allowing stored image re-transformation
- Red, green, blue output channels
- Real-time processing, including image subtraction and averaging
- Full-color imaging to 36 bits/pixel using 3 boards
- Multiple camera inputs supported

Typical Applications

- Inspection
- Graphics
- Paint Systems
- Medical Imaging
- Research and Development
- University Research

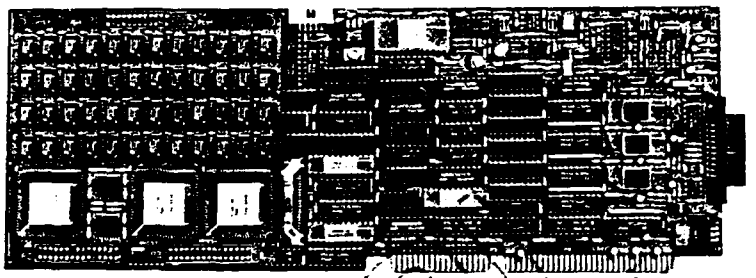

Technical Description

The **FG-100-AT** is a single-slot image processing board that captures video signals, stores images in frame memory, and simultaneously displays the image on an external monitor in monochrome or pseudocolor. In addition, 4096 × 12 bits of input look-up table memory are available so that real-time operations can be performed on live and/or stored images. Sixteen 256 × 8-bit LUTs are available for each of the board's three output channels.

The FG-100-AT incorporates Imaging Technology's proprietary new CMOS gate array chips. These arrays reduce the overall power consumption of the board, while simultaneously increasing its functionality and reliability.

Figure 1 is a block diagram of the FG-100-AT architecture.

Digitization Logic and the Input Look-Up Table

The FG-100-AT accepts a standard RS-170/330 (or 50 Hz CCIR) video signal. This analog signal is digitized to 8 bits of accuracy at a rate of 30 times per second with a flash A/D converter, providing a range of 256 gray levels.

A key feature of the FG-100-AT board is the **feedback input look-up table** that allows images in frame memory to be processed in real time. This look-up table consists of 4096 locations, each of which is 12 bits wide. Depending on the operation desired, this table can be used as either a single 4096 × 12-bit LUT or 16 separate 256 × 8-bit LUTs. As shown in Figure 1, inputs to the LUT can come from: the video source (up to 8 bits); the frame memory (up to 12 bits); or the LUT Select Register. The various combinations that are possible provide the ability to perform any/all of the following in real time:

- Transform incoming imagery prior to storage
- Transform previously stored images
- Arithmetic operations
- Implement graphic overlays, display windows, and area-of-interest processing
- Add or subtract a constant from a full-screen image
- Add, subtract, or average two images to six bits of accuracy

Frame Memory

The FG-100-AT board contains a 512 × 512 × 12-bit frame memory to store digitized images. Designed to allow simultaneous acquire, display, and CPU read/write access operations, the frame memory can be used in several modes: in one, 8 bits are used for the image and four are available for windowing and graphic overlays; in another, two 6-bit images can be stored for processing and display. The advanced memory architecture of the FG-100-AT allows users to randomly access individual pixels at very high rates. This facilitates the implementation of image processing algorithms on the IBM Personal Computer AT.

Furthermore, individual bit planes can be protected from CPU access or video acquisition, facilitating the implementation of graphic overlays.

The frame memory allows panning and scrolling of images on a pixel-by-pixel basis and zooming of any portion of an image by factors of 2, 4, or 8.

In addition, frame memory can be accessed either directly or indirectly. If indirect access is desired, pointer registers are used. These registers can be set to automatically increment or decrement (by factors of 1, 2, 4, 8, or 16) after memory read/write cycles. Direct access gives users the ability to easily move a memory-mapped window through frame memory.

Display Logic

The video output display logic optionally consists of one or three channels, each with its own D/A converter and 16 256 × 8-bit programmable look-up tables. These LUTs can be selected either statically (via registers) or dynamically (via the data stored in bits 8-11 of the frame memory), allowing the use of overlays without loss of image data. The LUTs are memory-mapped and can be changed at any time without streaking the display.

Synchronization Modes

The FG-100-AT operates in a variety of synchronization modes. Most commonly, the module will lock itself to the video source via its on-board dual-stage phase-locked loop. This allows locking onto not only standard RS-170/330 signals, but also such unstable sources as commercial videocassette recorders.

Alternatively, the FG-100-AT can use its internal crystal to generate system timing. The internal crystal also takes over if the external sync is lost, assuring continuity and consistency of the image in frame memory.

Full-Color Image Processing

To perform full-color image processing, three FG-100-AT boards are required. In this configuration, one module is designated a master and generates the system timing for the others. Each board can then digitize, store, and display one color primary: red, green, or blue. NTSC composite color is not supported.

IBM Personal Computer AT Bus Interface

The interface between the FG-100-AT and the IBM Personal Computer AT consists of sixteen I/O-mapped registers that allow programs to control the functions of the board and transfer status/control to the IBM Personal Computer AT.

In addition, the FG-100-AT supports a vertical blank interrupt. The interrupt can be configured via jumpers to eight priority levels supported by the AT.

Register Base Address +

0	SRU Control
2	External Mask
4	Scan Mask
6	Frame Memory Data
8	X Pointer
A	Y Pointer
C	Pointer Control
E	CPU Address Control
10	X Spin Constant
12	Y Spin Constant
14	Pan
16	Reserved
18	Scroll
1A	Board Status/Control
1C	Scan Control
1E	Look-Up Table Select

Power Requirements

(To be determined)

NOTE

Be sure to consult the specifications for your personal computer and any other boards you are using to determine whether sufficient power is available.

Imaging Technology, Inc., PC Vision, FG-100AT Frame Grabber

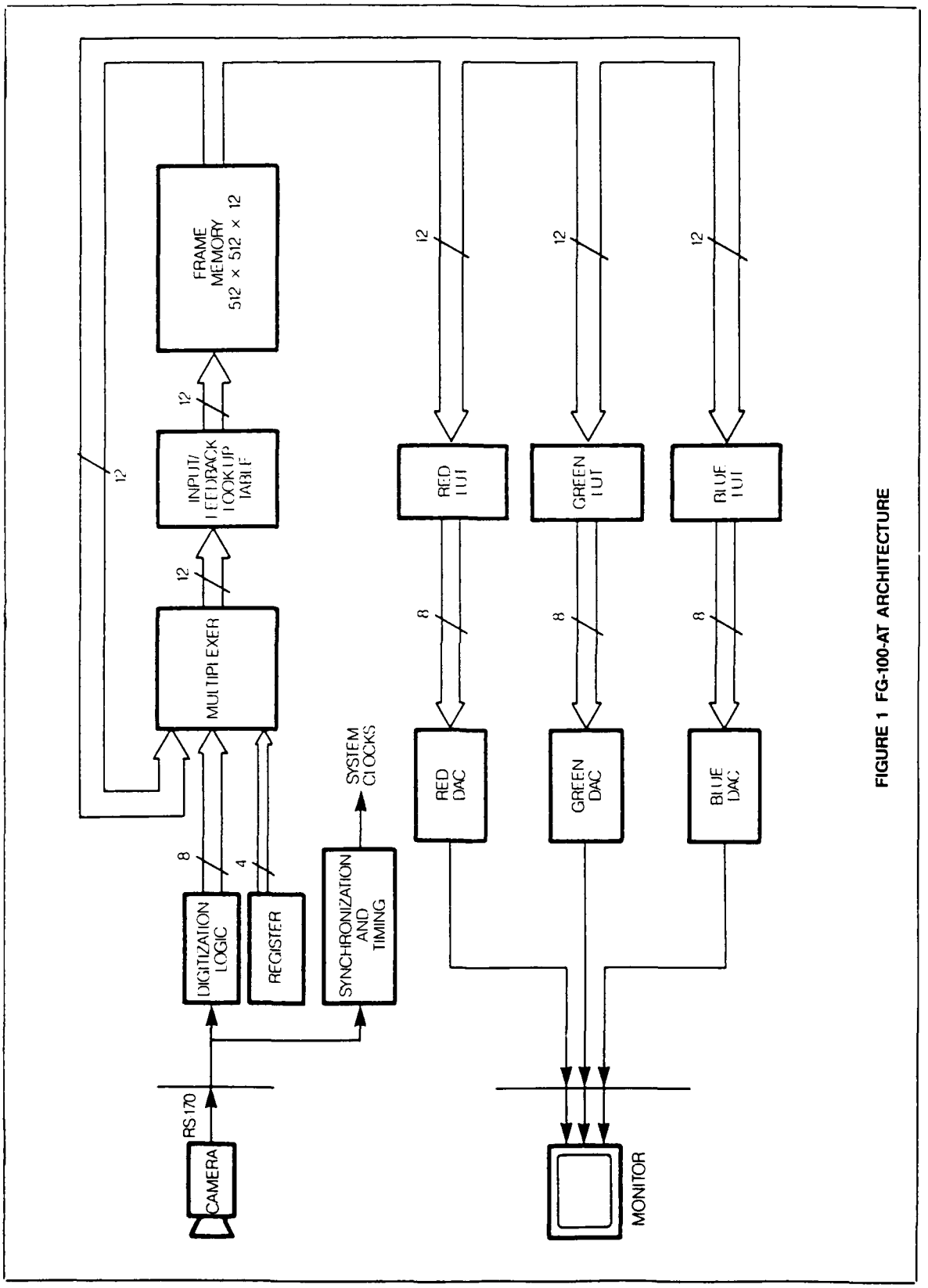

FIGURE 1 FG-100-AT ARCHITECTURE

Ordering Information

FG-100-AT-Hz-D

Hz = U (60 Hz) or E (50 Hz)
D = 1 or 3 (number of D/A converters)

Notes:

1. Hz does not affect price.
2. All documentation and cables are included.
3. When ordering, please include a description of the typical configuration in which the board(s) will be used. For example, if intending to use three boards for full-color processing, please note that.

Imaging Technology Incorporated also designs and manufactures a complete line of image processing modules and accessories that are compatible with Multibus, Q-Bus, VMEbus, and IBM PC architectures. For additional information, contact our Sales Department at the number below.

All specifications subject to change without notice.

General Electric, Model 2505, Solid State Video Camera

TN2505 SERIES TECHNICAL INFORMATION

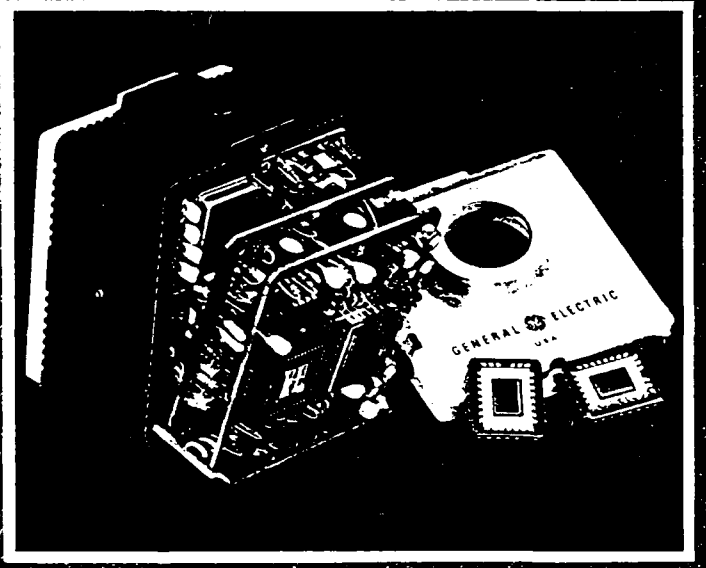

GENERAL ELECTRIC

General Electric, Model 2505, Solid State Video Camera

SPECIFICATIONS

ELECTRICAL	
Input Voltage	
Power Supply Module	120VAC ± 15% (TN 2505) 50/60Hz 220VAC ± 10% (TN 2506) 50Hz
Camera	+ 12 to + 35 VDC
Input Power	2.5 Watts
Sensor Format	244 Vertical, 388 Horizontal (TN2505) 290 Vertical, 416 Horizontal (TN2506) (CCIR)
Image Format	11 Millimeters Diagonal
Composite Video	1 Volt p-p into 75 Ohms RS-170
Sync	Internal RS-170, Linelock Crystal, External H&V, Genlock or Compulock
S/N Ratio	50 dB at Saturation
Geometric Distortion	0%
Spectral Response	350 to 1100 Nanometers
ALC Range	2.6 Million to 1 With fl. 8-360 Auto-Iris Lens
Gray Scale	10 shades of gray, Minimum EIA Standard Chart
Modulation Transfer Function	Better than 80% at 250 lines
Scan Rate	525/60 TN 2505 625/50 TN 2506
Sensitivity	Full output (1 Volt composite) at .8fc faceplate (0dB gain) .4fc faceplate (+ dB gain) Useable video at .2fc faceplate (0dB gain)
Outputs	
I/O Conn.	Clock (14.3MHz)TN 2505, H&V *Drive (Non-buffered)*
Iris	Gnd, Video, + 10 VDC
Video	Composite, 1 Volt p-p RS-170
Inputs	
I/O Conn.	+ 6 & + 12dB Gain, Sync, Injection Inhibit.
Power	+ 12 to + 35 VDC

ENVIRONMENTAL	
Temp. Range	0 to 50 C.
Humidity	95% Non-condensing
Shock	50G (½ sinewave at 10ms duration)
Vibration	6 G's at 500Hz. *For applications requiring greater loading we recommend using the two piece camera configuration.*

MECHANICAL	
Weight:	13.5oz
Camera Dimensions	(3.37" x 3.0" x 3.04")
Lens Mount:	Standard C Mount 1.00-32 Thread
Camera Mount: (top and bottom)	¼-20 Thread
Video Connectors	BNC

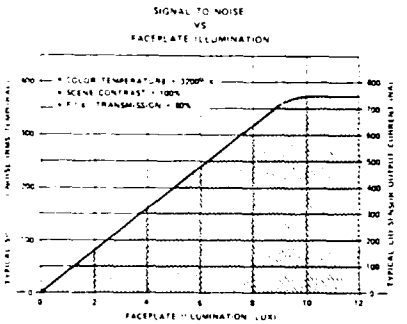

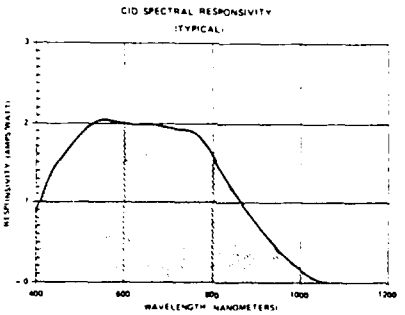

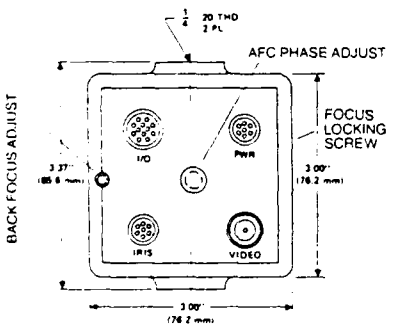

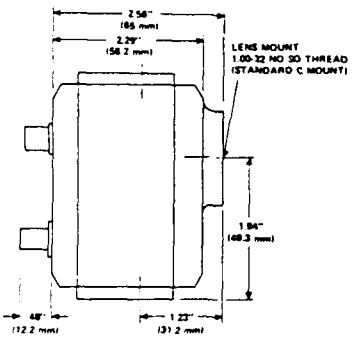

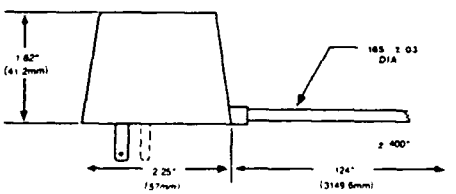

For further information contact:
Marketing Manager, Electronic Camera Operation
GENERAL ELECTRIC COMPANY
890 7th North Street
Liverpool, New York 13088
(315) 456-2808/2945

PRINTED IN USA

GET-6803

General Electric, Model 2710, Solid State Video Camera

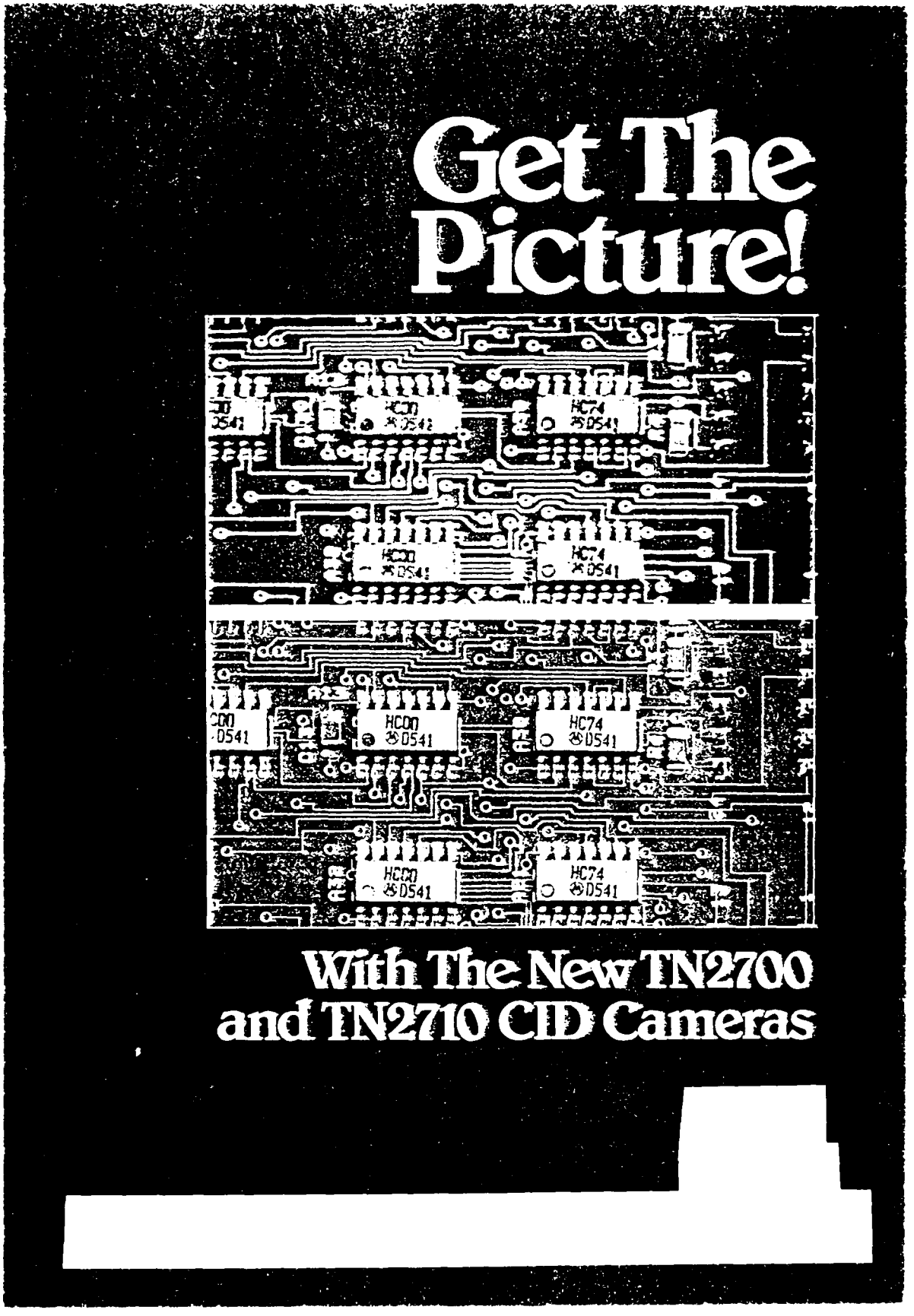

General Electric, Model 2710, Solid State Video Camera

SPECIFICATIONS

ELECTRICAL	
Input Voltage	
Power Supply	120VAC ± 15%, 50/60 Hz
Module	220VAC ± 10%, 50 Hz
Camera	+ 10.5 to + 18 VDC
Input Power TN2700 6 Watts, TN2710 8 Watts	
Sensor Format	484 Vertical, 377 Horizontal (TN2700) 484 Vertical, 754 Horizontal (TN2710)
Image Format	11 Millimeters Diagonal
Composite Video	1 Volt p-p Into 75 Ohms RS170
Sync	Internal RS170, Linelock Crystal, External H&V, Genlock
[1]S/N Ratio	TN2700 50db (Saturated Signal/ RMS Noise) TN2710 49db (Saturated Signal/ RMS Noise)
Geometric Distortion	0%
Spectral Response	200 to 1100 Nanometers with Quartz Faceplate 350 to 1100 Nanometers with Glass Faceplate
Gamma	1.0 to 0.5 continuously variable
ALC Range	2.6 Million to 1 with fl.8-f360 Auto Iris Lens
Gray Scale	10 shades of gray, Minimum EIA Standard Chart

ENVIRONMENTAL	
Temp Range — 30C to + 50C	
Humidity	— 95% Non-Condensing
Shock — 50G (½ sinewave at 10ms duration)	

Modulation Transfer Function	Better than 80% at 250 TV lines (TN2700) Better than 80% at 500 TV lines (TN2710)
Scan Rate	525 lines at 60 Hz, 2:1 Interface
[2]Sensitivity Full Output (1 volt composite at 0.3fc faceplate (0db gain) [3]Useable video at .01fc faceplate (x4 db gain & AGC)	
Outputs	
I/O Conn.	Clock (14.3 MHz), H&V Drive, Video
Iris	Gnd, Video, + 12 VDC
Video	Composite, 1 Volt p-p, RS170
Inputs	
I/O Conn	x2 & x4 Gain, Sync, Injection Inhibit, AGC Inhibit, Power, V-Drive
Power	+ 10.5 to + 18 VDC
Automatic Gain Control	Selectable — 8:1 Gain Range

MECHANICAL	
Weight:	24 oz.
Lens Mount:	Standard C Mount 1.00-32 Thread
Camera Mount:	¼-20 Thread
Connectors	
Video	BNC
Lens	7 Pin Viking
Power	7 Pin Viking
I/O	15 Pin "D"

NOTES:
[1] - Gamma = 1, Contours off, measured on Rhode & Schwartz Noise Meter @ 10 KHz 4.2 MHz
[2] - Foot Candle measurements with 3200^{o}K source
[3] - Useable Video defined as S/N = 1

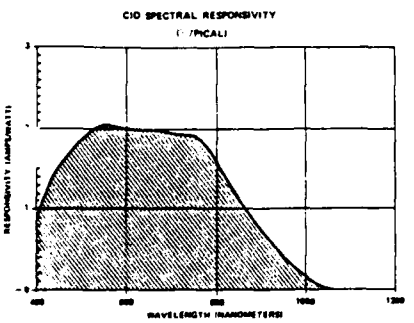

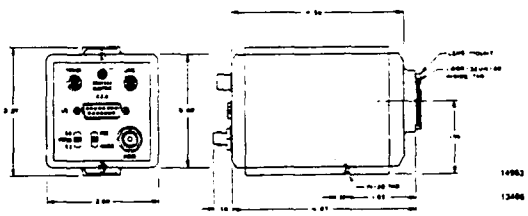

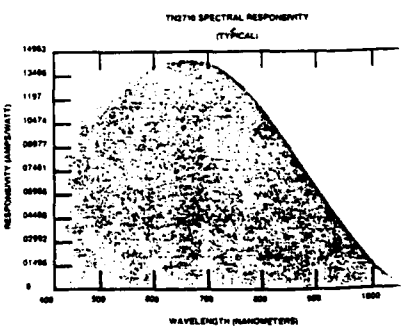

Sony, Model PVM-1271Q, Color Video Monitor

SONY

TRINITRON® COLOR VIDEO MONITOR

PVM-1271Q/1371QM

OPERATING INSTRUCTIONS page 2

Before operating the unit, please read this manual thoroughly and retain it for future reference.

MODE D'EMPLOI page 13

Avant la mise en service de l'appareil, prière de lire attentivement ce mode d'emploi et de le conserver pour toute référence ultérieure.

BEDIENUNGSANLEITUNG Seite 22

Vor Inbetriebnahme lesen Sie bitte diese Bedienungsanleitung aufmerksam durch, und bewahren Sie sie zum späteren Nachschlagen gut auf.

GEBRUIKSAANWIJZING blz. 31

Lees de gebruiksaanwijzing aandachtig door alvorens het apparaat in gebruik te nemen.
Bewaar de gebruiksaanwijzing voor eventuele naslag.

BRUKSANVISNING sidan 40

Läs igenom bruksanvisningen noggrant innan du använder apparaten och bevara den för framtida bruk.

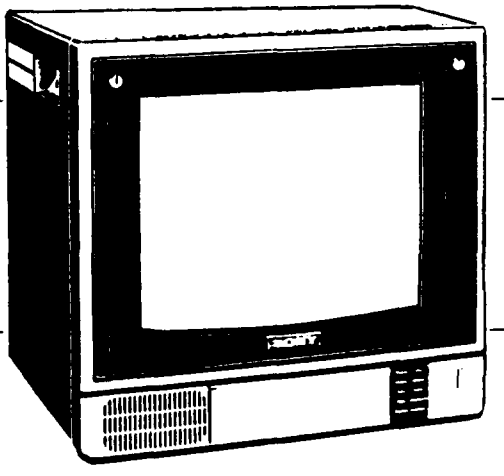

Sony, Model PVM-1271Q, Color Video Monitor

SPECIFICATIONS

Color system	PAL, SECAM, NTSC and NTSC$_{4.43}$ systems, switched automatically
Picture tube	Trinitron tube Approx. 33 cm (13 inches), 90-degree deflection, Super Fine Pitch 0.25 mm (Approx. 31 cm picture measured diagonally)
Resolution	RGB inputs : 600 lines, 640 × 200 dots Composite input : 550 lines
Color temperature	PVM-1271Q : 9,300°K PVM-1371QM : 6,500°K (Can be changed to either temperature by an internal switch. For switching of the color temperature, consult your authorized Sony dealer.)
Frequency response	10 MHz (−3 dB, RGB) 5.5 MHz (−3 dB, composite video)
Horizontal linearity	±8%
Vertical linearity	±5%
Line pull range	Horizontal ±500 Hz Vertical 8 Hz
Overscan of the picture	5%
Underscan of the picture	9%
Return loss	4 MHz, 35 dB (LINE A, LINE B)
Zooming	Within 2%
Convergence	Central area 0.6 mm Periphery 0.8 mm
Brightness	More than 35 foot-lamberts

Inputs	VIDEO IN : BNC connector VTR : 8-pin connector, Pin No. 2 (pin No. 6 : ground) composite 1 Vp-p ±6 dB, sync negative, 75 ohms and high impedance switchable
	AUDIO IN : mini jack VTR : 8-pin connector, Pin No. 1 (pin No. 5 : ground) −5 dBs, high impedance
	EXT SYNC IN : BNC connector composite sync 2 - 8 Vp-p, negative, 75 ohms and high impedance switchable
	RGB IN : BNC connector 0.7 Vp-p, ±6 dB, 75 ohms, non composite
	AUDIO (RGB) IN : mini jack −5 dBs, high impedance
	CMPTR : 25-pin connector For details, see "CMPTR connector".
Outputs	VIDEO OUT : BNC connector
	AUDIO OUT : mini jack Output level 1 W
	EXT SYNC OUT : BNC connector
	RGB OUT : BNC connector
	AUDIO (RGB) OUT : mini jack Loop-through
Power requirements	PVM-1271Q : 120 V ac, 50/60 Hz PVM-1371QM : 220 - 240 V ac, 50/60 Hz
Power consumption	PVM-1271Q : 105 W max. PVM-1371QM : 90 W
Dimensions	Approx. 346 × 339 × 388 mm (w/h/d) (13⅝ × 13⅜ × 15⅜ inches)
Weight	Approx. 14.5 kg (31 lb 15 oz)

CMPTR connector (25-pin)
Pin assignment

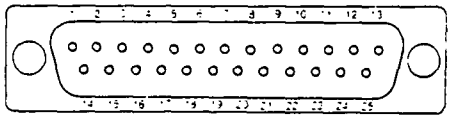

Pin No.	Signal	Signal level
1*	IBM select	High state (5 V) : IBM mode Low state : 3 Bit TTL
2	Audio select	High state (5 V or open) : Audio inputs from pin 13. Low state (less than 0.4 V) : Audio inputs from the LINE A AUDIO IN jack
3	H. sync or composite sync	Negative polarity When the high state is selected at pin 9 : 1 V p-p, 75-ohm terminated When the low state is selected at pin 9 : TTL level
4	Blue input	Positive polarity When the high state is selected at pin 9 : Analog signal (0.7 V p-p, 75-ohm terminated, non sync) When the low state is selected at pin 9 : Digital signal (TTL level)
5	Green input	
6	Red input	
7	+ 12 V power supply	0.3 A max
8	+ 5 V power supply	0.6 A max
9*	Analog/digital mode select	High state (open) : Analog signal (0.7 V p-p) Low state (ground) : Digital signal (TTL level)

11

Daedal Corp. Series 20,000, Precision Rotary Table

ROTARY MOTION — POSITIONING TABLES

2

SERIES 20000 Rotary Positioning Tables

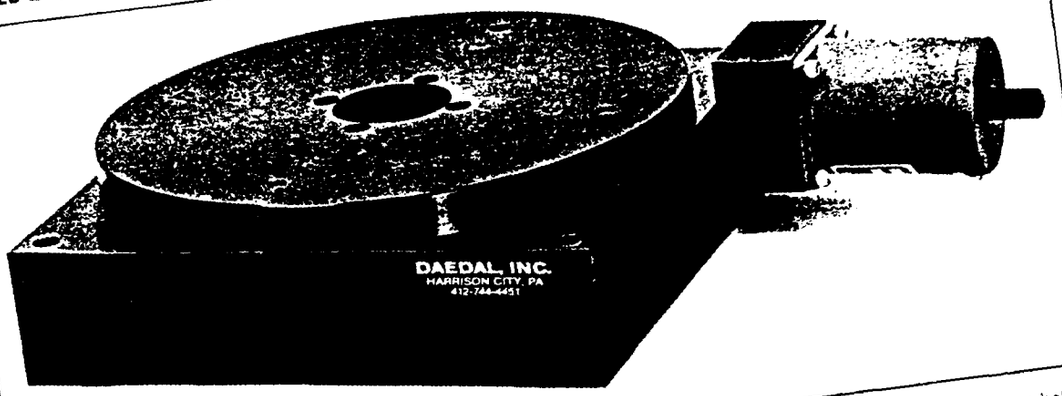

Daedal rotary positioning tables are designed for precise motor driven rotary positioning and indexing. These tables are low in profile, exhibit the highest standards of quality, and offer years of proven reliability and performance. With table diameters of 5, 6, 8, 10, and 12 inches, and load capacities up to 200 pounds, they are the ideal choice for a broad range of rotary positioning applications.

These tables feature a high quality angular contact ball bearing system which is stiffly pre-loaded to minimize runout, while producing extremely smooth rotation of the table top. A precision worm gear drive provides precise point to point angular positioning - free of any backlash to assure bidirectional accuracy and repeatability. The standard selection of gear ratios provides added flexibility in establishing table speed and resolution, especially when using a stepping, micro-stepping, or DC servo motor to drive the table. A mounting block and shaft coupling are provided for easy - direct mounting of any Nema 23 flange type motor. If desired, standard modifications can be made to accomodate larger frame size motors.

These tables are offered in two performance grades . . . precision grade and standard grade. The precision grade is offered for applications demanding more critical performance characteristics, while the standard grade is offered, at lower cost, for applications which are not as critical.

The housing and table top are constructed of heat treated aluminum-protected with a hard black anodized surface finish. Convenient mounting holes, with locking threaded inserts, are provided in the table top to securely mount customer payloads. A clearance hole, through the center of the table, can be utilized as a clear aperture for passing an optical beam, or for easy access to the table top from below. Available as standard options are solid table tops (with no clearance hole), and raised table tops (to clear the motor mtg. block when the payload size exceeds the table diameter). In addition, the table top is easily removed to permit custom modification.

These versatile rotary tables are designed to operate in any orientation ranging from horizontal to vertical, and can be directly mounted to Daedal linear tables to create integrated multi-axis positioning systems. Also, by driving these tables with Daedal micro-stepping motors and controls, very cost effective systems can be created ranging from simple rotary indexing, to computerized motion control for automated position.

Typical applications including precise mirror alignment for laser setups, fiber optics alignment, tracking systems, automated quality control setups, pan and tilt systems.

Variables for selection include desired table diameter, load capacity, gear ratio, and performance grade. Home position switch, special table tops, and rotary encoders are standard options.

Features

- Low profile design
- Lightweight aluminum housing with attractive black anodized protective finish
- Rigid angular contact ball bearings for smooth wobble free rotation
- Pre-loaded worm gear drive for accurate reliable positioning
- Convenient mounting holes with locking stainless steel threaded inserts
- Choice of gear ratios

ROTARY MOTION — POSITIONING TABLES 2

SERIES 20000 Rotary Indexing Tables cont.

TABLE DIA.	GEAR RATIO	LOAD CAPACITY HORIZ. (lb.)	LOAD CAPACITY VERT. (lb.)	REPEATABILITY (arc-min.) STD.	REPEATABILITY (arc-min.) PREC.	ACCURACY (arc-min.) STD.	ACCURACY (arc-min.) PREC.	REQ'D INPUT TORQUE (in-oz)	WEIGHT (lbs.)	PRICE STANDARD	PRICE PRECISION
5.00"	180:1 90:1 36:1	25	10	0.5 0.5 0.5	0.2 0.2 0.2	10.0 10.0 12.0	3.0 3.0 5.0	15 15 18	6	$ 891 891 891	$ 990 990 990
6.00"	180:1 90:1 45:1	40	15	0.5 0.5 0.5	0.2 0.2 0.2	10.0 10.0 12.0	3.0 3.0 5.0	15 15 18	8	940 940 940	1,106 1,106 1,106
8.00"	180:1 90:1 36:1	75	25	0.5 0.5 0.5	0.2 0.2 0.2	10.0 10.0 12.0	3.0 3.0 5.0	15 15 20	15	1,078 1,078 1,078	1,348 1,348 1,348
10.00"	180:1 90:1 45:1	200	40	0.5 0.5 0.5	0.2 0.2 0.2	10.0 10.0 12.0	3.0 3.0 5.0	20 20 24	29	1,560 1,560 1,560	2,074 2,074 2,074
12.00"	180:1 90:1 45:1	200	40	0.5 0.5 0.5	0.2 0.2 0.2	10.0 10.0 12.0	3.0 3.0 5.0	20 20 24	32	1,640 1,640 1,640	2,195 2,195 2,195

TABLE DIA. (A)	DIMENSION CHART B	C	D	E	F	G	H	J	K	L
5.00	1.00	5.00	4.00	1.75	.31	1.11	1.66	3.00	4.00	1.38
6.00	1.75	6.00	5.00	2.00	.38	1.23	2.04	4.00	5.00	1.38
8.00	1.75*	8.00	6.00	2.50	.50	1.57	2.04	4.00	6.00	1.38
10.00	2.00	10.00	9.00	3.00	.75	1.81	3.03	6.00	8.00	1.38
12.00	2.00	10.00	9.00	3.00	.75	1.81	3.03	8.00	10.00	2.38

*1.00 Dia. on 8.00" Dia. Table With 36:1 Gear Ratio

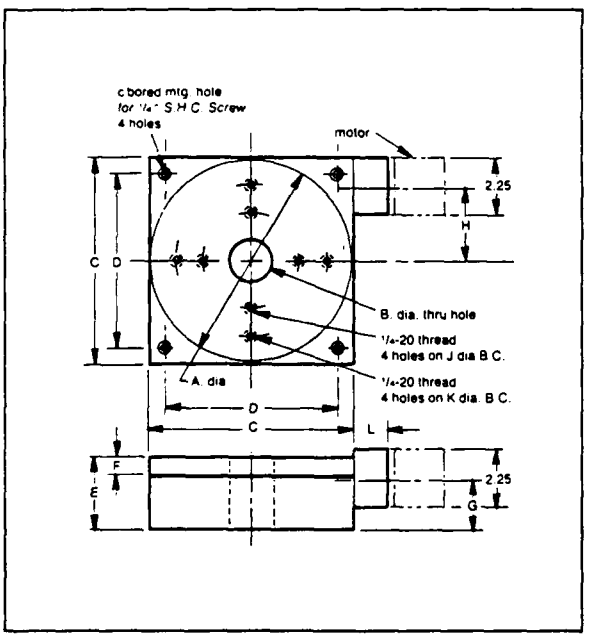

Specifications:

Construction: aluminum-stainless steel
Finish: black anodize
Travel range: 360° continuous
Runout:
Precision Grade: .001 in.
Standard Grade: .003 in.
Concentricity:
Precision Grade: .0001 in.
Standard Grade: .0005 in.

Ordering Information:

To determine the correct model number for a desired table, use the model number code as shown below, and follow the example given. When adding options, consult the factory.

MODEL NO. CODE:

2 08 02 -P

ROTARY TABLE SERIES

TABLE DIAMETER
5, 6, 8, 10, 12 in.

GEAR RATIO*
01 = 180:1
02 = 90:1
04 = 45:1
05 = 36:1
*Refer to the gear ratio column in specification chart for availability in selected table diameter.

GRADE
S = Standard
P = Precision

The example above calls for a precision grade rotary table having an 8.00" diameter table top, and a 90:1 gear ratio.

ATMOSPHERIC OPTICAL SYSTEMS FEB. 1988

PRELIMINARY OPERATIONS MANUAL
(1 Feb. 88)

WHOLE SKY IMAGER
(EO Camera System 5)

R.W. Johnson

UNIVERSITY OF CALIFORNIA SAN DIEGO

SCRIPPS INSTITUTION OF OCEANOGRAPHY

MARINE PHYSICAL LABORATORY San Diego, CA 92152-6400

Prepared for
Air Force Geophysics Laboratory, Air Force Systems Command
United States Air Force, Hanscom AFB, Massachusetts 01731

APPENDIX D

WHOLE SKY IMAGER
(E/O Camera System 5)

PRELIMINARY OPERATIONS MANUAL
(1 Feb 88)

This preliminary manual summarizes the basic support procedures required for the normal operation of the Whole Sky Imager. It is intended as a checklist operational guide for the use of on-site host personnel in performing their periodic inspection and assessment of the system's performance.

System maintenance and trouble shooting instructions are not included in this summary note, but are available under separate cover.

UCSD/MPL POINTS OF CONTACT

1. Richard W. Johnson, (619) 534-1772, AV 553-5800
2. John S. Fox, (619) 534-1770, AV 553-5800
3. Jack R. Varah, (619) 534-1768, AV 553-5800

TABLE OF CONTENTS

LIST OF ILLUSTRATIONS

1.0 SYSTEM DESCRIPTION

The basic Whole Sky Imager (WSI) system is contained in two mechanical assemblies. These assemblies are illustrated photographically in Figs 1 & 2, and as block diagrams in Figs 3 & 4. The external and internal assemblies (Figs 1 & 2) are normally interconnected by a set of 100 foot control cables which provide system power, synchronization and data logging capability.

In its most basic form, each of these WSI systems consists of a computer controlled solid-state video camera that provides calibrated, multi-spectral imagery suitable for the automatic extraction of local contrast transmission and cloud cover information. Imbedded within the control computer are prototype and proprietary extraction algorithms necessary to provide these numerical products. In addition to radiometrically calibrated imagery, advanced algorithms are available to provide near real-time products of the data acquisition, processing and display sub-systems in the form of continuously updated digital presentations of selected operational quantities. For the WSI task of generating cloud field statistics, these algorithms are withheld from the field systems, and they are used only during post-archival processing, thus each field system is operated in automatic data acquisition and archival modes only.

An auxiliary mounting pedestal illustrated in Fig. 5 is associated with the WSI system to provide a standardized base for the camera, and to provide some measure of environmental control. The 2 ft X 2 ft insulated pedestal is 4 feet high and contains a 1500 watt, 5120 Btuh electric heater with built-in fan, and a 5000 Btuh air conditioner for summer cooling. These heating and cooling units are automatically controlled by 115VAC in-line thermostats which are mounted within the pedestal adjacent to the camera baseplate.

2.0 HOST PERSONNEL RESPONSIBILITIES

The WSI system is designed to operate in automatic data acquisition and archival modes with a minimum of operator interaction. Thus, once the system has been installed and initialized by UCSD/MPL technical staff, it requires only those services outlined in Table A, "WSI Data Site: Host Support Notes."

The six tasks outlined in Table A can be further summarized into the three items listed below.

I. Visually inspect system status DAILY. Report abnormalities.

II. Remove data tapes & replace whenever indicated on monitor:
   a. On WEEKLY schedule if operation is normal.
   b. As indicated in the event of system fault or power failure.

III. Periodically substitute solar attenuator arms.
   a. Change arms in accordance with schedule illustrated in Fig. 6.

IV. Periodic inspection of sensor housing. Report abnormalities.
   a. Open box and check thermostat settings and verify heater & A/C operation.
   b. Note instrument purge pressure (1st and 2nd regulator stages).
   c. General visual inspection of dome and occulter/attenuator and housing.

V. Weekly removal, cleaning and replacement of external computer air filter.

Checklists to assist in conducting the tasks listed above are provided in the following section.

TABLE A

WSI DATA SITE: HOST SUPPORT NOTES

DURING DATA COLLECTION INTERVAL
(ESTIMATED 2 YRS)

1. Provide daily visual inspection of camera assembly. Wipe or brush optical dome lightly if required to remove snow, heavy dew, thick dust, etc.
2. Provide daily visual inspection of console assembly. Observe video monitor to determine normal image quality and solar attenuator position.
3. Provide weekly unloading and replacement of data cassette with subsequent mailing to UCSD/MPL. (Cassettes provided by UCSD/MPL as well as procedural training).
4. Provide periodic substitution of solar attenuator arms to compensate for seasonal declination changes. (Change schedule and appropriate arms provided by UCSD/MPL. Normal change cycle is at two week intervals, extending to twelve weeks twice a year).
5. Provide telephone contact with UCSD/MPL in the event of system malfunction, and assist in preliminary fault assessment.
6. Permit intermittent access to site by UCSD/MPL personnel to effect system repair/replacement as required.

NOTE: UCSD/MPL will provide written instruction manuals as required to assist host personnel in accomplishing items listed above.

TABLE B

Solar Attenuator Arm Change Schedule

Date	Remove Arm No.	Install Arm No.
9 Nov	2	1
2 Feb	1	2
22 Feb	2	3
12 Mar	3	4
29 Mar	4	5
16 Apr	5	6
7 May	6	7
6 Aug	7	6
27 Aug	6	5
14 Sep	5	4
1 Oct	4	3
19 Oct	3	2
9 Nov	2	1

3.0 WSI OPERATIONAL CHECKLISTS (REF. TABLE A)

A. DAILY VISUAL INSPECTIONS

1. Camera Assembly
   a. Wipe or brush optical dome lightly, if required.
   b. Clear occultor drive of debris, if required.
   c. Check pedestal stability & alignment.
2. Console Assembly
   a. Check monitor for normal image quality.
   b. Check monitor image for solar attenuator position, i.e., sun's image within attenuator boundary.
   c. Check monitor for normal image cycle, i.e., four frame sequence and stable standby.
   d. Check standby image for correct annotation, i.e., time/date and filter ident.
   e. Check solar attenuator position at LAN, i.e., support rod vertical, solar image on vertical center line.
3. Accessory Control Panel
   a. Indicator lights cycling normally.
   b. Attenuator & Iris readouts changing normally.

B. DATA TAPE REPLACEMENTS

The 8 mm tape cassette that is used in the EXB-8200 streaming tape drive is designed to hold approximately 2.2 Gigabytes of data. This is in excess of the amount normally expected from a continuous seven day data collection cycle. Thus the normal operating procedure is to change data tapes every seven days during the normal evening reset cycle.

In the event of an EXB-8200 write failure, or a total system power failure, the corrective action is to remove and replace the data tape as instructed on the monitor. This will initiate the automatic re-boot sequence and the system will return to normal operation.

1. Normal WEEKLY (7 day) reloading sequence.

   After seven continuous days of operation, the system will automatically STOP, EJECT THE TAPE, and CUE the screen.

   a. Remove data tape from tape drive.
   b. Insert NEW data tape into tape drive.
   c. Close the tape drive door.

   The system will now automatically stand-by and resume data collection at the next occurring sunrise.

2. Abnormal FAULT or POWER LOSS reloading sequence.

   If a tape write fault, or a system power interruption occurs, the system will automatically STOP, EJECT THE TAPE, and CUE the screen. Operator response is as in the normal WEEKLY sequence.

   a. Remove data tape from tape drive. (Partially filled tapes will NOT be reused.)
   b. Insert NEW data tape into tape drive.
   c. Close the tape drive door.

   The system will now automatically re-boot and proceed through its self test routine. Upon satisfactory completion of self test the system will automatically STOP, EJECT THE TAPE, and CUE the screen.

   a. Close the tape drive door.

   The system will now automatically stand-by and resume data collection at the next occurring sunrise.

   Note that after a FAULT or POWER loss restart as in item 2 above, less than seven days may remain before the normal WEEKLY reloading day occurs. In this event, the normal WEEKLY

schedule should be re-initiated by operator intervention at the end of the normally designated 7th day. This re-initiation is most easily accomplished by inducing a POWER LOSS restart sequence. i.e., Turn off system power momentarily. Turn power back on and proceed as in item 2.

C. SOLAR ATTENUATOR ARM REPLACEMENT

The solar attenuator is an equatorially driven device that is designed to prevent direct solar illumination from falling upon the camera fisheye lens. This shadowing of the lens prevents undesirable stray light from entering the optical system and biasing the imagery collected by the camera.

The attenuator is designed to track the sun's position automatically from sunrise to sunset, and then during the evening hours, reset itself to the next mornings start position.

There is no automatic adjustment to compensate for the systematic drift that naturally occurs in solar declination with changes in the season. This necessary adjustment is accomplished manually by periodically replacing the occultor support arm.

The required seven support arms, each of slightly different length are provided by UCSD/MPL as is the Solar Attenuator Arm Change Schedule, See Fig. 6. Two Attenuator Frame assemblies with glass filters are provided to facilitate arm changeover procedures.

The arm change procedure is to be accomplished during the evening reset interval on the dates indicated in Fig. 6.

1. Loosen the three retaining screws on the small external shroud panel, and remove panel.

2. Insert 3/32" allen wrench (UCSD/MPL provided) into each of two 10-32 X 3/8" attenuator arm retaining set screws, and loosen each about one turn.

3. Lift arm from slotted drive disc.

* 4. Remove square attenuator frame from arm by loosening two 4-40 FH Nylok attachment screws.

* 5. Attach square attenuator frame to newly selected attenuator arm. Assure that arm and frame mate flat-to-flat. Tighten 4-40 screws securely.

6. Insert newly selected attenuator arm into slotted drive disc, and tighten both 10-32 allen retaining set screws.

7. Inspect installation for secure attachment of Frame-to-Arm, and Arm-to-Disc.

* Steps 4 & 5 are accomplished, using alternate Attenuator Frame, in office environment prior to visiting rooftop camera location.

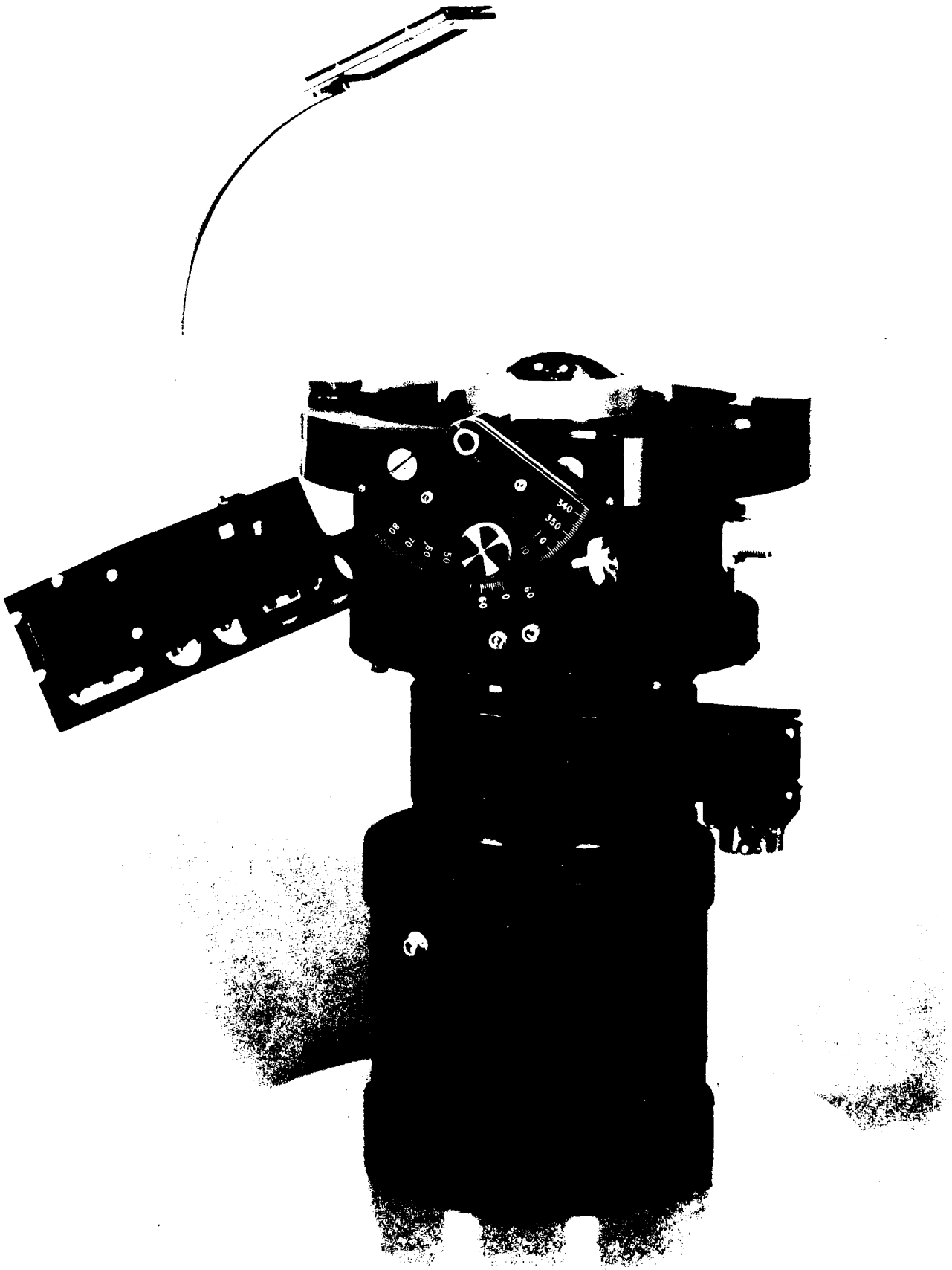

Fig. 1. (a) WSI Camera assembly, w/o shroud. (EO Camera System 5)

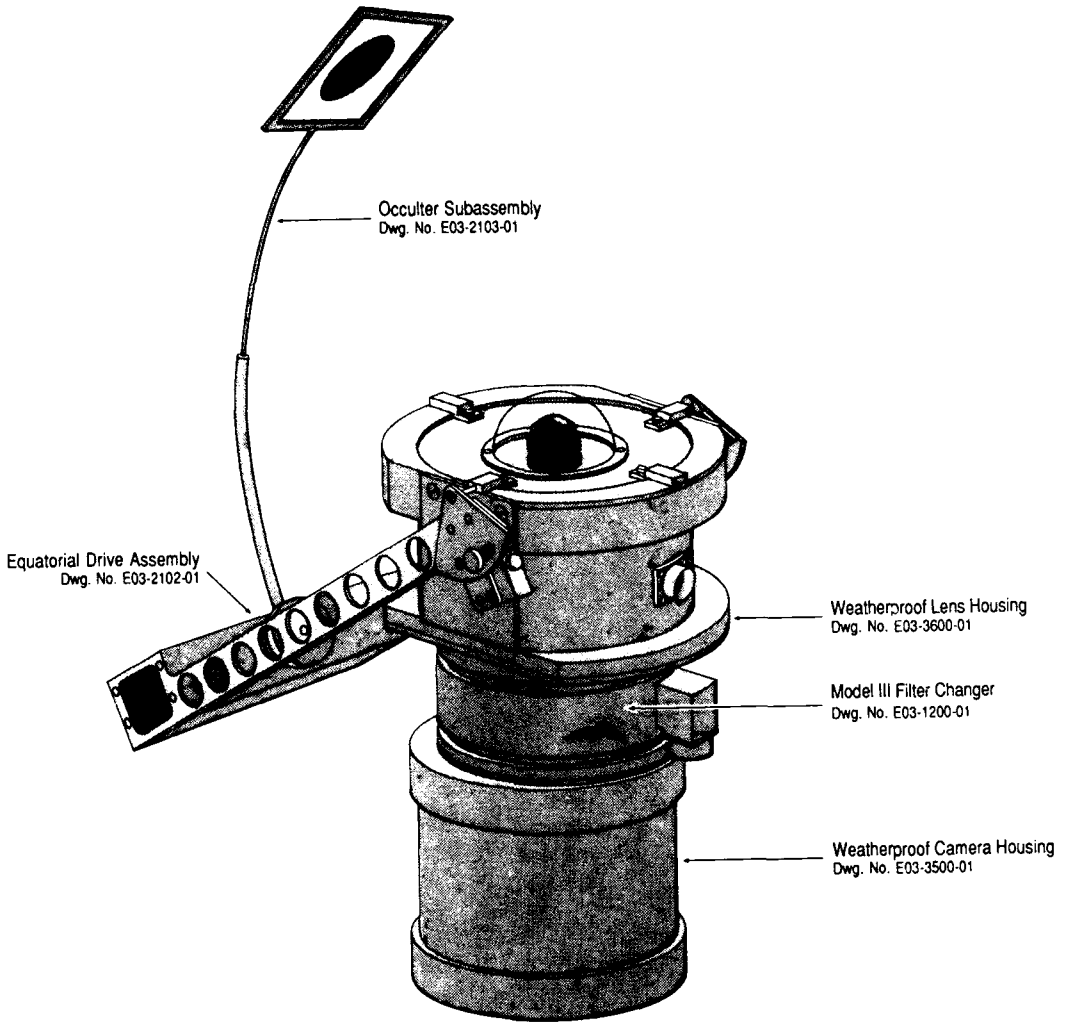

Fig. 1. (b) Artist's Conception of WSI Camera assembly, w/o shroud. (EO Camera System 5)

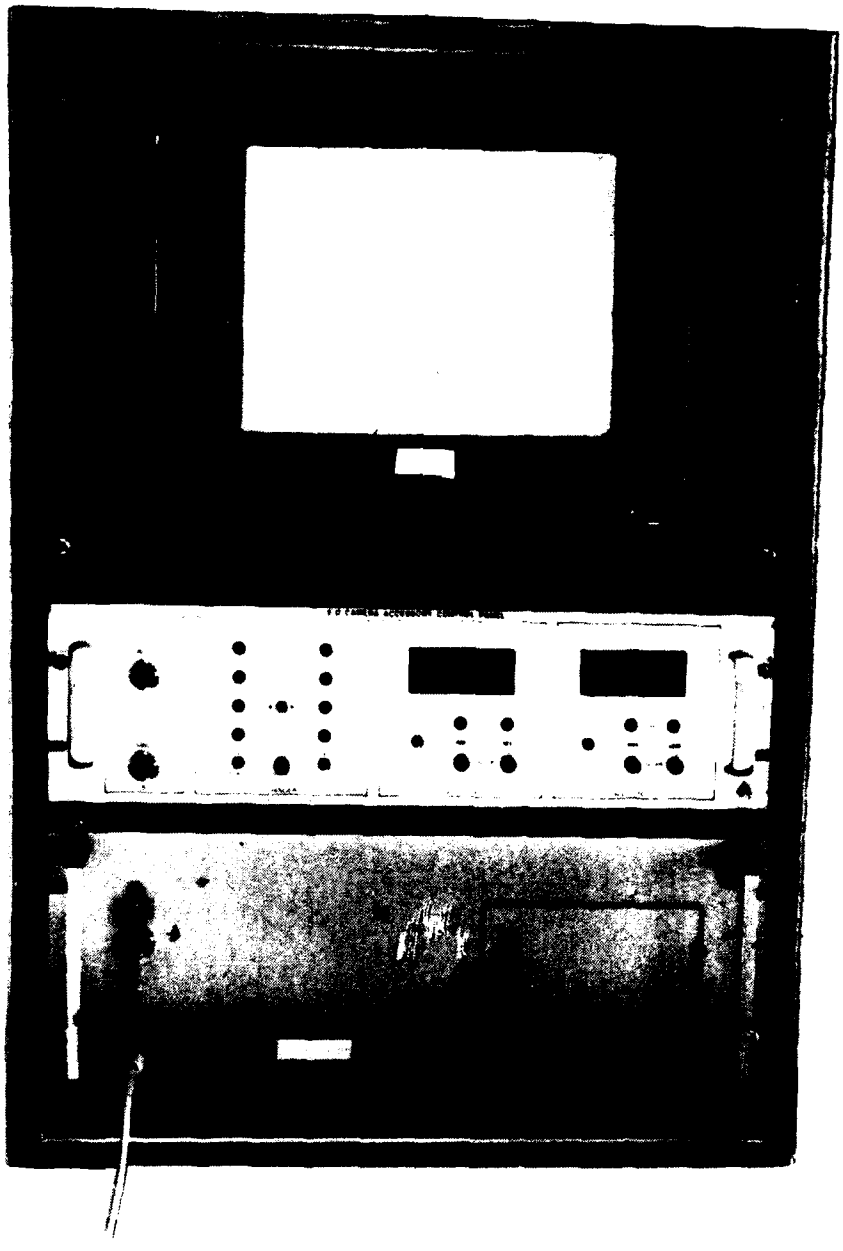

Fig. 2. WSI Control Console Assembly. (EO Camera System 5)

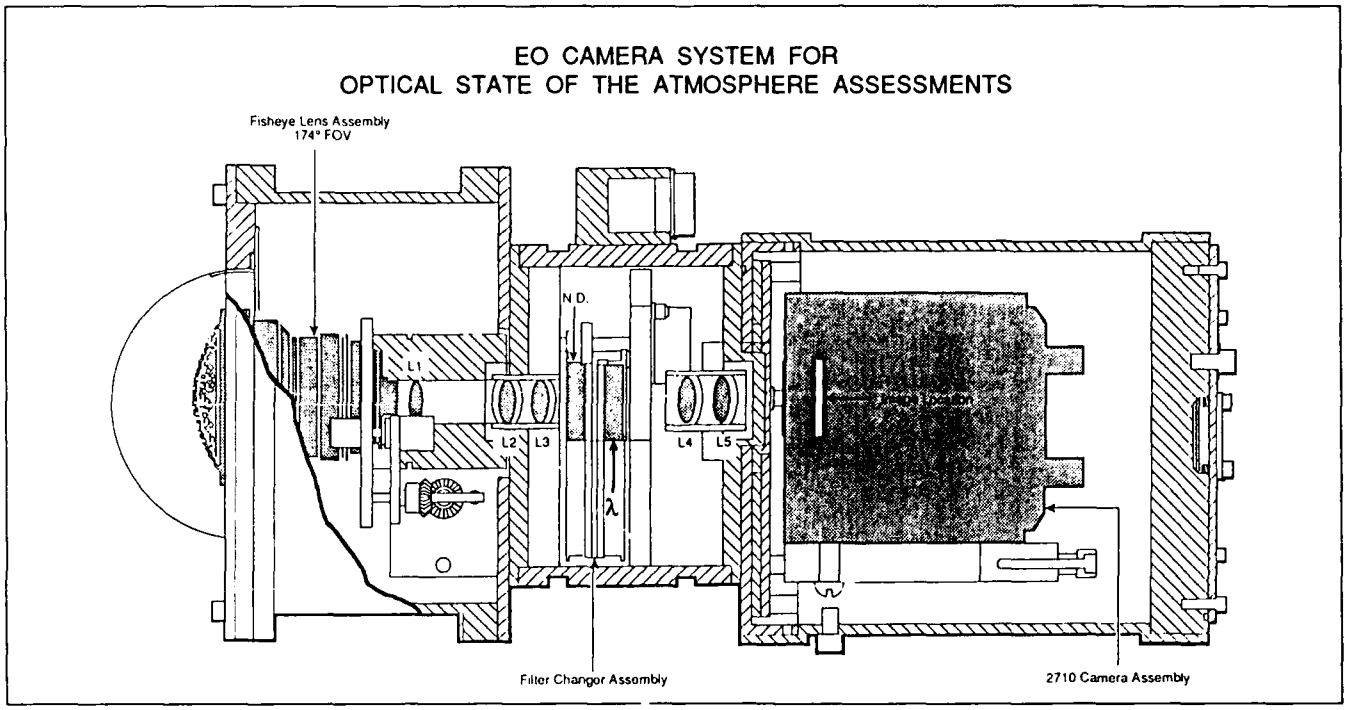

Fig. 3. WSI Camera Schematic. (EO Camera System 5)

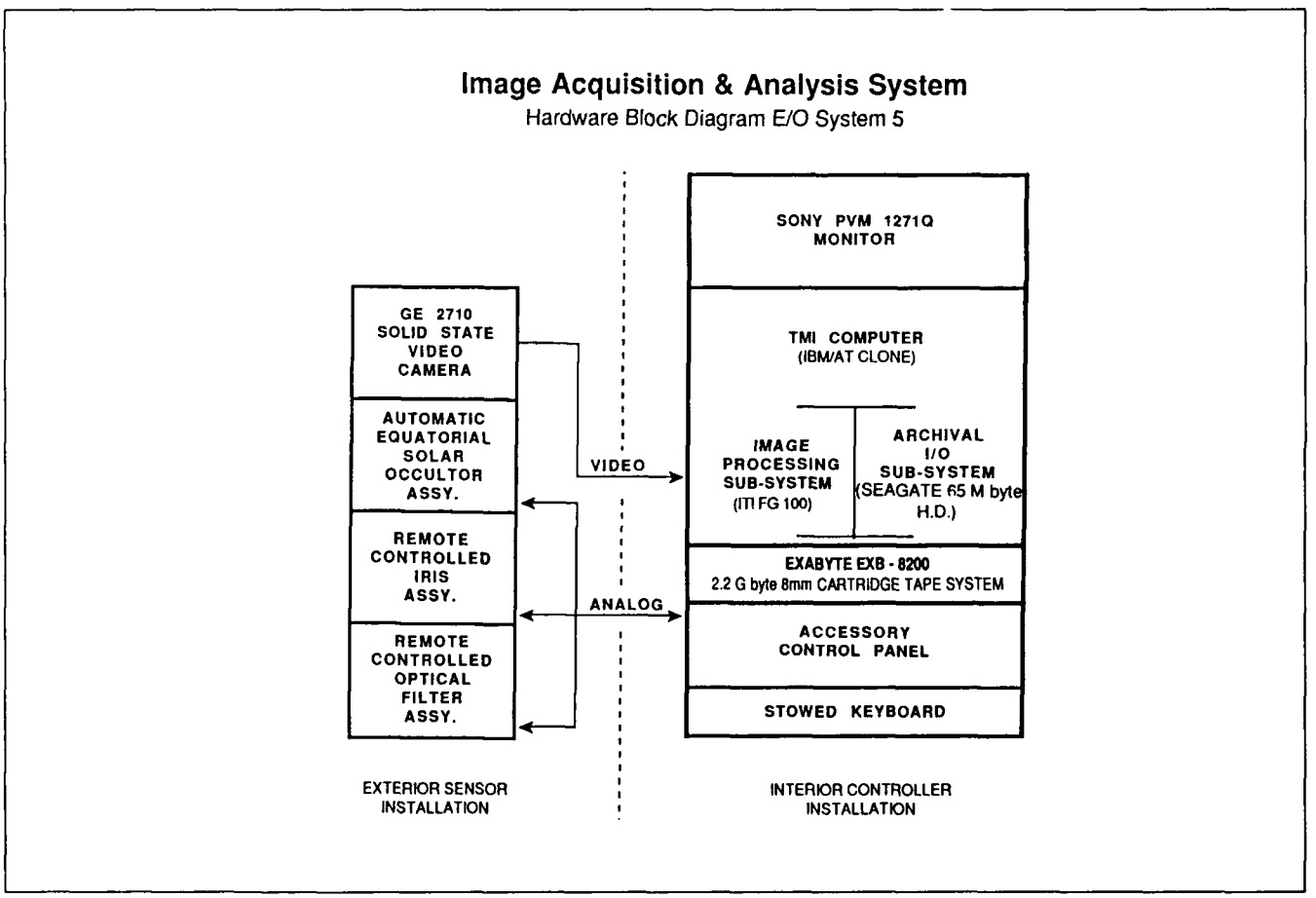

Fig. 4. WSI System Block Diagram. (EO Camera System 5)

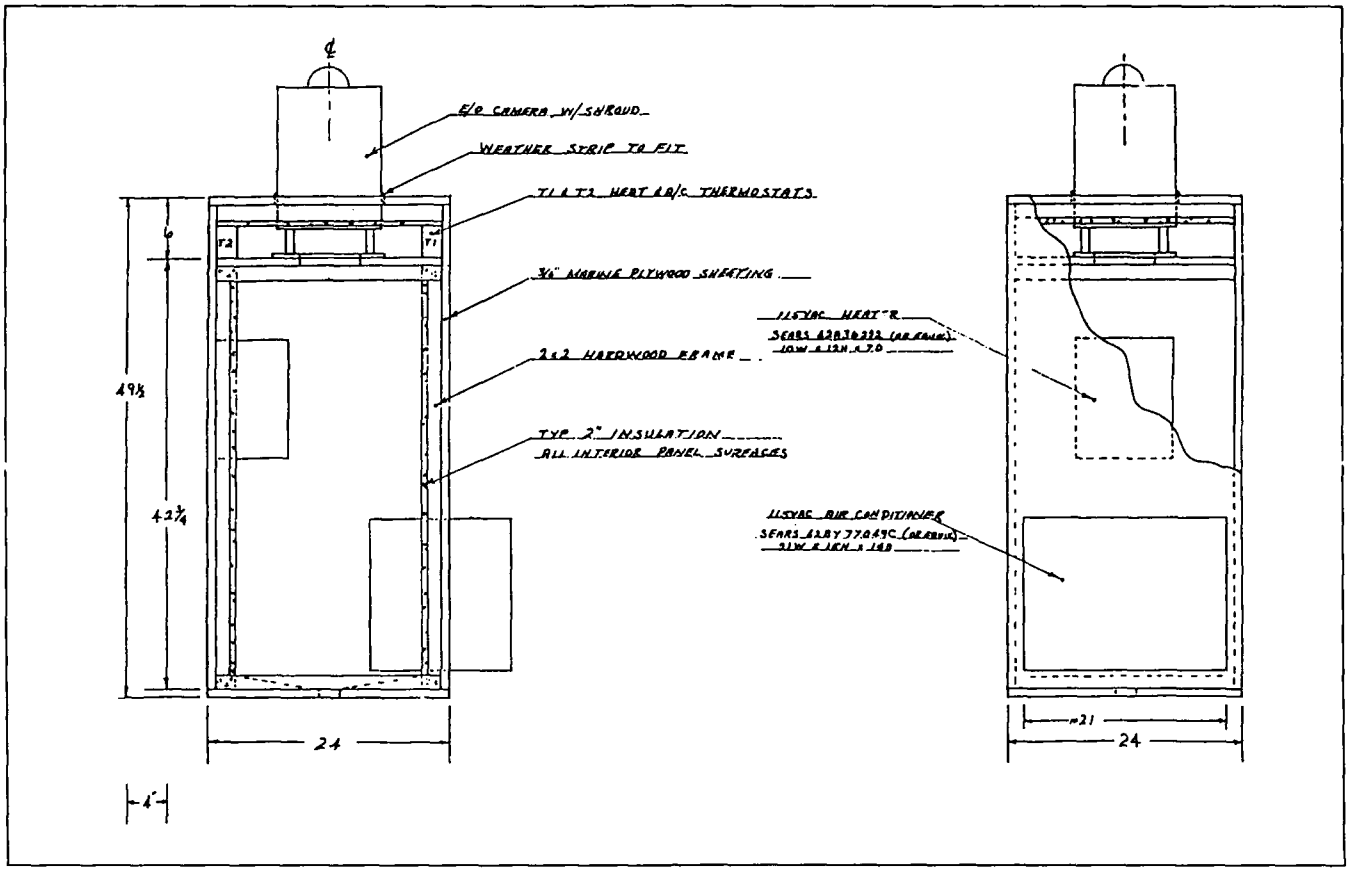

Fig. 5. EO Camera Pedestal (typical). (EO Camera System 5)

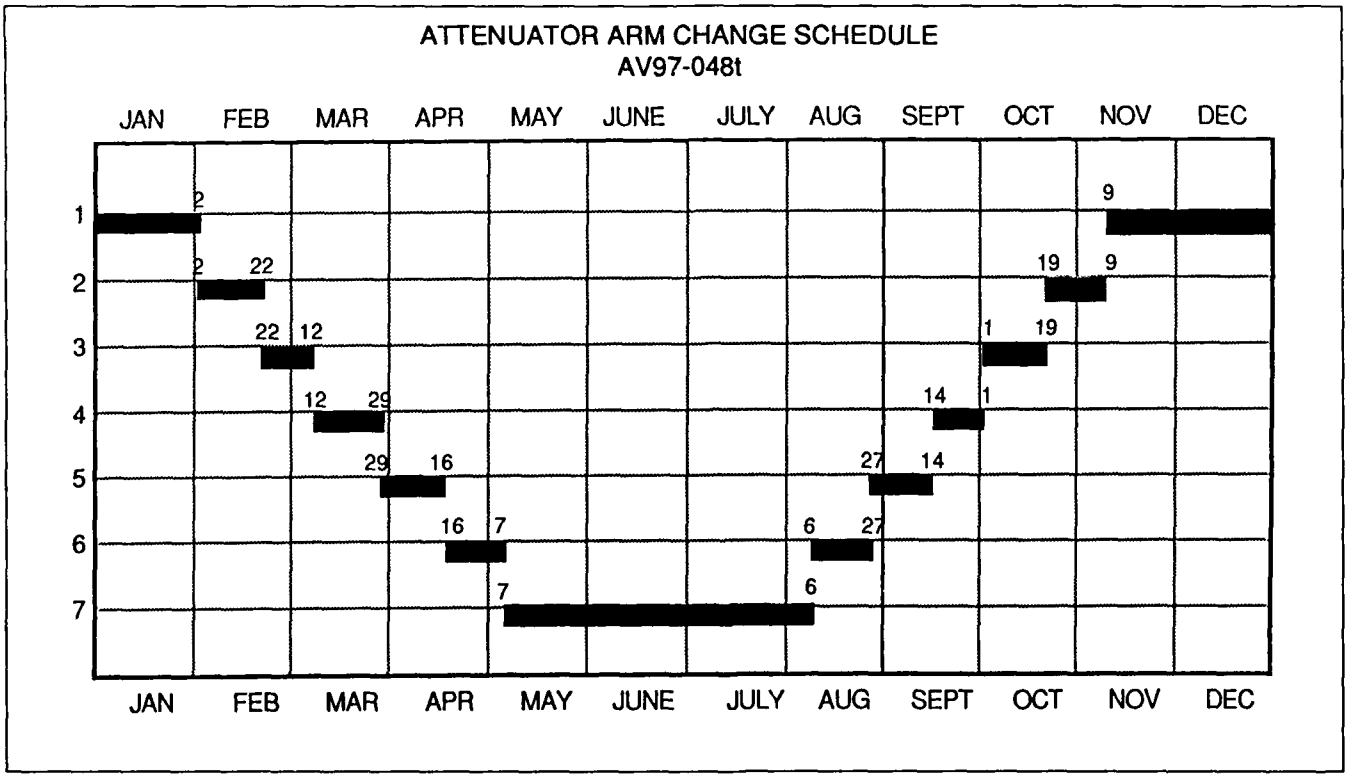

Fig. 6. Attenuator Arm Change Schedule. (EO Camera System 5)

NOTES

NOTES